Characterisation of a novel member of the Trim family as a novel pantropic viral inhibitor

Yuxin Song

Numéro National de Thèse : 2022ENSL0003

THESE

en vue de l'obtention du grade de Docteur, délivré par

l'ECOLE NORMALE SUPERIEURE DE LYON

Ecole Doctorale N° [340]
Biologie Moléculaire, Intégrative et Cellulaire (BMIC)

Discipline : **Sciences de la vie et de la santé**

Soutenue publiquement le 08/09/2022 par :

Yuxin SONG

Characterisation of a novel member of the Trim family as a novel pantropic viral inhibitor

Caractérisation d'un nouveau membre de la famille Trim en tant que nouvel inhibiteur viral pantropique

---

Devant le jury composé de :

Dr. Yves GAUDIN	Directeur de recherche, I2BC Paris Saclay	Rapporteur
Prof. Audrey ESCLATINE	Professeure des Universités, I2BC	Rapporteure
Dr. Magda MAGIERA	Chargée de recherche, Institut Curie	Examinatrice
Prof. Mathias FAURE	Professeur des Universités, CIRI	Examinateur
Dr. Andrea CIMARELLI	Directeur de recherche, CIRI, ENS de Lyon	Directeur de thèse

Numéro National de Thèse : 2022ENSL0003

THESE

en vue de l'obtention du grade de Docteur, délivré par

l'ECOLE NORMALE SUPERIEURE DE LYON

Ecole Doctorale N° [340]
Biologie Moléculaire, Intégrative et Cellulaire (BMIC)

Discipline : **Sciences de la vie et de la santé**

Soutenue publiquement le 08/09/2022 par :

Yuxin SONG

Characterisation of a novel member of the Trim family as a novel pantropic viral inhibitor

Caractérisation d'un nouveau membre de la famille Trim en tant que nouvel inhibiteur viral pantropique

---

Devant le jury composé de :

Dr. Yves GAUDIN	Directeur de recherche, I2BC Paris Saclay	Rapporteur
Prof. Audrey ESCLATINE	Professeure des Universités, I2BC	Rapporteure
Dr. Magda MAGIERA	Chargée de recherche, Institut Curie	Examinatrice
Prof. Mathias FAURE	Professeur des Universités, CIRI	Examinateur
Dr. Andrea CIMARELLI	Directeur de recherche, CIRI, ENS de Lyon	Directeur de thèse

Content

Acknowledgments

During the four years of my PhD, I progressed a lot both scientifically and personally, and in addition had a super nice experience living in France. First of all, I would like to thank the members of the jury for judging my thesis work.

At the same, I would like to thank my thesis director sincerely, Andrea CIMARELLI for helping me with the application of CSC scholarship, for helping me with the design of the subject and the guidance in the experiment and the writing of this manuscript. His rigor and enthusiasm for scientific research inspired me to continue in the field of scientific research.

I also would like to thank Drs. Henri GRUFFAT and Frederick ARNAUD for being members of my thesis monitoring committee. Thanks for the kind advice on the experiments and also concerns for my daily life that helped me running smoothly my thesis work.

I would like to thank all the members of the team with whom I worked with during my thesis: Lucie,

Xuan-Nhi, Anuj, Léa, Stéphanie, Mathilde, Li, Clara, Federico, Alexandre, Florent, Severine, Giulia, Clement, Raphael, Amandine and Charlotte. Thanks for the daily company and the advice in experiments.

Finally, I would like to thank all the people from the CIRI, the ENS, the Platim, the Cytometrie and the surrounding laboratories (OR, TEV, EBV and EVIR team) for the help during my experiment and thesis.

From a personal point of view, I want to thank my parents, who make me feel free to study abroad. Thanks all my friends for their company and the cherished experiences in these four years. I would like to thank the China government for the fellowship support and official aid during the Covid19 restrictions which allows me to continue my studies.

Abstract

To identify novel cellular modulators of HIV-1 infection in IFN-stimulated myeloid cells, we have carried out a screen that combines functional and evolutionary analyses in THP-1-PMA cells that led us to the Tripartite Motif Protein 69 (Trim69), a poorly studied member of the Trim family of innate immunity regulators. Trim69 inhibits HIV-1, primate lentiviruses and the negative and positive-strand RNA viruses VSV and SARS-CoV2, overall indicating it is a broad-spectrum antiviral factor. Trim69 binds directly to microtubules and its antiviral activity is intimately linked to its ability to promote the accumulation of stable MTs, a specialized subset of microtubules. By analyzing the behavior of primary blood cells, we provide evidence that a program of MT stabilization is commonly observed in response to IFN-I in cells of the myeloid lineage and Trim69 is the key factor behind this program.

Overall, our study identifies Trim69 as the first antiviral innate defense factor that regulates the properties of microtubules to limit viral spread, highlighting the possibility that the cytoskeleton may be a novel unappreciated fighting ground in the host-pathogen interactions that underlie viral infections.

Résumé

Afin d'identifier de nouveaux modulateurs cellulaires de l'infection par le VIH-1 dans les cellules myéloïdes stimulées par l'IFN, nous avons réalisé un criblage qui combine des analyses fonctionnelles et évolutives dans les cellules THP-1-PMA. Ce criblage nous a conduit à la protéine Tripartite motif protein 69 (Trim69), un membre peu étudié de la famille Trim des régulateurs de l'immunité innée. Trim69 inhibe le VIH-1, les lentivirus de primate et les virus à ARN à brin négatif et positif VSV et SARS-CoV2, indiquant globalement qu'il s'agit d'un facteur antiviral à large spectre. Trim69 se lie directement aux microtubules (MT) et son activité antivirale est intimement liée à sa capacité à favoriser l'accumulation de MT stables, un sous-ensemble spécialisé de microtubules. En analysant le comportement des cellules primaires du sang périphérique, nous apportons la preuve qu'un programme de stabilisation des MT est couramment observé en réponse à l'IFN-I dans les cellules de la lignée myéloïde et Trim69 est le facteur clé derrière ce programme.

Dans l'ensemble, notre étude identifie Trim69 comme le premier facteur de défense innée antiviral qui régule les propriétés des microtubules afin de limiter la propagation virale, soulignant la possibilité que le cytosquelette soit un nouveau terrain de combat méconnu dans les interactions hôte-pathogène qui sous-tendent les infections virales.

Abbreviations

+TIPs	plus-end tracking proteins
αTAT1	Tubulin acetyl transferase 1
25HC	Cholesterol-25-hydroxylase
2LTRs	2 long terminal repeat circles
3CLPro	3C-like proteinase
ABTB2	Ankyrin Repeat And BTB Domain Containing 2
ACE2	Angiotensin-converting enzyme 2 receptor
Ad5	Adenovirus 5
AIDS	Acquired Immunodeficiency Syndrome
AIM2	Absent in Melanoma 2
AKAP2	A-Kinase Anchoring Protein 2
ALIX	ALG-2-interacting protein
AP-1	Activator protein-1
APOBEC3A	Apolipoprotein B mRNA editing enzyme, catalytic polypeptide-like 3A
ARF	ADP ribosylation factor-like;
ARL13B	ADP-ribosylation factor-like 13B
ATG-3	Autophagy related 3
BAZ1A	Bromodomain Adjacent to Zinc Finger Domain 1A
BICD2	Bicaudal D2 adaptor
BLAST	Basic Local Alignment Search Tool
Bpp	Bayesian *Phylogenetics* and Phylogeography
BUSTED	Branch-site Unrestricted Statistical Test for Episodic Diversification
CA	Capsid
CAMSAP	Calmodulin-regulated spectrin-associated *protein*
CC	Coiled-coil
CCPs	Cytosolic carboxypeptidases
CCR5	C-C chemokine receptor type 5
CCY-1	Coiled-Coils Y protein 1
CD4	Cluster of Differentiation 4
CDK-5	Cyclin-dependent kinase 5
CFLAR	CASP8- and FADD-like apoptosis regulator
cGAS	Cyclic GMP-AMP synthase
CHX	Cycloheximide
CITED2	CBP/p300-interacting transactivator with glutamic acid/aspartic acid-rich carboxyl-terminal domain 2
CLASPs	Cytoplasmic linker associated proteins
CLIP170	CAP-Gly domain containing linker protein 1
CME	Clathrin-mediated endocytosis
COS	C-terminal subgroup one signature
CPSF6	Cleavage and polyadenylation specificity factor subunit 6

CRISPR/Cas9 KO	Clustered Regularly Interspaced Short Palindromic Repeats/*CRISPR*-associated protein 9 knockout
CTT	C-terminal tails
CXCR4	C-X-C chemokine receptor type 4
CypA	Cyclophilin A
DCs	Dendritic cells
DENV	Dengue Virus infection
DGINN	Detection of Genetic INNovation
DHCs	Dynein heavy chains
DICs	Dynein intermediate chains
DLCs	Dynein light chains
DLICs	Dynein light intermediate chains $
DMVs	Double membrane vesicles
dox	Doxycycline
EB	End binding *protein*
EEF1A1	Elongation factor 1-alpha 1
eIF2α	Eukaryotic translation initiation factor 2α
Env	Envelope
ER	Endoplasmic reticulum
ERGIC	ER-Golgi intermediate compartment
EURT	Entry/ Uncoating assay based on core-packaged RNA availability and Translation
Fez1	Fasciculation and elongation protein zeta 1
FIL	Filamin-type immunoglobulin;
FL	Full length (in retroviral DNA)
FL	Fusion loop (in structure SARS-CoV2 Spike)
FMD	Foot and mouth disease
FN3	Fibronectin type 3
FUBAR	Fast, unconstrained bayesian approximation for inferring selection
G	Glycoprotein
Gag	Group-specific antigen
GFP	Green fluorescent protein
Glu-tubulin	Detyrosinated tubulin
Gp120/gp41	Glycoproteins 120 and 41
GST	Glutathione-S-transferase protein
HAP1	Huntingtin-associated protein 1
HDAC6	Histone deacetylase 6
Hel	Helicase
HIV	Human immunodeficiency virus
HR1 and 2	Heptad repeat 1 and 2
HSP90	Heat shock protein HSP90
HTLV	Human T cell leukemia virus
HTT	Huntingtin
HYPHY	HYpothesis testing using *PHYlogenies*
IB	Inclusion Bodies

ICs	Intermediate chains
IFITM3	Interferon-induced transmembrane protein 3
IFN	Interferon
IGF2BP3	Insulin-like growth factor 2 mRNA-binding protein 3
IKK	Inhibitor of nuclear factor kappa B kinase complex
IL2	Interleukin 2
IN	Integrase
IntDen/area	Integrated Density weighted for area
IP10	IFN-inducible protein-10
IRF	IFN regulatory factor
JAK	Just Another Kinase, Janus Kinases
JHM virus	Mouse hepatitis *virus* (MHV) strain *JHM*
L	RNA-dependent RNA polymerase
LBPA	Lysobisphosphatidic acid
LCs	Light chains
LDL	Low-density lipoprotein
leC	Complement of the genomic leader region
LICs	Light intermediate chains
LILRA3	Leukocyte immunoglobulin like receptor
LLPS	Liquid-liquid phase separation
LPAR1	Pysophosphatidic acid receptor 1
M	Matrix protein
MA	Matrix
MAPs	Microtubule-associated proteins
MATH	Meprin and tumor-necrosis factor receptor-associated factor homology
MAVS	Mitochondrial antiviral-signaling protein
MDA5	Melanoma differentiation-associated protein 5
MEME	Multiple Em for motif elicitation
MOI	Multiplicity of infection
MSSS	Minus-strand strong stop
MT	Microtubule
MTOC	Microtubule-organizing center
MVB	Multivesicular bodiy
Mx1	MX Dynamin Like GTPase 1
MyD88	Myeloid differentiation primary response 88
N	Nucleoprotein
NC	Nucleocapsid
Nef	Negative factor
NEMO	NF-kappa-B essential modulator-like
NF-κB	Nuclear factor κB
NFAR1/2	Nuclear factor associated with dsRNA 1 and 2 proteins
NHL	NCL-1/HT2A/LIN-41 protein
NS3	Non-structural protein 3
NTD	N-terminal domain

NUMA	Nuclear mitotic apparatus protein
Nup358	Nuclear protein 358
P	Phosphoprotein
PAML	Phylogenetic analysis by maximum likelihood
PAMPs	Pathogen-associated molecular patterns
PBLs	Peripheral Blood *lymphocytes*
PCM1	Pericentriolar material 1
PCT-1	Procalcitonin
PEDV	Porcine Epidemic Dhiarrea virus
PHA	Phytohemagglutinin
PHD	Plant homeodomain
PIP3	Phosphatidylinositol-3- phosphate
PKR	Double- stranded RNA-activated protein kinase
Plpro	Papain like protease
PMA	Phorbol 12-myristate 13-acetate
Poh1	Proteasome 26S subunit, non-ATPase 14 (PSMD14-
Pol	Polymerase
PRR	Pattern recognition receptors
PS	Phosphatidylserine
PSMB8	Proteasome subunit beta type-8
PTMs	Post translational modifications
qPCR	Quantitative polymerase chain reaction
RAG1	Recombination activation gene 1
RBCC	RING; B-Box and CC
RBD	Receptor-binding domain
RdRp	RNA-dependent RNA polymerase
Rev	Regulator of expression of virion proteins
RIG-I	Retinoic acid-inducible gene I
RING	Really Interesting New Gene
RLRs	(RIG-I)-like receptors
RRE	Rev-responsive element
RT	Reverse Transcriptase
S	Spike
SAM	S-adenosyl-L-methionine (SAM)-dependent
SAMHD1	Sterile alpha motif and HD domain-containing protein 1
SARS-CoV2	Severe acute respiratory syndrome *coronavirus* 2
SARS-Cov2 nsp	Non-structural proteins of SARS-Cov2
SARS-Cov2 ORFs	Open reading frames of SARS-Cov2
SD1 and 2	Subdomains 1 and 2
SIRT2	Sirtuin 2
soTrim69	Saguinus oedipus Trim69
SPRY	Sp1A kinase and Ryanodine receptors domain
STAT	Signal Transducer and Activator of Transcription
TAK1	TGF-β-activated kinase 1

TAB2	TAK1-binding protein 2
Tat	Transactivator
TBK1	TANK-binding kinase 1
TFIIIA	Transcription factor 3A
TLRs	Toll-like receptors
TM	Transmembrane domain
TMPRSS2	Transmembrane serine protease 2
TNPO3	Transportin-3
TOP1	Topoisomerase 1
TPR	Tetratricopeptide repeats
Tr	Trailer
TRAM	Translocating-chain associated protein
trC	Complement of the genomic trailer region
Trim	Tripartite motif protein
TTL	Tubulin tyrosine ligase
TTL	Tyrosine-tubulin ligases
TUBA	Tubulin alpha
Ubc13	Ubiquitin-conjugating enzyme 13
Ube2	Ubiquitin-conjugating enzyme E2 variant
UEV1A	Ubiquitin-conjugating enzyme E2 variant 1A
VCP	Valosin-containing protein
Vpu and Vpr	Viral proteins U and R
VS	Vesicular Stomatitis
VSIV	Indiana VSV serotype
VSNJV	New Jersey VSV serotype
VSV	Vesicular Stomatitis virus
YAP	Yes-kinase associated protein

Figures and Tables List

Introduction

Results

Introduction

1. The family of Tripartite motif (TRIM) Proteins

1.1 Discovery

The history of the discovery of the Trim family can be started at the beginning of the 90s, upon the identification of a novel type of cysteine-rich sequence motif that was identified in seven proteins, among which the human V(D)J recombination activation gene (RAG1) and the Really Interesting New Gene (RING1) (Freemont et al., 1991; van Lohuizen et al., 1991). In this domain, the spacing between the two cysteine/histidine pairs was distinct and closer than what was usually found in other zinc finger proteins and this led the authors to propose the existence of a novel protein domain that they named RING finger ($CX_2CX_{9-27}CXHX_2CX_2CX_{6-17}CX_2C$, in which the numbers indicate the number of residues within each cysteine or histidine (**Figure 1**).

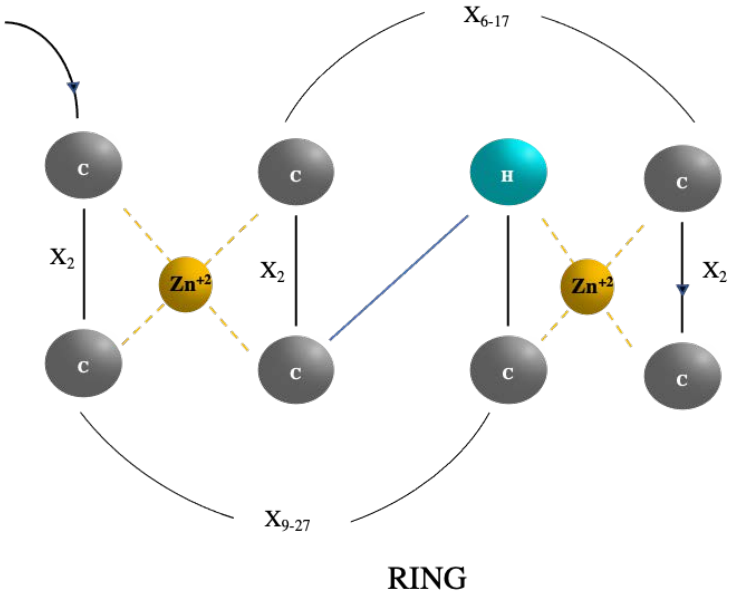

Figure 1. Topological representation of the RING domain and coordinating Zinc ions. *The RING finger domain. Primary sequence organization of the RING domain. C represent cysteine that coordinates zinc. H denotes the histidine ligand. X can be any amino acid, the number 2 refers to amino acid residues in the spacer regions between the zinc ligands. (picture adapted from* (Freemont, 1993) *and* (Saurin et al., 1996)

This domain was later reported to play a critical role in mediating the transfer of ubiquitin both to heterologous substrates, as well as to the RING proteins themselves, indicating therefore that this domain could represent a characteristic signature of E3 ubiquitin ligases (Joazeiro & Weissman, 2000). Subsequent studies identified several other proteins in which this RING domain was flanked by yet a second novel cysteine histidine box, which was first identified in the sequence of the Xenopus transcription protein TFIIIA (Miller et al., 1985) and that was named B box. This domain resembled other known zinc finger proteins domain, but displayed an unusually short distance between the two which was of 27 amino acids. This kind of box can occur in two flavors, B-box1 and B-box2, which share a similar but distinct pattern of Cys/His residues arrangement, mainly a cysteine in B-box1 and a histidine in B-box2 (Table 1).

	Consensus sequence
RING	C-X_2-C-X_{9-27}-C-X-H-X_2-C-X-$_{6-17}$-CX_2-C
B-BOX-1	C-X_2-C-X_{7-12}-C-X_2-C-X_4-C-X_2-[CH]-X_{3-4}-H-X_{4-9}-H
B-BOX-2	C-X_2-H-X_{7-9}-C-X_2-[CDHE]-X_4-C-X2-C-X_{3-6}-H-X_{2-4}-[CH]

Table 1. Consensus sequences for the RING and B-box domains 1 and 2 within members of the TRIM family *(from* (Meroni & Diez-Roux, 2005)).

A third features was then identified in a predicted coiled-coil domain (CC) immediately downstream to the B box domains (Borden et al., 1995). Using these three features (RING, B-box and CC), under the hypothesis that proteins that share common domain organization may reveal large families with interesting properties, over 80 novel protein members were identified (Saurin et al., 1996), which led to the initial definition of the large Trim family that we know nowadays. In addition to the three elements that define the family, a large number of Trim proteins possess a variable C terminal domain that confers specificity of action. In addition, TRIM proteins can form homodimers or heterodimers or even multimers with other TRIM proteins (**Figure 2b**) (Hatakeyama, 2017; Reymond et al., 2001) which is likely to diversify even more their functions and regulation.

First thought to be metazoan-specific, now some members of this family have been identified in plants and fungi (Crawford et al., 2018; Marín, 2012; Sardiello et al., 2008; Williams et al., 2019), which indicates that the evolution of the TRIM family is very broad. As a whole, Trim proteins are present in most eukaryotic cells and most of them are interferon type I (IFN-I) inducible (L. Wang & Ning, 2021) which suggests a role in antiviral responses.

1.2 Structure and classification groups

Members of the TRIM family are divided into two large groups. The first is characterized by a conserved structural arrangement of the three common N-terminal domains (RING; B-Box and CC, or collectively RBCC, **Figure 2a**) (Hatakeyama, 2017). This RBCC motif is usually followed by more diverse C-terminal regions that are specific for each TRIM and are often used to

classify TRIM proteins into 11 subgroups (C-I to C-XI, **Figure 2b**). The second group includes TRIM-like proteins that share a similar overall domain organization, but lack one or multiple subdomains that compose the RBCC core. Until recently, this group was composed of seven members that contained only PRY and SPRY domain or else additional domains (PHD, BROMO, FN3 or Pyrin) but that lacked the prototypical RING, B box and/or coiled-coil domain (see **Figure 2**).

As said above, the really interesting new gene (RING) domain that most members of the TRIM family possess is an E3-ubiquitin ligase activity domain (Borden, 1998). This enzymatic activity can thus control many events either through a direct control of the effector protein through substrate degradation by the 26S proteasome, or by conjugation to non-degradative ubiquitin chains that can modulate the activity of the RING targets. As such, Trim family members ensure control activities in many cellular processes, and have been implicated in intracellular signaling, innate immunity, transcription, autophagy, and carcinogenesis (Koepke et al., 2021a; McNab et al., 2011), despite the fact that a large number of TRIM proteins have been identified over the years, only a few have been well characterized to date.

The B-Box domain(s), following the RING domain, is (are) also zinc-binding motifs that occur in two flavors: B-box1 and B-box2. While mostly conserved, their presence is not absolute in the TRIM family (Reymond et al., 2001), with some TRIMs that possess only a B-box 2 domain or cys-his boxes with spacers distinct than those typical of a B-box. As said above, the main difference is in the second potential coordination residue, which is a cysteine in B-box1 and a histidine in-box2 ((Reymond et al., 2001). Depending on the diversity in size and sequence

within the variable region across the B-box1, the B1 box domain may enhance the activity of the RING domain and thus contribute to regulate E3-ubiquitin ligase activity (Borden, 1998). This may be mediated by the ability of B-boxes to mediate hetero-dimerization of different TRIM proteins.

Following the B-Box domains is the coiled-coil domain, which is composed of a long coiled coil region of approximately 100 residues which also play an important role in TRIM dimerization, and potentially higher-order oligomerization (Napolitano & Meroni, 2012).

The subclassification of the group I is based on the composition of sequences in the C-terminal region after the RBCC motif. This region represents the most variable portion of the protein and is generally responsible for the interaction of TRIM proteins with their cellular or viral targets, regulating both protein-binding specificities (van Gent et al., 2018) and subcellular localization (Ebner et al., 2017; Reymond et al., 2001; Short & Cox, 2006a). It is essentially based on their C-terminus that the TRIM family is divided into eleven groups (C-I to C- XI) (Reymond et al., 2001).

The most common TRIM C-terminal domain is the ∼61 amino acid long PRY domain and the ∼140 amino acid long Sp1A kinase and Ryanodine receptors (SPRY domain). These two domains are either present in a PRY-SPRY combination (also known as RFP-like, or B30.2, which is only found in vertebrates (D'Cruz et al., 2013), or the SPRY domain is present alone as most commonly found in mammals, plants, and fungi (Esposito et al., 2017; Rajsbaum et al., 2014; Sardiello et al., 2008). Additional domains present at the C terminus of TRIM family members include: the fibronectin type 3 domain (FN3), the plant homeodomain, the COS box, the NHL domain as well as the bromodomain (McNab et al., 2011). Below is a schematic

presentation of these C-terminal domains (**Figure 2**).

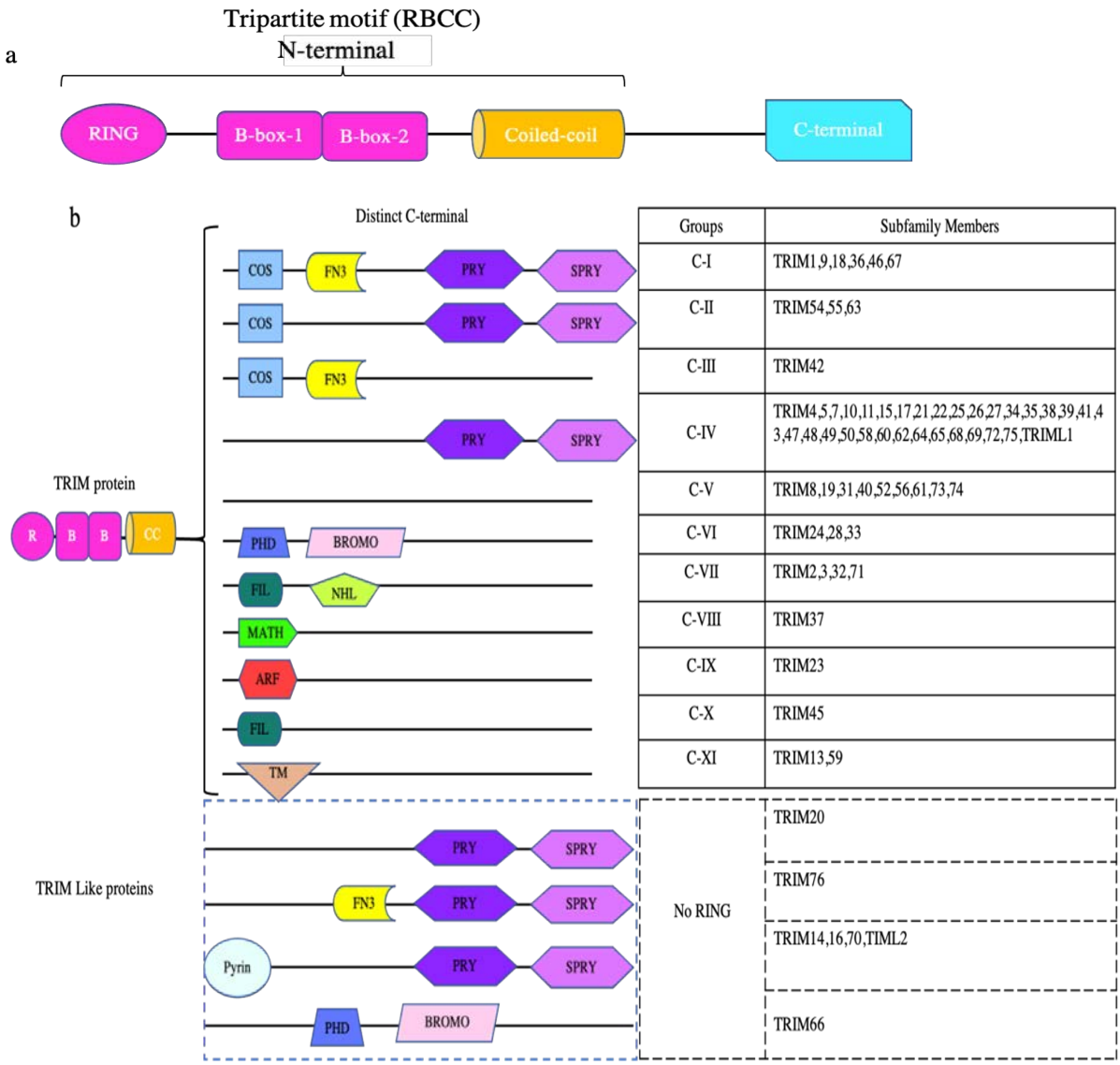

Figure 2. ***Structure and classification of the TRIM family.*** *(a) Modular representation of typical TRIM proteins: Ring domain (R), two B-boxes (BB1 and BB2), coiled-coil domain (CC) and distinct C-terminal regions. (b) Classification of TRIM proteins (from C-I to C-XI) in addition to an unclassified group lacking an identifiable RING-finger domain (no RING). PRY, PRY domain; SPRY, SPRY domain; COS, C-terminal subgroup one signature; FN3, fibronectin type 3; NHL, NHL domain; ARF, ADP ribosylation factor-like; BROMO bromodomain; FIL, filamin-type immunoglobulin; MATH, meprin and tumor-necrosis factor receptor-associated factor homology; PHD, plant homeodomain; TM, transmembrane.*

1) The SPRY /PRY-SPRY domain:

Approximately two thirds of the TRIM/RBCC proteins possess this 170 residues domain, also known as RFP-like domain that was first identified in TRIM27/RFP. The reported functions of the PRY-SPRY domain are diverse, yet predominantly involved in mediating protein-protein interactions (Nisole et al., 2005a). In most instances this protein-interaction entails binding of ubiquitination targets and determining E3 ligase specificity as discussed for individual TRIMs in detail below. Moreover, the PRY-SPRY domain is critical for the direct antiviral restriction activity of certain TRIMs, such as TRIM5alpha (Yap et al., 2005).

2) Cos box:

A distinct feature of MuRFs is that the C-terminal fraction of their HD domain (spanning predicted helices H2–H3) contains a conserved sequence motif, termed the COS (C-terminal subgroup One Signature)-box. This motif is also found in TRIM classes C-I and C-III, where it occurs just prior to a FnIII variable domain. The structure of the isolated COS-box from MID1 has been elucidated using NMR. Functionally, the COS-box is thought to mediate the association of its containing TRIMs to cytoskeletal structures. The COS-box of MID1 has been shown to associate with microtubules, while the COS box of MuRF1 was seen to interact with the sarcomere in transgenic mouse muscle. Always localized downstream of the coiled-coil domain, the COS one bears very little amino acid conservation across different TRIM members (around 30-40 percentage identity). The domain is present in a relatively restricted number of TRIM proteins as in TRIM18 and TRIM1 (also known as Midline protein 1 and 2, MID1 and MID2, respectively) (Baldini et al., 2020).

3) Additional C terminal domains:

One of the less frequent C-terminal domains within the TRIM/RBCC family is the NHL domain derived from the NCL-1/HT2A/LIN-41 protein in which it was originally described. This domain consists of 2–6 repeats of an approximately 40-residue sequence that resembles the WD repeat and that assembles to form a multiblade propeller structure (Slack & Ruvkun, 1998). TRIM proteins containing this domain are known to bind specific RNA sequences and to play important roles in fertility and development (Connacher & Goldstrohm, 2021). The TRIM/RBCC proteins that contain a plant homeodomain (PHD) are instead found in nuclear proteins and are thought to be involved in chromatin-mediated transcriptional regulation (Ivanov et al., 2007). They can be associated to a bromodomain (BROMO) that recognizes acetylated lysine residues, such as those on the N-terminal tails of histones. The fibronectin type 3 (FN3) domain has been described to be involved in binding to DNA and heparin. In addition, filamin-type immunoglobulin domains might be involved in dimerization and actin crosslinking (Ozato et al., 2008). Finally, ADP ribosylation factor-like (ARF) domains are involved in intracellular vesicular trafficking, and a MATH (meprin and tumor-necrosis factor receptor (TNFR)-associated factor (TRAF) homology) domain is necessary and sufficient for self-association and receptor interactions by some TRAF proteins (Esposito et al., 2017).

2. General functions

TRIM proteins are involved in broad and important cellular processes such as apoptosis, cell cycle regulation, cell proliferation, oncogenesis and innate immunity (Koepke et al., 2021a). The most studied functions of many TRIM proteins remain however related to innate and adaptive immunity (Nisole et al., 2005b; Venuto & Merla, 2019). Indeed, over the past decade, TRIM proteins were shown to serve important roles in the regulation of three major pathways involved in innate immune processes (**Figure 3**): (a) the regulation of cell cytokine production; (b) the modulation of autophagy; (c) the direct targeting of viral components, which leads to their degradation or to the inhibition of specific steps in the life cycle of different viruses. Here, we will illustrate the diversity of these functions through two examples: TRIM5alpha and TRIM21.

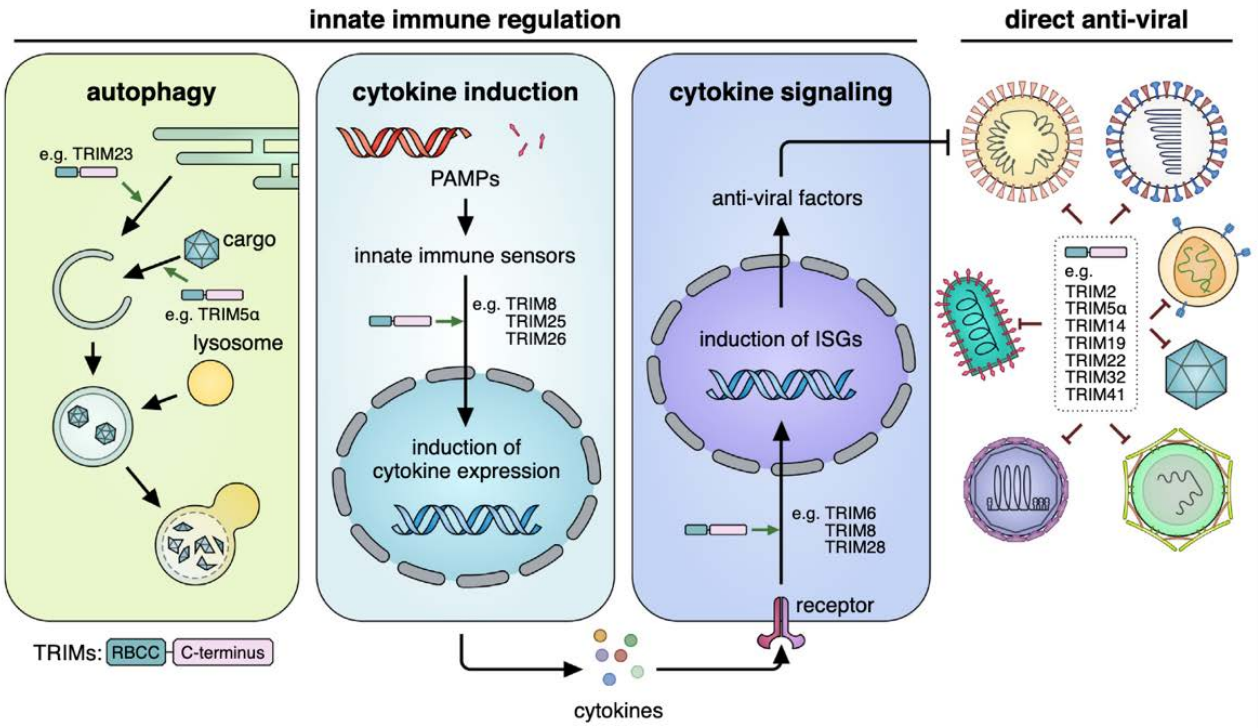

Figure 3. Schematic involvement of TRIM protein in the regulation of three major pathways. *(1) Modulation of autophagy, a cell-intrinsic autodigestive pathway that limits the*

replication of certain viruses; (2) regulation of cytokine induction and cytokine-mediated antiviral innate immune responses; (3) direct targeting of viral components, which triggers their degradation or inhibits the specific steps in the lifecycle of viruses (from (Koepke et al., 2021b).

1) The example of TRIM5α

Perhaps in the case of innate immunity and retroviral infection, the most studied member of the TRIM family is TRIM5α (T5α). T5α is a cytoplasmic protein that was functionally identified as an anti-HIV-1 restriction factor using a cDNA expression approach in which cDNAs of cells from Rhesus monkeys were expressed in human cells with the goal of transferring cell resistance to infection (Stremlau et al., 2004).

TRIM5α is a 493 amino acid residues protein in humans, belongs to C-IV group and presents the typical TRIM structure with a RING, two B-Boxes and CC domains followed by a PRY-SPRY domain (**Figure 4a**).

TRIM5 primary transcripts give rise to the expression of five additional isoforms following alternative splicing (gamma, iota, kappa and epsilon in addition to the longest isoform which is alpha) (Battivelli et al., 2011). While all contain a RING-B-box and CC domain, only the alpha isoform bears a PRY-SPRY domain and indeed the remaining isoforms cannot inhibit viral infection directly. On the contrary, due to the fact that they can interact with the long isoform, they can exert a dominant negative effect on T5α and decrease the extent of viral inhibition.

An interesting feature of T5α is that the protein expressed in one species does not inhibit infection of a virus specific to this species, but it can potently inhibit infection by viruses of other species (Sawyer et al., 2005; Stremlau et al., 2004, 2005). For instance, the human T5α

does not restrict HIV-1 infection because HIV-1 has developed manners to circumvent it by binding to cyclophilinA (Kim et al., 2019; Sokolskaja et al., 2006; Towers et al., 2003; Yap et al., 2004). On the other hand, human T5α can inhibit infection by other retroviruses suggesting that this factor has played an important role in limiting viral transmission from one species to the other (Hatziioannou et al., 2004; Diehl et al., 2008).

A plethora of studies have reported how mechanistically T5α can recognize and surround viral capsids leading to their degradation (Black & Aiken, 2010; Ganser-Pornillos et al., 2011; Biris et al., 2012; Grütter & Luban, 2012). This particular step can be visualized in real time by confocal microscopy (Y.-L. Li et al., 2016) and has also been shown to lead to IFN signaling, thus coupling detection of the viral pathogen, its direct disruption as well as signaling leading to the stimulation of the IFN pathway in a single protein (Grütter & Luban, 2012).

While all initial studies indicated that HIV-1 could not be restricted by human Trim5α, recent evidence indicates that HIV-1 avoids this targeting simply by masking itself with Cyclophilin A (CypA), a cellular protein very abundant in the cell, that is specifically bound by HIV-1 to shield itself from recognition (Sokolskaja & Luban, 2006). It is of interest that in Owl monkeys, a retro-transposition event substituted precisely the PRY-SPRY domain of Trim5α with the protein cyclophilin A, the first cellular protein identified as an HIV-1 Gag interacting protein. The resulting Trim-Cyp fusion is indeed a very potent inhibitor of HIV-1 (Luban et al., 1993) (**Figure 4b**).

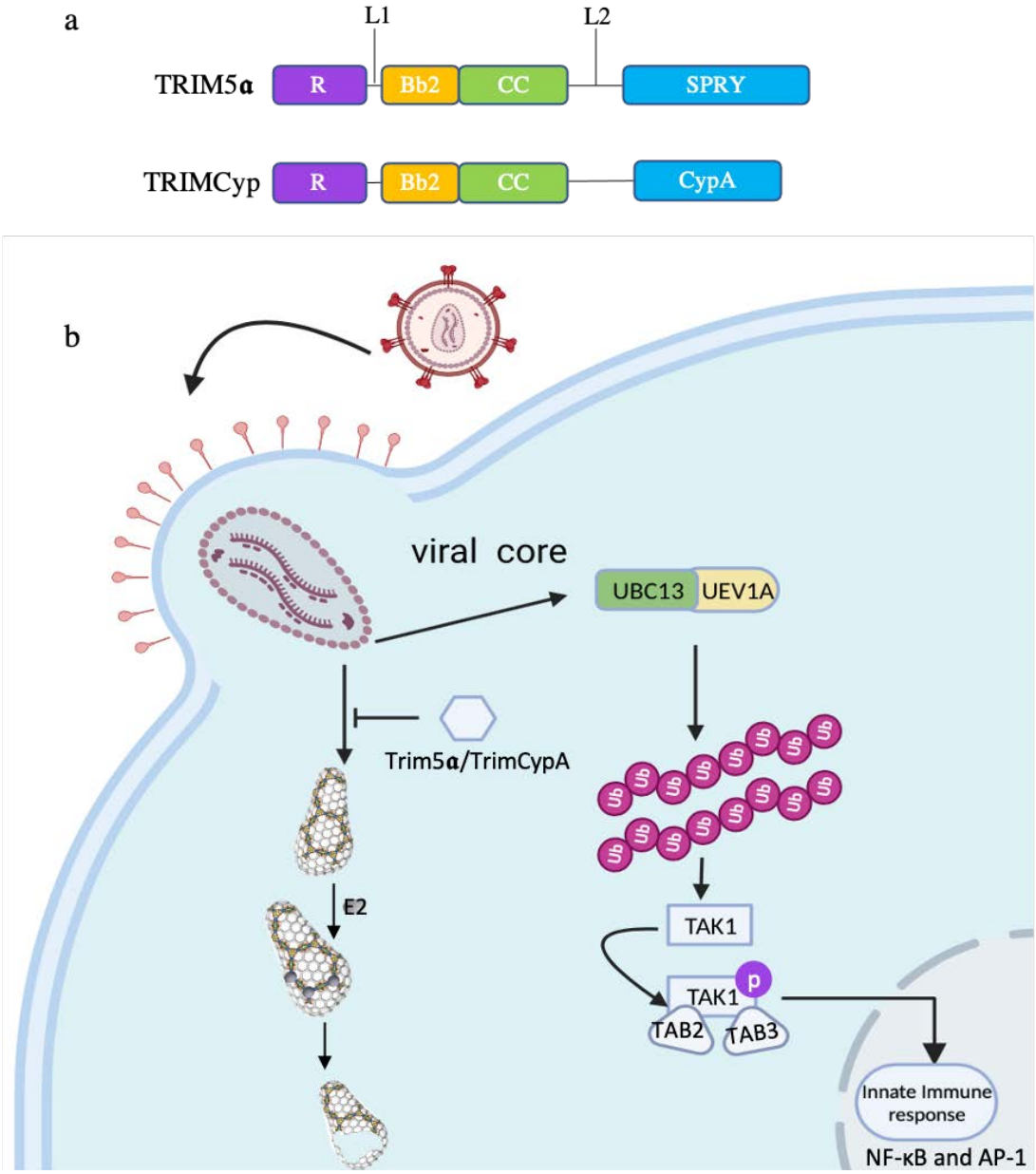

Figure 4. The structure of TRIM5α/TrimCypA and their roles in retrovirus infection.

a) Composed by a common tripartite motif (TRIM, also known as RBCC motif), including R (RING), Bb-2 (B-box 2) and CC (coiled-coil) domains. Linker 1 (L1) connects RING and B-box 2, and the RBCC scaffold to the capsid-binding domains, SPRY in TRIM5α and CypA in TRIMCyp are connected by Linker 2 (L2). B) The retrovirus capsid is engaged by TRIM5α in the cytoplasm of the infected cell and forms a hexagonal lattice on top of the capsid. This leads to aberrant uncoating of the capsid (the RING domain of TRIM5α recruits an E2 enzyme (Ubc13), after the core is disassembled and blocks retrovirus infection. Concomitantly, TRIM5α binding to capsid triggers its E3 ligase activity, and in concert with the E2 ubiquitin (Ub)-conjugating enzyme complex UBC13–UEV1A generates free lysine 63 (K63)-linked Ub chains, which in turn are catalysts in the autophosphorylation (P) of the TAK1 complex (includes TAK1, TAB2, and TAB3). Activation of the TAK1 complex by autophosphorylation results in the induction and expression of NF-κB- and MAPK responsive inflammatory genes, thereby leading to an innate immune response in the infected cell.

2) The example of TRIM21

A second and really different example of relationship between TRIM molecules and innate responses is provided by TRIM21 (or Ro52) (Mallery et al., 2010; McEwan et al., 2011, 2013; Fletcher & James, 2016). TRIM21 was initially cloned as an antigen recognized by autoantibodies present in the sera obtained from lupus erythematosus patients (Ben-Chetrit et al., 1988, 1990). TRIM21 is a typical member of the family and possesses the classical RING, B-box, CC and PRY-SPRY domain organization. The remarkable features of TRIM21 is the intracytoplasmic recognition of the Fc portion of antibodies, which are recognized through the PRY-SPRY domain (James et al., 2007) (**Figure 5a**). A number of non-enveloped viruses enter cells despite the fact that their capsids are coated with antibodies. TRIM21 is capable of detecting such antibody-virus complexes leading to their ubiquitination (through its RING domain), and to its subsequent degradation via the proteasome (Hennig et al., 2008; Mallery et al., 2010; McEwan et al., 2013). Recent studies indicated that this mechanism of action could also be observed for enveloped viruses when certain viral antigens could make complexes with antibodies and become therefore susceptible to TRIM21-mediated degradation (Mallery et al., 2010) . As observed in the case of Trim5α, recognition of its substrate leads to the activation of the IFN signaling pathway via NF-kB, AP-1, IRF proteins that converge in TAK1 kinase complex activation and IFN production (Fletcher et al., 2015; McEwan et al., 2013) (**Figure 5b**). Thus, also in this case TRIM21 recognizes its targets and also initiate a danger signal that can be passed to other cells.

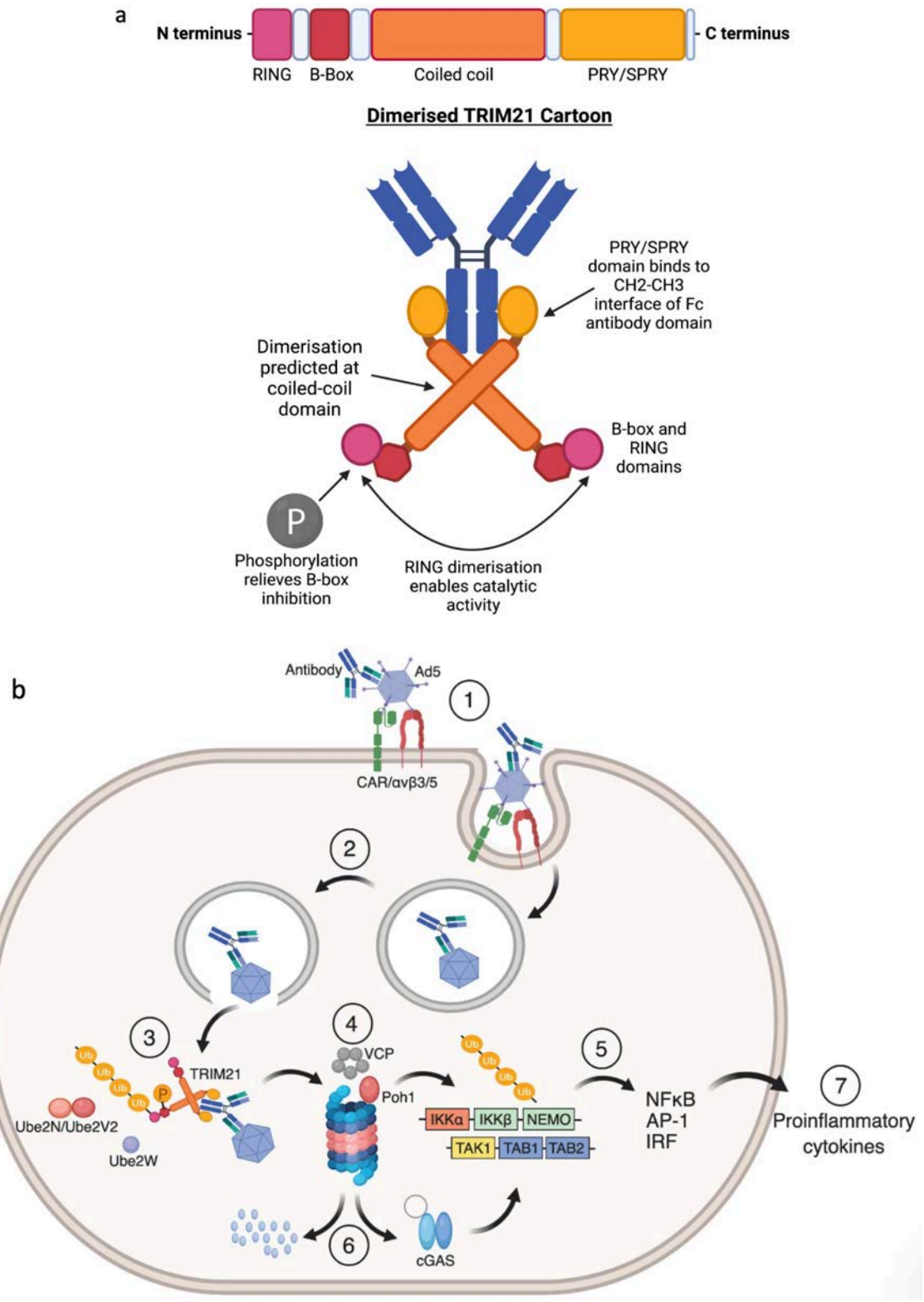

Figure 5. TRIM21 structure and Mechanism of TRIM21 mediated anti-viral activity*. A) Schematic representation of the domain organization of TRIM21 and cartoon representation of dimerised TRIM21 binding with the constant region (Fc) of an antibody. B) Mechanism of action of TRIM21 in 7 steps: (1) a virus, Adenovirus 5 in figure, engages its entry receptors at*

the cell surface, which triggers endocytosis of the virus/antibody complex and loss of fiber from the Ad5 capsid. (2) Fiber loss exposes protein VI that lyse the endosomal membrane which allows the virus/antibody complex to escape to the cytosol. (3) TRIM21 binds to the Fc part of the antibody in which auto-inhibition is released by B-box phosphorylation and undergoes auto-ubiquitination by the E2 enzymes Ube2W and Ube2N/Ube2V2. (4) This directs the Ad5/antibody complex to VCP and the proteasome for degradation. (5) Liberation of K63-linked ubiquitin chains by Poh1 activates IKKα-IKKβ-NEMO and TAK-TAB1-TAB2 which in turn induces NF-κB, AP-1 and IRFs resulting in the production of pro-inflammatory cytokines and in an anti-viral state. (6) Exposed viral genomes trigger a second wave of immune signaling via the cytosolic DNA sensor cGAS. (from (Foss et al., 2019))

3. Trim69

TRIM69, also known as RNF36 (ring finger protein 36; or Trif) was initially isolated from a rat testis library by Ogawa and colleagues in 1998 utilizing the polymerase chain reaction with degenerate primers to amplify novel TRIM family members (Ogawa et al., 1998). Subsequently, the human TRIM69 gene (hTRIM69) was identified (GenBank:No.AY305385) on the basis of its differential expression between a library of human round spermatid-specific cDNA and one of human primary spermatocytes (G. Liang et al., 2004; X. Zhang et al., 2003). As such, the initial reports suggested that TRIM69 could be important in spermatogenesis. hTRIM69 maps to chromosome 15q21 and consists of eight exons and seven introns. It belongs to the C-IV subfamily of the TRIM family and also contains the common characteristic features of the family: a RING finger domain with an E3 ubiquitin ligase activity; two B-boxes domain, a Coiled-coil domain, and a PRY-SPRY domain (**Figure 6**).

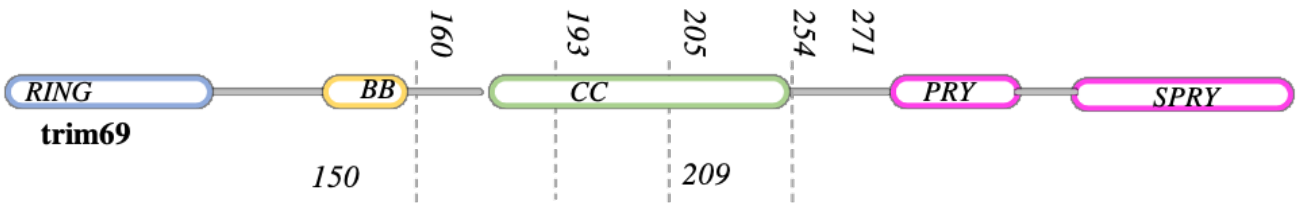

Figure 6. A schematic presentation of the structure of TRIM69. *The domain structure of TRIM69 molecule is composed by RBCC motif (a RING domain with an E3 ubiquitin ligase activity, two B-boxes and coil-coiled domain) and PRY-SPRY in the C-terminal.*

TRIM69 has been the subject of few studies overall and has been associated or reported to participate to various biological processes, such as cell growth, apoptosis, differentiation,

innate immune responses, and cancer development, but most of these studies were only associative (Cambiaghi et al., 2012). In one study, TRIM69 was known mostly for its role in zebrafish brain development (Han et al., 2016), by regulating in an unclear manner p53-dependent apoptosis.

Overall, not much was known about this protein. The first report of antiviral activity of TRIM69 was published in 2018 in a study in which this protein was identified as an antiviral factor against Dengue Virus infection (DENV) (K. Wang et al., 2018). In this study, TRIM69 was shown to directly interact with the non-structural protein 3 (NS3) and to promote its polyubiquitination and degradation. In light of the effects of NS3 in DENV replication, this degradative action was of high interest. In 2019, one study contradicted however the antiviral role of TRIM69 against DENGUE virus, but reported alongside a second report, an antiviral role against the Vesicular Stomatitis Virus (VSV) a negative-strand RNA virus of the *Rhabdoviridae* family, genus Vesiculovirus.

In these studies, the exact mechanism of action of TRIM69 was not identified although one of the two indicated a block in pioneer transcription (see below). Whether the E3-ubiquitin ligase activity of Trim69 was required as well as the intracellular distribution of this protein remains to be clearly defined. Of interest however, both studies reported that resistance to TRIM69 arouse spontaneously in cell culture through the accumulation of a mutation in the phosphoprotein P (Kueck et al., 2019; Rihn et al., 2019). As we will explain more in detail below, the P protein plays numerous roles in the life cycle of VSV and of *Rhabdoviridae* in general. How a single point mutation in the P protein allows the virus to escape the antiviral effects of

TRIM69 as well as how TRIM69 interferes with VSV replication and also whether it acts on other viruses were currently unknown questions that my thesis work attempted to address.

4. An introduction to Retroviruses and RNA viruses

What follows is a brief and schematic description of the key steps of the viral life cycle of the three viruses examined in my study.

4.1 The human immunodeficiency virus type 1 (HIV-1) and primate lentiviruses

HIV-1 was identified as the causative agent for the Acquired Immunodeficiency Syndrome (AIDS) in 1983 (Barré-Sinoussi et al., 1983; Gallo et al., 1984; Levy et al., 1985). HIV-1 belongs to the *Retroviridae* family and to the *Lentivirus* genus. Together with the human T cell leukemia virus (HTLV-1 and 2) and with HIV-2 it is the only retrovirus to infect humans to date. The human population is currently infected by HIV-1 which is the causative agent of AIDS worldwide, as well as in a much minor proportion by a close relative, HIV-2, which is essentially restricted to some regions of Western and Central Africa and is much less pathogenic. HIV-1 infection results in a chronic exhaustion/depletion of CD4 T cells that are the main targets of the virus replication and that lead to the collapse of immune system functions, exposing the organism to secondary infections that are fatal. The availability of virus specific drugs directed against the virus enzymes (reverse transcriptase, protease and integrase) has completely reshaped the disease so that in developed countries and with a prompt detection and treatment, infected individuals can carry out a normal life and keep the virus under control.

1) Structure of the HIV-1 genome

The genome of HIV-1 follows a typical organization of retroviruses in that it has a length of approximately 9.8 kb, it is flanked by two long terminal repeats (LTRs) and bears three large open reading frames: Gag, Pol and Env. In addition however, the genome of HIV-1 codes for several non-structural proteins absent in other retroviruses and playing key roles in pathogenesis: Tat and Rev that acts at the transcriptional and mRNA export phase; Nef, Vpu and Vpr that play different roles in viral replication (Frankel & Young, 1998) (**Figure 7a**).

The structural proteins Gag, Pol and Env are translated as large polyprotein precursors (either Gag, Gag-Pol fusion and Env) that are further processed by the viral protease (PR for Gag and Gag-Pol) or by the cellular furin in the case of Env. Specifically, Gag (p55) is processed to p17 (Matrix), p24 (Capsid), p7 (NucleoCapsid) and p6 proteins; Pol is processed to p10 (Protease), p66/p51 (Reverse Transcriptase), and p31 (Integrase). Envelope is translated as a single precursor (gp160) that is then processed in the ER-Golgi in gp120 (the external part of the Envelope protein) and the transmembrane gp41. After assembly at the plasma membrane, virion particles are released in the extracellular milieu where the process of maturation (the complete proteolytic digestion of Gag and Gag-Pol operated by the viral Protease) results in an infectious virion particle. In this particle the viral RNA is contained within a structure called the viral core or the viral capsid, composed by the viral protein CA (**Figure 7b**). Given that their role is not at play in my work, the role of viral non-structural proteins will not be detailed in this manuscript.

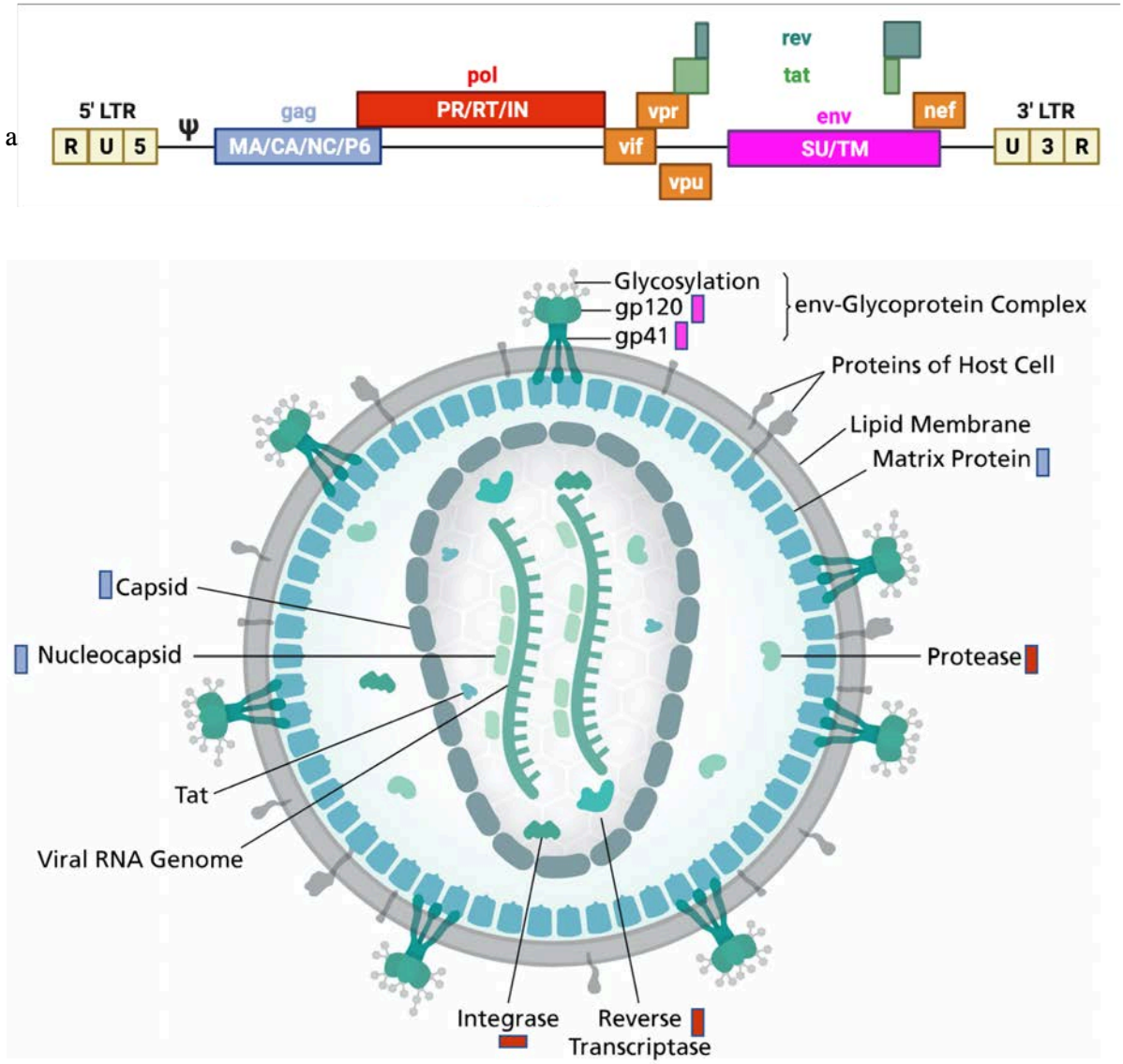

Figure 7. Arrangement of the HIV genome and virion particle's structure. a) *The viral RNA genome is flanked by two long terminal repeats and codes for the three large open reading frames common to all retroviruses Gag, Pol and Env, in addition to a number of non-structural proteins that play a role in virus pathogenesis.* ***b)*** *The mature virion particle derives its membrane from the plasma membrane of the host cell in which envelope glycoproteins trimers are embedded. The inner layer of the membrane anchors the Gag-derived MA proteins. The capsid is found at the center of the virion in the form of an icosahedrical capsid that contains the two copies of gRNA, NC, p6, RT, IN plus Vpr (from* (Frankel & Young, 1998).

2) The life cycle of HIV-1

i. Early phases of the viral life cycle (from entry to integration)

Cell entry begins with the binding of the viral gp120 to the CD4 receptor and to the chemokine coreceptors CCR5 or CXCR4 (**Figure 8**). Following binding, a conformational change in gp41 allow the viral membrane to fuse with the cellular one, leading to the entry of the viral capsid inside the cell cytoplasm. In the case of HIV, cell fusion takes place at the plasma membrane although a productive virus entry endosomal pathway has also been described (Permanyer et al., 2010).

What happens to viral cores inside the cell remain highly debated. Viral cores are complexes of the viral CA, viral enzymes required for the reverse transcription and integration of the viral genome, the viral nucleocapsid chaperone protein (NC) and of course the viral genome. This complex must travel from the entry point to the nucleus, must reverse transcribe the viral RNA into double-stranded DNA and must pass through the nuclear pore for integration to occur. In the meantime, this complex should also evade sensing and recognition by cellular defenses. The classical view proposed that upon entry, the viral core shed part of CA to allow both transport and reverse transcription (Campbell & Hope, 2015; Yamashita & Engelman, 2017). However, this view has been challenged over the years by evidence indicating that CA can reach the nucleus and influence integration, and that intact or semi-intact capsids could be visualized inside the nucleus (Beck & Hurt, 2017; Campbell & Hope, 2015; Lusic & Siliciano, 2017; Wilbourne & Zhang, 2021; Yamashita & Engelman, 2017). These notions are important because according to its conformation, viral nucleoprotein complexes may be more or less apt to bind to specific factors or to be transported, all questions pertinent here. Indeed, the viral core of HIV-1 and CA in particular is bound to a number of co-factors that allow it to perform efficient infection: Cyclophilin A (that masks CA from recognition of the restriction factor

TRIM5a), CPSF6 and Nup358 that are required to dock the capsids at the nuclear pore etc (Malim & Bieniasz, 2012; Wilbourne & Zhang, 2021) (**Figure 8**).

ii. Late phases of the viral life cycle

Once the viral DNA is integrated into the host chromatin, the viral genome is transcribed by the host transcription machinery with the help of the Tat transactivator that is required for the extension of transcripts from the viral LTR promoter. While most of the first viral RNAs are spliced leading to the production of the viral proteins Tat, Rev and Nef, the accumulation of Rev leads to the accumulation of unspliced RNAs, as a result of the binding of viral RNAs to the viral protein Rev on the Rev-responsive element (RRE) that promotes the export of single and unspliced viral mRNAs from the nucleus. Translation from viral RNA gives raise to structural polyproteins that reach the plasma membrane giving raise to novel virion particles (**Figure 8**).

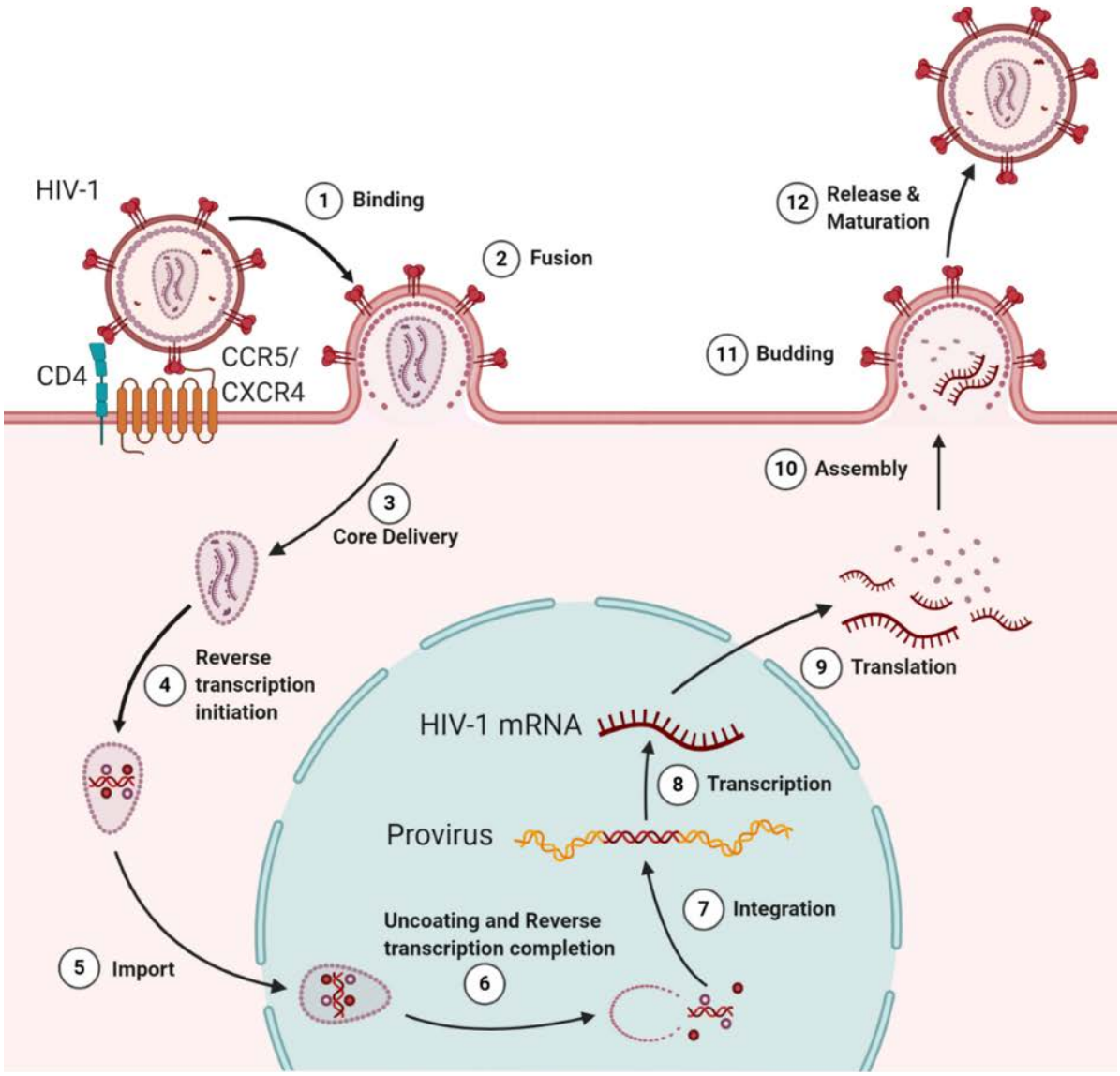

Figure 8. ***The HIV life cycle.*** *Early phases of the viral life cycle (1-7): 1. Env binds to the CD4 receptor and co-receptor (CCR5 or CXCR4) on the host cell surface. 2. Fusion of the viral and cellular membranes releases the viral core into the cytoplasm. 3. The viral core then traffics to the cell nucleus where it docks at the nuclear pore. 4-5. Reverse transcription converts the viral RNA genome into double-stranded DNA, forming the pre-integration complex (PIC) that is imported into the nucleus. 6-7. The viral genome is then integrated into the host cell chromosome. Prior to or during nuclear import, the capsid disassembles in a process termed uncoating. Late phases of the viral life cycle (8-12): 8-9. Proviral transcription yields viral RNAs that are exported to the cytoplasm for viral protein production. 10-11. Genome-length viral* RNA and viral proteins are assembled to package into virions for budding. 12.Release of virion particles and maturation (from (Ganser-Pornillos & Pornillos, 2019))

4.2 The Vesicular Stomatitis Virus (VSV)

Vesicular stomatitis virus (VSV) is an enveloped, negative-strand RNA virus that belongs to the *Vesiculovirus* genus of the *Rhabdoviridae* family. VSV is an insect-borne virus that can be transmitted by arthropods to several animals such as swine, rodents, cattle, mule and horse but can also infect humans and other species (Fultz & Holland, 1985). The early history of the VSV has been reviewed in 1952 (Hanson, 1952). Outbreaks of unidentified causes in cattle of South Africa have been described in the early 1800s and were then reported by Theiler in 1901 in horses and mules in Transvaal, South Africa. Affected animals presented increased temperature and decreased appetite, followed by marked salivation, formation and then rupture of vesicles on the gums, tongue and lips, leaving broad ulcerations. This disease was later on characterized by Oltsky (1926) and Cotton (1927) as vesicular stomatitis (VS) (reviewed in (Howatson, 1970). In endemic areas, VS outbreaks are seasonal, often associated to the transitions between the rainy and dry seasons. In cattle and pigs the symptoms are clinically similar to foot and mouth disease (FMD), animals presented high fever, marked salivation and the formation/rupture of vesicles on the gums, tongue and lips that often resulted in broad ulcerations. However, despite similar symptoms, VS, but not FMD animals undergo rapid recovery and only rarely result in the death of the animals (Hanson, 1952; Letchworth et al., 1999; Rodríguez, 2002). In humans, VSV induces very mild influenza-like symptoms.

VSV was isolated from the tongue epithelium of a cattle in Richmond, Indiana in 1925 (Cotton, 1926, reviewed in (Lichty et al., 2004). There are two major serotypes (according to their

spectrum of neutralization): New Jersey (VSNJV) was isolated in 1926 and Indiana (VSIV) was isolated in 1925 (Hanson, 1968; G. Liu et al., 2021), which represent the larger proportion of infections and additional minor serotypes include Cocal and Alagoas, as well as Piry, Isfahan and Chandipura, which identified to infect humans and domestic animals (Bhatt & Rodrigues, 1967; Tesh et al., 1977). Among them, VSIV is further sub-divided into four distinct serological complexes, Indiana 1 contains vesicular stomatitis Indiana virus (VSIV), Indiana 2 contains Cocal virus (COCV), Indiana 3 contains vesicular stomatitis Alagoas virus (VSAV), and Indiana 4 contains Morreton virus (MORV), however, these have not been shown to cause natural outbreaks in livestock (Bhatt & Rodrigues, 1967; Tesh et al., 1977).

1) Genome and virion structure

The genome of VSV is located within the internal RNP complex of the virus and consists of single-stranded, negative-sense RNA of around 11 kb flanked by a 3' 47 nucleotide leader (Le) sequence and by a 59 nucleotides trailer (Tr) at the 5' terminus ((Whelan & Wertz, 1999; Luo, 2012). The VSV RNA successively encodes the nucleoprotein (N), phospho-protein (P), matrix protein (M, involved in virus assembly and budding), glycoprotein (G, widely used for pseudotyping in light of its broad cellular tropism), and the RNA-dependent RNA polymerase (L). The N, P and L proteins are associated with the RNA molecule and compose the transcriptionally active nucleocapsid (NC). The NC is enveloped by a lipid bilayer which is derived from the host cell plasma membrane and which is acquired during the budding process. G is a transmembrane glycoprotein that is involved in virus entry (Beilstein et al.,

2015). Most of the M protein is located beneath the viral membrane and bridges the NC and the lipid bilayer (**Figure 9**).

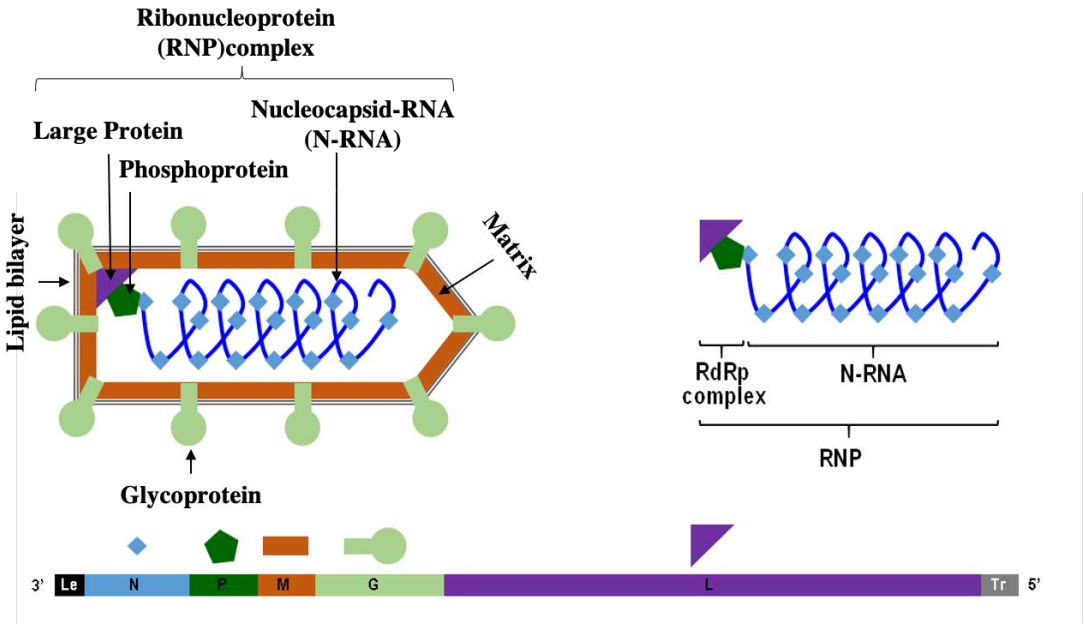

Figure 9. Genome composition and virion structure of VSV. *A diagram of the characteristically bullet-shaped virion is shown above as a representation of the VSV genome. The negative-sense, single-stranded RNA genome (depicted in blue within the virion) is completely covered by the nucleoprotein (N), which, together with the phosphoprotein (P) and the RNA-dependent RNA polymerase (L), forms the viral ribonucleoprotein complex (RNP). The matrix protein (M) condenses the nucleocapsid and drives virion budding. The glycoprotein (G) decorates the surface of the virion. The VSV genome is arranged in the order 3'-(leader), N, P, M, G, L, (trailer)-5'.*

The five viral proteins are assembled into a characteristically bullet-shaped virus particle, 180 nm in length and 75 nm in diameter that acquires a plasma membrane envelope in which the viral glycoprotein G is inserted (Lichty et al., 2004). Within the virion particle, the viral RNA is completely coated with the viral nucleoprotein (N) that condenses the RNA in a helical N-RNA

complex (Barr et al., 2002). The P protein bridges interactions between N-RNA and the RdRp large L proteins (Green & Luo, 2009) to form the ribonucleoprotein (RNP) (**Figure 9**). In addition, VSNJV and VSIV both encode two additional non-structural proteins, known as C and C', initiating from downstream start codons in the P gene although the very existence of these alternative open-reading frames has not been fully clarified (Peluso et al., 1996; Spiropoulou & Nichol, 1993)

N Protein

The X-ray crystallography showed the atomic structures of the N-proteins of VSV in complex with RNA (Green et al., 2006). Complexes contain 10 N-protein monomers in which each N-protein is associated with 9 nucleotides of the RNA. N-RNA interactions are mainly coordinated by basic amino acid side chains that interact with the RNA's phosphate groups, including the corresponding six residues for VSV, Arg143, Arg146, Lys155, Lys286, Arg317 and Arg408 (Luo et al., 2007). Higher-order complexes are stabilized by an N- and a C-terminally protruding extension, which interact with the neighboring N-protein monomers to form a circular assembly (Luo et al., 2007). N-protein is thus essential for RNP formation and is an essential factor during replication and transcription (Riedel et al., 2020).

P Protein

The VSV P protein is 265 amino acids, usually presented as a dimer with a non-globular molecule containing structured domains separated by disordered regions (Ding et al., 2006;

Gerard et al., 2007; Green & Luo, 2009; Jamin & Yabukarski, 2017). The P protein carries out multiple functions during transcription and replication of the VSV genome, such as bridging the L protein and the N–RNA template (Mellon & Emerson, 1978), stimulating RNA synthesis from the L polymerase at both the initiation and elongation steps (De & Banerjee, 1984; Emerson & Yu, 1975; Morin et al., 2012; Ogino & Green, 2019), and chaperoning the N protein to replication complexes within the cell ((Masters & Banerjee, 1988; Peluso, 1988).

M Protein

The VSV M protein is a 229 amino acid small protein (26.6 kDa) present in around 1,800 molecules per virion (McCreedy & Lyles, 1989). It is composed of a positively charged N-terminal part, which has eight lysine residues in the first 20 residues (Gaudier, 2002) important for membrane docking. In addition, the flexible amino-terminal part of VSV M contains two motifs, ^{24}PPPY^{27} and ^{37}PSAP^{40}, that constitute potential late domains, which are found in the proteins of many enveloped viruses and have the ability to recruit cellular partners that are involved in the ultimate step of the budding process (Raux et al., 2010). M proteins play a major role in assembly and budding processes (Mebatsion et al., 1999). In the cell, M proteins can be found mainly in the cytoplasm (80%), the plasma membrane (10 to 20%) (Ye et al., 1994) and the nucleus and have been described to inhibit cellular transcription, by interacting with the RNA polymerase II TFIID complex (Ahmed & Lyles, 1998; Flood et al., 2000). Furthermore, P has been shown to interfere with nucleocytoplasmic transport of host mRNAs (Glodowski et al., 2002; Gustin, 2003; Petersen et al., 2000) by interacting with NUP98, and also to inhibit cellular translation by modifying the initiation complex eIF4F through

dephosphorylation of the initiation factors eIF4E and 4E-BP1 (Connor & Lyles, 2002). Finally, it was also shown to participate in apoptosis induction (Desforges et al., 2002)

G Protein

VSV-G is a class III virus fusion protein (A. A. Albertini et al., 2012). Its structure consists four domains: a β-sheet lateral domain, a central trimerization domain, a pleckstrin homology domain (PH domain), and a fusion domain containing two very short FLs positioned at the tip of a three-stranded β-sheet (Roche et al., 2006, 2007). VSV G is responsible for attachment to the cellular receptor and for entry into the cell. In light of its large tropism, the G protein is often used to drive fusion of different viral particles (including HIV-1 particles) in a large spectrum of cells. As the pH drops in early endosomes, G changes conformation to allow fusion between the viral envelope and the endosomal membrane releasing the viral content in the cell cytoplasm, where RNA replication starts (Roche et al., 2006, 2007)). Interactions between the G and M proteins have also been shown to increase budding efficiency (Swinteck & Lyles, 2008). Apart from roles in fusion and particle assembly, G has been shown to also participate in cytotoxicity (Hoffmann et al., 2010).

L Protein

VSV L protein is the viral RNA polymerase and it consists of an N-terminal ring-like structure and a flexible C-terminal appendage containing three globular domains (called CRs or blocks I–VI) (Poch et al., 1990; B. Liang et al., 2015). This enzyme contains also a 2’-O-MTase activity important for RNA synthesis (Sleat & Banerjee, 1993) and cap formation (Grdzelishvili et al.,

2005). The P protein as well as its N-terminal fragment was found to induce large conformational changes in the L protein and to be important for viral synthesis (Jenni et al., 2020; Rahmeh et al., 2010).

2) Life cycle

After binding to its receptor(s), the VSV virus enters the cell via the endocytic pathway (Cureton et al., 2009). The acidic pH (≤6.3) environment within early endosomes triggers conformational rearrangements in G protein that in turn drive viral-cellular membranes fusion and lead to the cytoplasmic release of the viral RNP (Baquero et al., 2015; White & Rock, 1981), constitutes the template for transcription of viral genes and the viral RNA polymerase (the L-P complex) is responsible for replication of the viral genome, the viral replication machinery takes place in specialized compartment or cytoplasmic inclusions (Heinrich et al., 2010) also known as viral inclusion Bodies (IBs). IBs concentrate N, P and L proteins and appear place of privileged viral replication (Dolnik et al., 2021; Heinrich et al., 2010, 2018). In Rhabies virus belonging to the same family as VSV but to the genus *Lyssavirus*, similar structures, or Negri bodies, appear very large within the cytoplasm and present features of liquid-liquid phase-separation in which viral material appear protected from the surrounding environment and possibly detection by cytosolic pattern recognition receptors (Nikolic et al., 2017). During transcription, a positive-stranded leader RNA, uncapped and non-polyadenylated, and five capped and polyadenylated mRNAs encoding the five viral proteins are synthesized from a single promoter at the 3’ end of the genome according to a pause-reinitiation mode regulated by specific sequences that flank each gene (of 23 nucleotides of length) (Rodrigues et al., 2002).

At a later stage of infection, the polymerase switches to replication of the viral genome, which yields nucleocapsids containing the full-length antigenome (sense) RNA, which in turn serves as template for the synthesis of the (antisense) RNA genome. During their synthesis, both the nascent-antigenome and the genome are bound by the N protein. Specific transfer of the N protein to viral RNAs rather than to the cellular mRNAs is mediated by the P protein, which acts as a chaperone by binding the N alone (N°) (Blondel et al., 2015). The neo-synthesized genomic RNPs then serve either as template for additional rounds of transcription and/or replication, or are transported to the cell membrane where they are assembled with the M and G proteins into virions. According to this replicative mode, RNAs and corresponding viral proteins are produced in a gradient-wise manner: N > P > M > G > L (Banerjee, 1987; Iverson & Rose, 1981) and then release from the cell through the budding process (**Figure 10**).

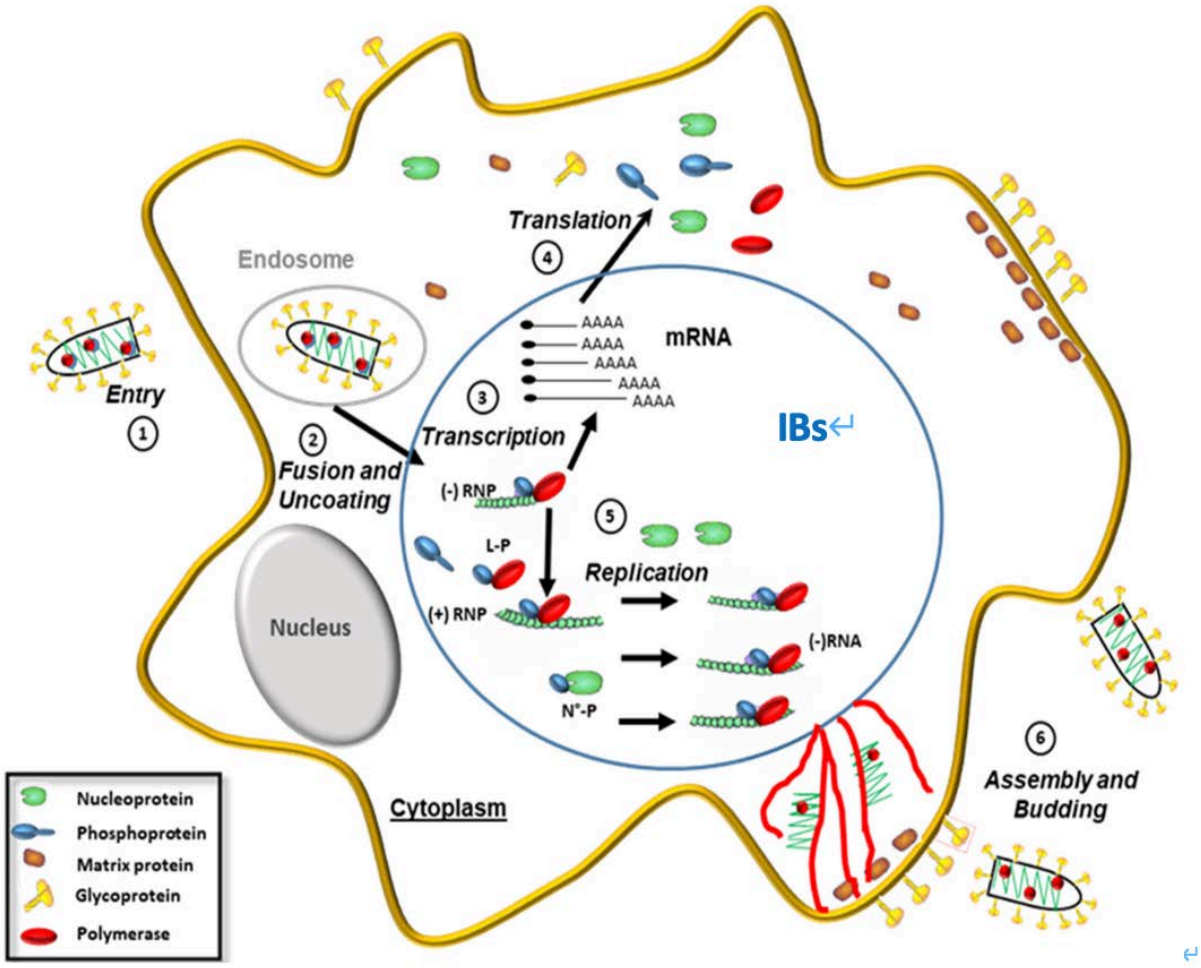

Figure 10. A schematic representation of the life cycle of VSV. *In the cytoplasm:1. entry phase involving the binding of viral particles to receptors. 2. Endocytosis followed by membrane fusion and RNPs release in the cytosol. 3. Transcription of viral mRNA. 4. Translation of viral mRNAs by the cell machinery. 5. Replication of the viral genome and 6. transport of viral RNP by microtubules to membrane virus assembly and progeny virus budding. Viral transcription and replication occur in viral replication compartments (IBs), which are phase-separated liquid compartments. (adopt from* (Asmi et al., 2018; Blondel et al., 2015)*)*

(1) Attachment, Entry, and Uncoating

Attachment of VSV to host cells is mediated by the glycoprotein which binds to the surface of cells. Due to VSV has a wide host spectrum suggested that VSV enters cells through highly

ubiquitous receptors. At first, phosphatidylserine (PS) has been proposed to be a VSV receptor (Schlegel et al., 1983), but was dispute due to PS is only present at the surface of apoptotic cells. However, by correlation and an excess of annexin V, which binds specifically and tightly to PS demonstrated that PS is not a receptor for VSV (Coil & Miller, 2004). Cells without gp96 or with catalytically inactive gp96 do not bind VSV G suggested the endoplasmic reticulum chaperone gp96 is essential for VSV infection and functional VSV G receptor at the cell surface, which most likely because it facilitates the correct folding of either a protein receptor or an enzyme required for the synthesis of a glycolipid receptor (Bloor et al., 2010). Furthermore, it is also demonstrated that gp96-deficient cells present obviously decrease in cell surface expression of four members of the extended LDL receptor family (LDL-R, LRP6, Sorl1 and LRP8) in gp96-deficient cells. Recently, other receptors of VSV have been identified, they are the members of the low-density lipoproteins receptor (LDL-R) family (Finkelshtein et al., 2013), which can only bind to VSV G by recombinant soluble CR2 and CR3 domains of LDL-R (Nikolic et al., 2018). In addition, a new cellular protein, leucine-rich repeat-containing G protein-coupled receptor 4 (Lgr4) is important for VSV infection (N. Zhang et al., 2017) but this still was dubious (Belot et al., 2019).

Following attachment to the cell, VSV uses clathrin-mediated endocytosis (CME) to enter the host cell (Cureton et al., 2009; Johannsdottir et al., 2009; Sun et al., 2005), which was shown to be dependent on dynamin (dynamin-2) pathway (Johannsdottir et al., 2009) or actin pathway. Since the average size of VSV (200 nm long) is significantly larger than the dimensions of typical clathrin-coated pits, the vesicles used for clathrin-mediated endocytosis

(CME) of VSV are not fully coated with clathrin and require actin polymerization for efficient internalization, but not for smaller VSV particles, such as the defective interfering (DI-T) particles (75 nm long) (Cureton et al., 2009, 2010).

VSV "*uncoating"* involves low pH trigger conformational changes in G protein, exposes the hydrophobic fusion loop, to induce fusion of viral envelope with endosomal membranes (Belot et al., 2019) and release of viral RNPs into the cell cytoplasm (Le Blanc et al., 2005; A. A. V. Albertini et al., 2012). This release appear dependent on the presence of the lysobisphosphatidic acid lipid (LBPA), which is only found in late endosomes and appears facilitated also by ALG-2-interacting protein 1 (AIP1/ALIX) and phosphatidylinositol-3-phosphate (Belot et al., 2019). Upon membrane fusion, the M protein dissociates from the nucleocapsid to permit transcription and replication to occur in the cell cytoplasm (G. Liu et al., 2021; Mire et al., 2010).

(2) Replication and Synthesis

VSV transcription and replication follow the membrane fusion event and are driven by the viral polymerase complex comprised of L (RdRp), N and P (Banerjee & Barik, 1992; Knudson, 1973). The RNP serves as template for viral RNA synthesis that starts with primary viral transcription accomplished by the incorporated viral polymerase complex (Moyer et al., 1986). The first step is primary transcription of the initial viral genome, mRNA synthesis starts at the 3'-end of the genomic and results in short, uncapped leader RNAs and 5'-capped, 3'-polyadenylated mRNAs, each of these reactions occurring co-transcriptionally. Viral mRNAs

are subsequently translated by host cellular machinery, and the accumulation of viral proteins, following a start-stop mechanism regulated by highly conserved gene start and gene end sequences located in UTRs and polyadenylation of the viral mRNAs by the viral polymerase slows down transcription at the gene ends that result in dissociation of the RdRp from the template to a descending gradient of viral mRNAs from the first (N) to the last (L) gene (N > P > M > G > L. N is thought to trigger the polymerase's switch from transcription to the 3' leader of the negative-sense genome and produces a complementary, positive-sense RNA molecule known as the anti-genome, which is immediately coated by N and subsequently serves as the template for the production of more genome (G. Liu et al., 2021) (**Figure 11**).

Newly synthesized genomes also serve as templates for the secondary transcription of viral genes, which, in combination with continued replication, results in the major amplification step of the replication cycle. Eventually, viral nucleoprotein complexes are condensed via interactions with M protein, which also drive budding of nascent virions from the plasma membrane at sites that are enriched with G protein (G. Liu et al., 2021; Lyles, 2013).

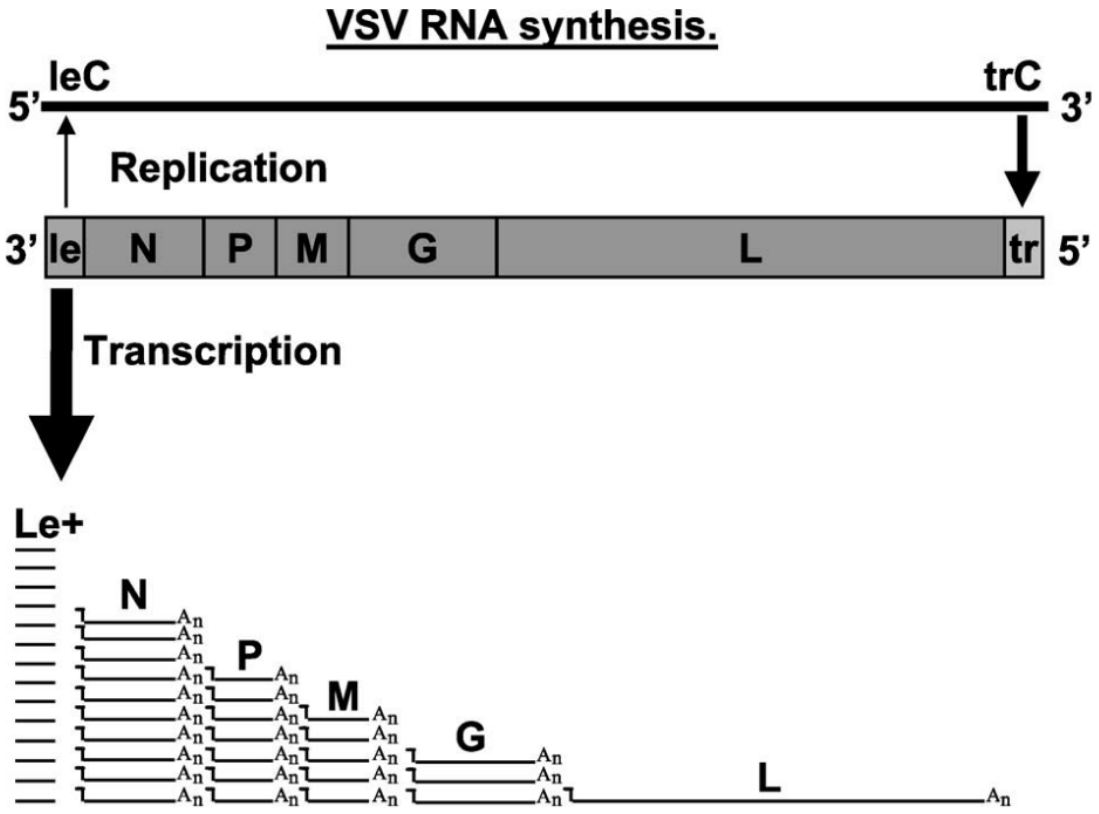

Figure 11. VSV genome organization and the products of VSV transcription and replication. *3'to 5'are the 3'50-nt leader region (le), and the genes encoding protein: the nucleocapsid protein (N), phosphoprotein (P), matrix protein (M), glycoprotein (G) and RNA-dependent RNA polymerase (L), respectively, followed by the 5' trailer region (tr). The products of transcription, the leader (Le+) and the five capped and polyadenylated monocistronic mRNA are indicated diagrammatically below the genome in their relative, respective, transcriptional abundance. The full-length antigenomic positive-strand RNA product of genomic replication is shown above the template. This positive strand antigenome subsequently serves as the template for abundant negative-sense genome synthesis. The ends of the positive strand are labeled, leC = complement of the genomic leader region, trC =complement of the genomic trailer region.*

(3) Assembly and Budding

VSV assembly occurs at the plasma membrane and is mediated by the viral M and G proteins. VSV RNA and the individual proteins are transported to the plasma membrane via different routes. The G protein is synthesized via the ER-Golgi secretory pathway, where it is glycosylated and finally transported to the plasma membrane (Moyer et al., 1986; Wilusz et al., 1983). Instead, VSV M is transported in an unclear manner in sites of assembly

independently of the G protein (Scales et al., 1997). The viral RNA-protein complex is assembled in the cytoplasm and transported to the plasma membrane in a microtubule dependent manner (Whitlow et al., 2008) where it associates with M protein (Loh et al., 2005).

After assembly, virus budding and release still depend on the function of the M protein and its cellular interacting partners. A PPxY motif present in the M protein interacts with the corresponding WW (tryptophan) domains of certain cellular partners promoting budding (for ex, the Yes-kinase associated protein (YAP) ((Swinteck & Lyles, 2008; T. Zhang et al., 1999). M protein interacts with dynamin1 and 2 also promotes viral assembly and budding (Flood & Lyles, 1999; Lyles, 2013).

4.3 The Severe Acute Respiratory Syndrome Coronavirus 2 (SARS-COV-2)

This virus is one of the latest of a large family of RNA viruses that normally cause mild flu-like symptoms in humans. The consequences of SARS-CoV2 infection are instead much more dramatic as it can be observed over the past couple of years. Coronaviruses are positive-strand RNA viruses that belong to the order of Nidovirales (family *Coronaviridae*). Within this family are four genera: the *alpha*, the *beta*, the *gamma* and the *delta* coronaviruses. Collectively Coronaviruses have a large spectrum of hosts and can infect all mammals and avian species.

1) Genome and virion structure

Their genome is one of the largest RNA viral genomes spanning a length of around 30kb, including two noncoding regions at both ends (W. Lu et al., 2020). Approximately two thirds of the 5'end of the SARS-CoV-2 genome encodes two overlapping polyproteins: pp1a and pp1ab, which are digested by two viral proteases into 16 non-structural proteins (NSPs) and are essential for viral replication and transcription (M.-Y. Wang et al., 2020).

Four ORFs at the 3'terminus of the viral genome code a canonical set of structural proteins that include the nucleocapsid (N), spike (S) protein, membrane (M) protein and envelope (E) protein, which are responsible for virion assembly and also participate in suppression of the host immune response. Between these structural genes, there are multiple accessory genes (ORF3a, ORF3b, ORF6, ORF7a, ORF7b, ORF8b, ORF9b, ORF10), involved in regulating viral infection and enhance its virulence (**Figure 12**).

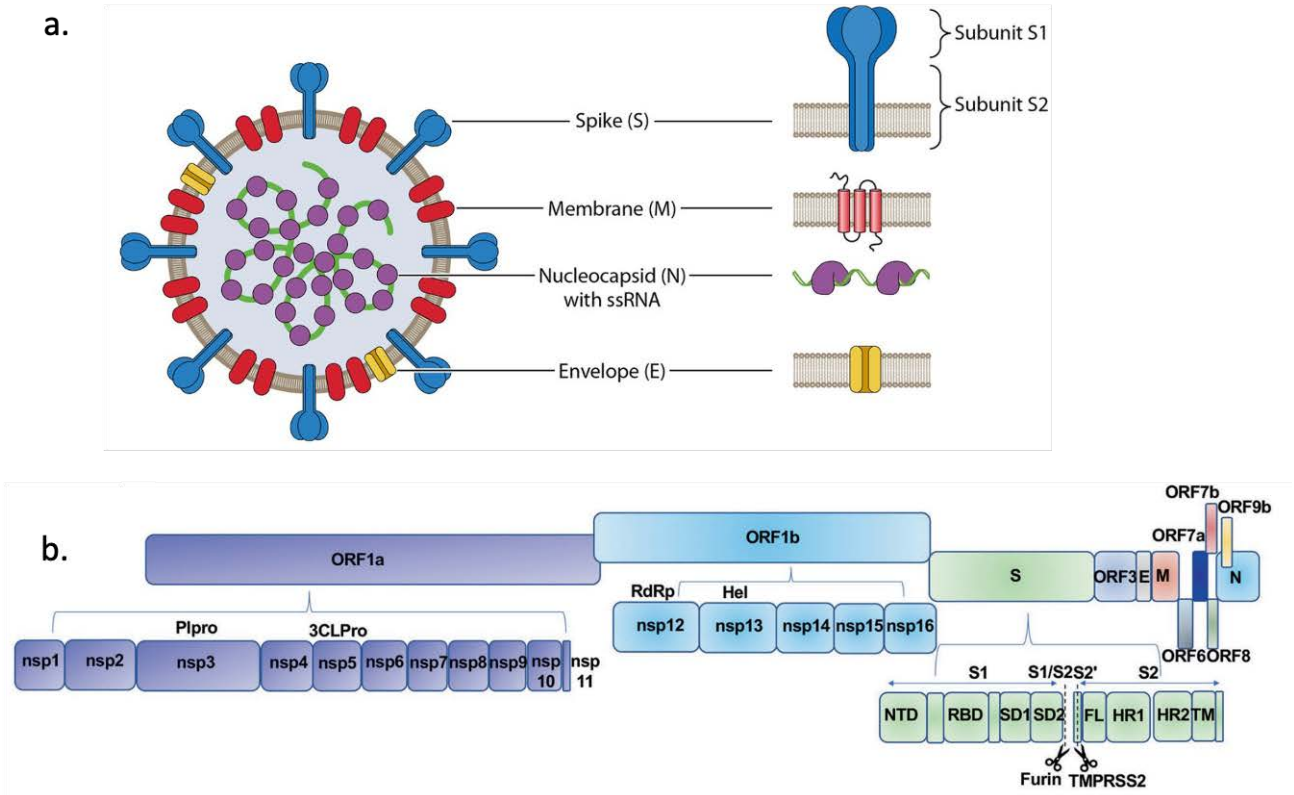

Figure 12. Schematic diagrams of the SARS-CoV-2 virion and genome*. a. Four structural proteins of SARS-CoV-2 include Spike protein (S), Membrane protein (M), Nucleocapsid protein (N), and Envelope protein (E). b. The genome includes ORF1a-ORF1b-S-ORF3-E-M-ORF6-ORF7 (7a and 7b)-ORF8-ORF9b-N in order. Sixteen nonstructural proteins (nsp1–11, 12–16) are encoded by ORF1a and ORF1b, respectively, and six accessory proteins were delineated. Plpro papain like protease, 3CLPro 3C-like proteinase, RdRp RNA-dependent RNA polymerase, Hel Helicase, S encodes NTD N-terminal domain, RBD receptor-binding domain, SD1 subdomain 1, SD2 subdomain 2, FL fusion loop, HR1 heptad repeat 1, HR2 heptad repeat 2, TM transmembrane domain. Dotted line indicates S1/S2 and S2' site cleavage by Furin and TMPRSS (from* (Synowiec et al., 2021)

S protein

The S proteins are homotrimeric class I fusion glycoproteins that are composed of two distinct functionally subunits: an N-terminal half (S1) and a C-terminal half (S2) (Walls et al., 2020), mediating attachment of the virus to host cell surface receptors and promoting subsequent fusion between the viral and host cell membranes to facilitate viral entry into the host cell (V'kovski et al., 2021). The surface-exposed S1 contains the receptor-binding domain (RBD) that specifically binds to the angiotensin-converting enzyme 2 receptor (ACE2) to enter target cells (Yan et al., 2020). The transmembrane S2 domain anchors the entire glycoprotein at the viral membrane surface and contains the fusion peptide, which mediates the fusion between the viral and the cellular membranes upon extensive conformational rearrangements (Arya et al., 2021).

M and E proteins

The membrane (M) protein is a type III glycoprotein, also identified as a negative regulator of the innate immune response because of its interaction with a common adaptor protein, MAVS (Norris & Ovádi, 2021). M also interacts with other structural viral proteins and plays a central organizing role in virion assembly as it directs the shape of envelope formation (de Haan et al., 2000) and provides the matrix to which the nucleocapsid can attach for budding (Neuman et al., 2011). Instead the envelope (E) protein is the shortest structural protein and it encodes a single α-helical transmembrane domain (Parthasarathy et al., 2008) that can self-assemble on membranes to form homopentamericion channels, that change the ion permeability of cellular membranes (Verdiá-Báguena et al., 2012). E proteins are mainly located in the ER-Golgi intermediate compartment (Liao et al., 2006) and are expressed abundantly inside

infected cells during the replication cycle. Only a small fraction of the E protein present within a cell is incorporated into the virion envelope (Abdelmageed et al., 2020).

N protein

The Nucleocapsid (N) protein is the main structural protein inside the virion and contains three intrinsically disordered regions (the N-arm, central linker region and C-tail) and two structural domains: the N-terminal domain (Drouin et al., 2021; Kirtipal et al., 2020) and the C-terminal domain (Zinzula et al., 2021). The N-NTD adopts a monomeric structure and works in RNA binding, while the CTD (N-CTD) exists as a dimer. The primary function of the N protein is to bind to the RNA genome to constitute the nucleocapsid complex essential for both viral RNA transcription as well as amplification. The N protein also plays a central role in antagonizing host immune responses (X. Lu et al., 2011).

2) The life cycle of SARS-CoV-2

The viral life cycle begins with the virus entry into the cell via endosomes via the attachment to the ACE2 receptor. Following the conformational changes of the S protein, the viral nucleoprotein complexes are released in the cell cytoplasm after viral to cellular membrane fusion (Shang et al., 2020). Subsequently, host ribosomes are hijacked to directly translate the positive-strand RNA genome in the two viral replicase polyproteins (pp1a and pp1ab), which are then processed into 16 mature non-structural proteins (NSPs) that assemble into replication–transcription complexes (RTCs) by the two viral coded proteases: the main protease (Mpro) and the papain-like protease (PLpro). These NSPs, among which is the viral

RNA polymerase then assemble to mediate viral RNA replication. The RTCs produce new gRNAs can be translate to yield additional non-structural proteins, serve as a template for further RNA synthesis or be packaged into new virions and a set of sub-genomic mRNAs (sg-mRNAs) that include open reading frames (ORFs) 2–9b, which encode the structural proteins, and also a number of accessory proteins, which enter the endoplasmic reticulum (ER), and the N protein attaches to the genomic RNA (+) strand to produce nucleoprotein complex. The nucleoprotein complex and the structural proteins move to the ER-Golgi intermediate compartment (ERGIC) where the virions assemble, mature, and bud off from the Golgi in the form of small vesicles. These vesicles travel to the host cell membrane where they are released into the extracellular region through exocytosis. The released virions infect a new set of cells initiate another round of infection (Jackson et al., 2022) (**Figure 13**).

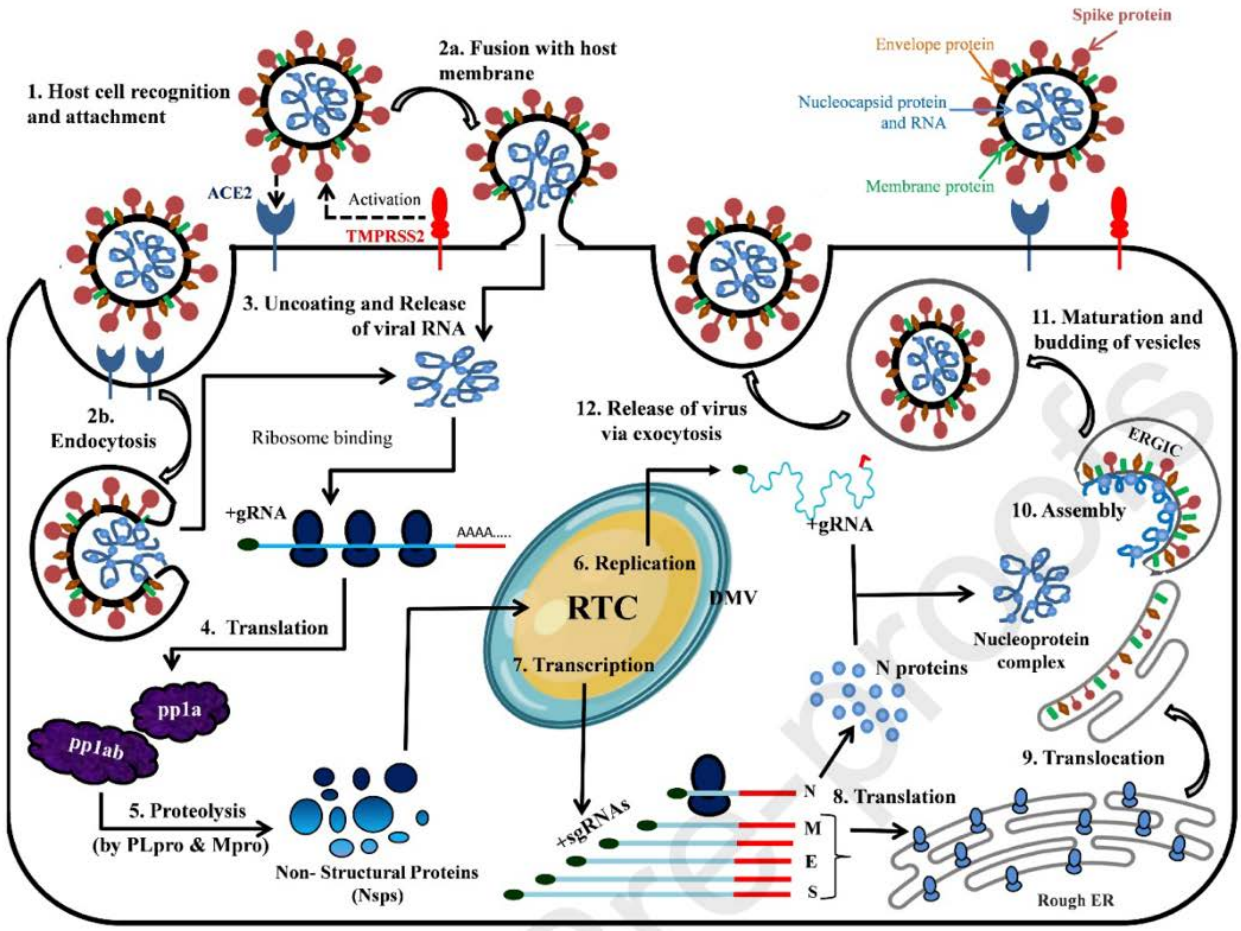

Figure 13. **The SARS-CoV- 2 life cycle.** *Step1-2: During the viral infection, SARS-CoV-2 injects its genome into the host cell via endosomes or direct fusion of the viral envelope with the host cell membrane, mediated by binding of the spike (S) protein to the human angiotensin-converting enzyme 2 (ACE2) at the cell surface. Step 3-4: the viral gRNA is uncoated and released into the host cell cytoplasm and translated by the host ribosomes. Step5: The translation products, polyproteins pp1a and pp1ab, are proteolytically cleaved into nonstructural proteins Nsp1 - 16 by the viral proteases, PLpro and Mpro. Several Nsps (Nsp2-16) along with other factors assemble together to form RTC complex inside the infected host cell. While Nsp2-11 are supposed to play a supporting role, Nsp12-16 provide the required enzymatic function for viral genome replication/transcription inside the RTC. Step6/7: The RNA (+) strand first gets replicated to the RNA (-) strand and then the negative-strand is used either for replication to the RNA (+) strand for new virion assembly or transcription of sub-genomic mRNAs. Step8: These sub-genomic mRNAs are translated to the structural proteins: S, M, E, N, and the accessory proteins. Step9-11: The S, M, and E proteins enter the endoplasmic reticulum (ER), and the N protein attaches to the genomic RNA (+) strand to produce nucleoprotein complex. The nucleoprotein complex and the structural proteins move to the ER-Golgi intermediate compartment (ERGIC) where the virions assemble, mature, and bud off from the Golgi in the form of small vesicles. Step12: These vesicles travel to the host cell membrane where they are released into the extracellular region through exocytosis. The released virions infect a new set of cells leading to disease progression (from* (Arya et al., 2021).

5. Cellular antiviral responses

Virus triggers a cellular response through the activation of pattern recognition receptors (PRRs), leading to the production and secretion of IFN and pro-inflammatory cytokines. Two major classes of PRRs are involved: Toll-like receptors (TLRs) and retinoic acid-inducible gene I (RIG-I)-like receptors (RLRs) via the recognition of pathogen-associated molecular patterns (PAMPs), result in the phosphorylate activation of the nuclear factor κB (NF-κB) and IFN regulatory factor (IRF) 3 and/or IRF7 and then induce the activity of the promoter regions of Type I IFNs and pro-inflammatory cytokines, respectively (Blondel et al., 2015), finally activate the JAK-STAT signaling pathway leading to synthesis of hundreds of interferon stimulated gene (ISG) products. Among, the RIG-I (also known as Ddx58) of RLRs has described are the major PRRs for activating an IFN response upon virus infection (Fujita et al., 2007; Kato et al., 2006; Ramos & Gale, 2011).

Although innate immune activation by RNA viruses preferentially occurs through intracellular RIG-I–like receptors (**Figure 14**), other nucleic acid recognition receptors, such as Toll-like receptors (TLRs) (**Figure 15**), play a role in finely programming the final outcome of virus infection. Among the TLR family, toll-like receptor 4 (TLR4) is at the plasma membrane as well as TLR3, TLR7 and TLR8, TLR9 in the endosomes, recognize viral RNAs or unmethylated DNA with CpG motif (Hornung et al., 2006) and transduce downstream antiviral signaling that culminates in the activation of transcription factors such as IFN regulatory factors 3 (IRF3), IRF7, IRF5 and/or nuclear factor κB (NF-κB) (Cureton et al., 2012), leading to the production of IFN and proinflammatory cytokines by the infected cells.

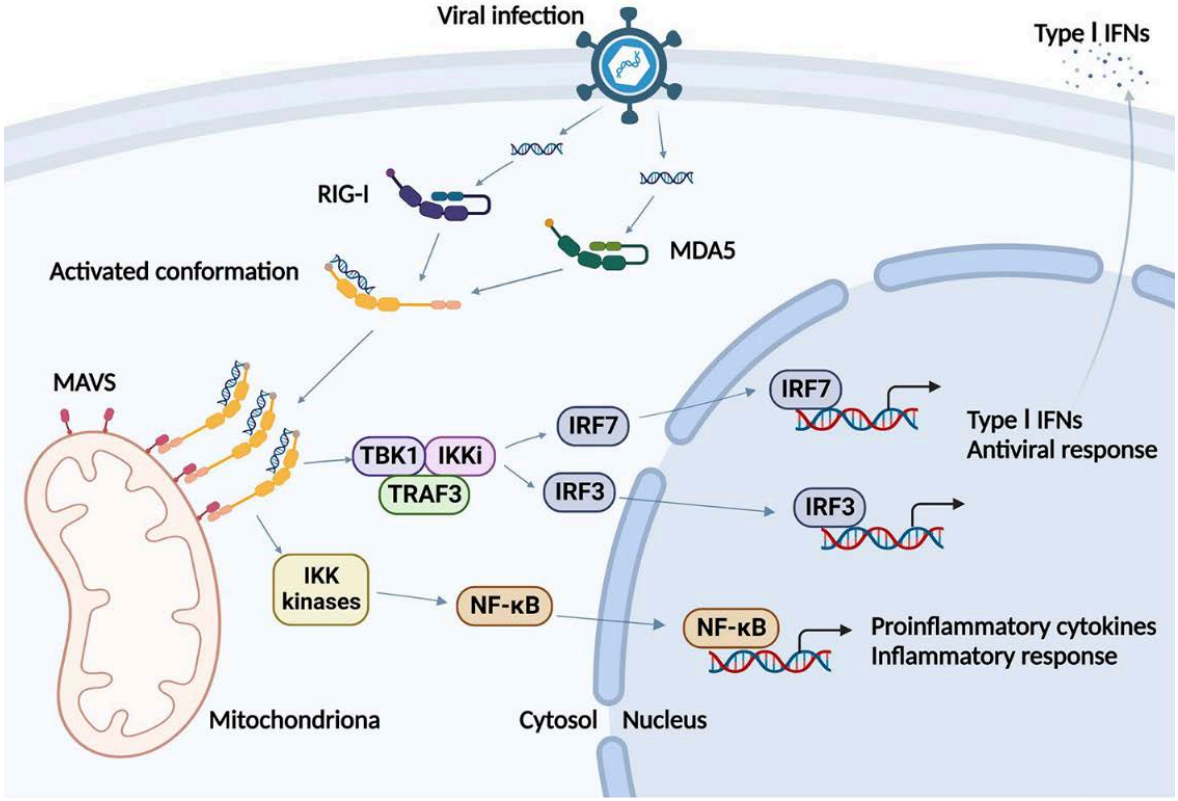

Figure 14. The signaling pathways of the RLR. *The RLR include RIG-I and MDA5 recognize dsRNA and soon convert to activated conformations. Then RIG-I and MDA5 form homopolymers and recruit MAVS, which then activate TBK1/IKK kinases to generate type I IFNs for antiviral responses and activate NF-κB to transcribe the proinflammatory cytokines for inflammatory responses. Abbreviations: RIG-I: retinoic acid-inducible gene I; MDA5: melanoma differentiation-associated protein 5; MAVS: mitochondrial antiviral-signaling protein;TBK1: TANK-binding kinase 1; IKK: I-kappa-B-kinase;IRF3/7: interferon regulatory factor 3/7; NF-κB: nuclear factor kappa-B; type I IFNs: type I interferons (from* (Song et al., 2022)*).*

PRR signaling results in production and secretion of IFN- α/β, which in autocrine or paracrine fashion, activate the JAK-STAT signaling pathway leading to synthesis of hundreds of interferon stimulated gene (ISG) products, such as Mx1 (Hastie et al., 2016; Sehgal et al., 2020).

Several other ISGs have been shown to inhibit VSV replication. This is the case of the enzyme cholesterol-25-hydroxylase, generates 25-hydroxycholesterol (25HC) which then suppresses VSV by blocking the membrane fusion step (Anderson et al., 1999; S.-Y. Liu et al., 2013). The double- stranded RNA-activated protein kinase (PKR) inhibits VSV translation (Stojdl et al., 2000) through the phosphorylation of the eukaryotic translation initiation factor 2α (eIF2α) (Krishnamoorthy et al., 2008) leading to subsequent translational shutoff (Baltzis et al., 2004; Harashima et al., 2010). Similarly, the promyelocytic leukemia (PML) protein interferes with VSV mRNA synthesis (Blondel et al., 2010) and IFITs proteins also inhibit viral translation (Schmeisser et al., 2010). The final step in the VSV life cycle, virus budding, is also inhibited by Tetherin, known antiviral factor discovered in the context of HIV. This protein blocks virion particle release from infected cells leading to retention of virion particles at the plasma membrane surface (Liberatore et al., 2017). In addition, the studies have showed autophagy plays an antiviral role in the Drosophila model for VSV via TLR-7-mediated recognition of VSV G protein stimulates the autophagy pathway (Dinh et al., 2011). During the course of our study, two papers documented an antiviral activity of Trim69 against VSV, but the underlying mechanism of inhibition was not presented. Overall, a handful of ISGs have been shown to inhibit VSV replication. On the other hand, the VSV M protein inhibits IFN induction by inhibition of host RNA synthesis and result in a block of the entire pathway (Ahmed et al., 2003; Marquis et al., 2020). As such the relationship between IFN, ISGs and viral replication is a complex and delicate one.

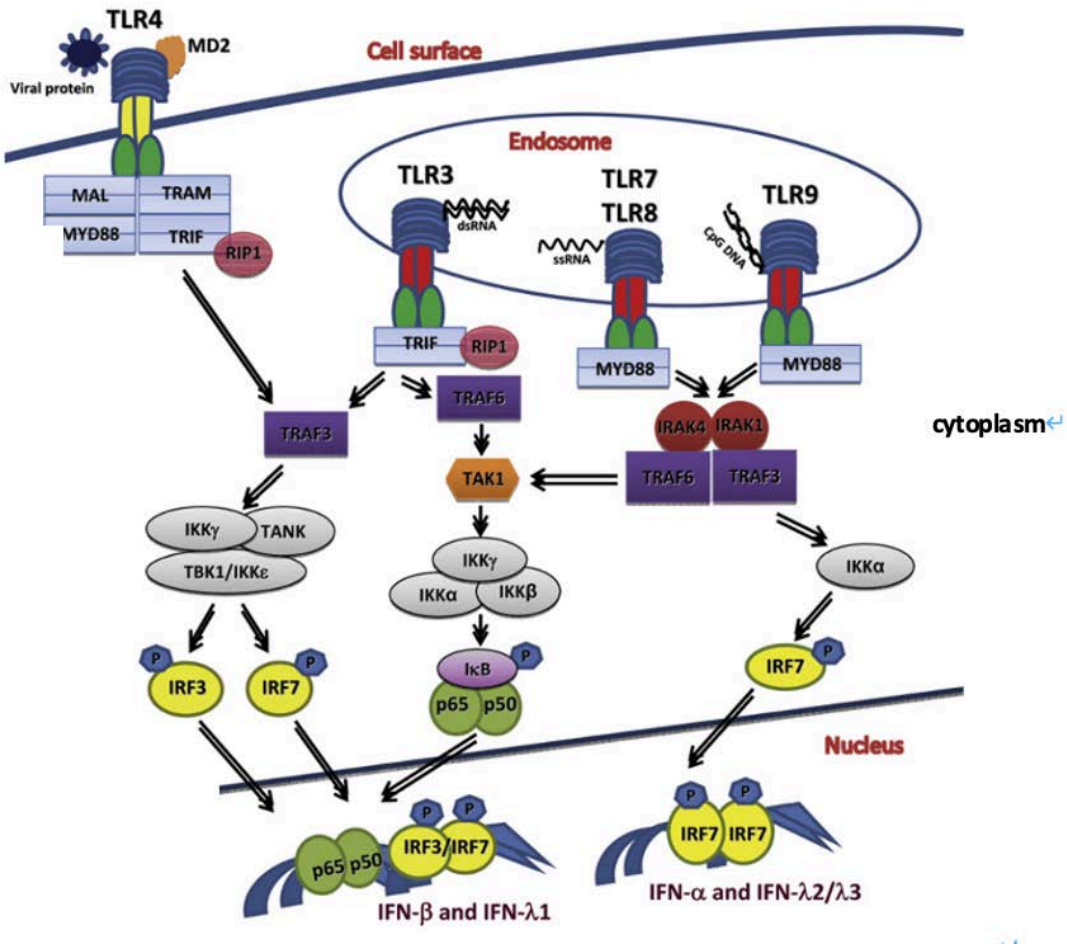

Figure 15. Viral proteins, dsRNA, ssRNA, and CpG DNA, initiates an antiviral innate immune response mediated by TLRs. *TLR4 are present on the cell surface and recognize viral proteins. TLR3, TLR7, TLR8, and TLR9 are intracellular viral nucleic-acid-sensing TLRs that are localized in endosomes, recognize Viral dsRNA, ssRNA, and unmethylated CpG DNA , respectively. To activate the TRIF-dependent pathway, TLR4 requires the bridging adaptor TRAM and its trafficking into endosomes. The MyD88-dependent and TRIF-dependent signaling complexes through a cascade of signaling events leading to the activation of several transcription factors including NF-κB, IRF3, and IRF7. NF-κB transcriptionally regulates the expression of inflammatory cytokines and chemokines while IRF3 and IRF7 control the transcription of type I and type III IFN genes.*

6. Microtubules

6.1 The structure and Organisation of microtubules

Microtubules are cytoskeletal filaments that play key roles in most if not all cellular functions (segregation of chromosomes, intracellular trafficking, etc (Alushin et al., 2014; Manka & Moores, 2018; Nogales et al., 1998; R. Zhang et al., 2015). Microtubules are hollow cylindrical tubes, composed of heterodimers of globular α-tubulin and β-tubulin molecules that associate in a head-to-tail fashion to form protofilaments, which associate laterally between themselves (Horio & Hotani, 1986; Downing & Nogales, 1998). The number of protofilaments that compose a microtubule is variable and if in cells this is of 13 protofilaments, this can vary in vitro from 10 to 15. Microtubules are polarized and present a plus and a minus end. The first is directed towards the exterior of the cell and is the site of active microtubule growth, while the second points towards the interior of the cell and grows more slowly (Akhmanova & Steinmetz, 2015; Desai & Mitchison, 1997; Martin & Akhmanova, 2018; Nogales & Wang, 2006) (**Figure 16**).

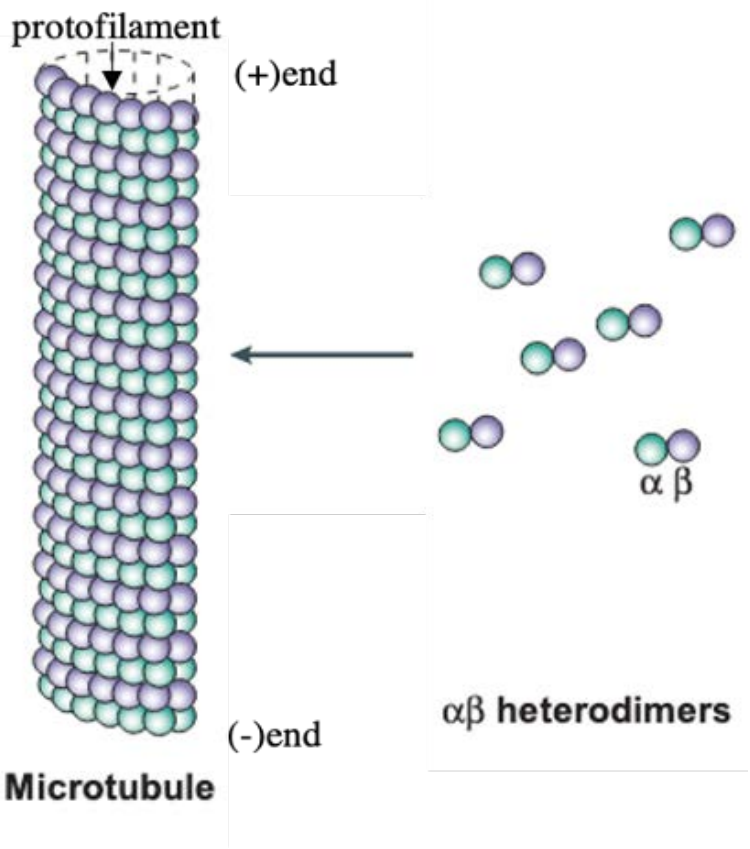

Figure 16. Structure of a microtubule. *αβ-tubulin heterodimers assemble into protofilaments, which form microtubules by lateral association resulting, typically, in a microtubule with 13 protofilaments. Microtubules have polarity with the minus-ends nucleating at the microtubule-organizing center (MTOC) and plus-ends extending to the cell periphery.*

Microtubules behavior is heavily influenced by interaction with a variety of MT-associated proteins (MAPs). These proteins can regulate MT dynamics by either stabilizing or destabilizing them, or even connecting them to other cellular structures, such as membranes or other cytoskeletal components. While MTs are generally very dynamic structures, their properties can be influenced by their post-translational status, which in this case can be very complex and has been defined as the 'tubulin code' (Verhey & Gaertig, 2007). This tubulin code refers

both to (a) expression of different α- and β-tubulin isotypes, and (b) post-translational modifications of tubulin (Wloga et al., 2017).

6.2 Microtubule-associated proteins (MAPs)

The dynamic instability of MTs (Mitchison & Kirschner, 1984) and their organization can be regulated by their interactions with other proteins, called microtubule-associated proteins (MAPs), which were initially discovered as proteins that co-purify with MTs in vitro after several cycles of polymerization and depolymerization (Cassimeris, 2009; Lloyd & Hussey, 2001; Sedbrook, 2004). There are different types of Microtubule associated proteins (**Figure 17**), based on their mode of action, MAPs can be classified into: (1) motile MAPs, interact with motor proteins that generate forces and movement, such as Kinesins or Dynein (Bhabha et al., 2016; Hirokawa et al., 2009); (2) enzymes that break or depolymerize microtubules, including katanin (McNally & Vale, 1993), spastin (Roll-Mecak & Vale, 2005), and fidgetin (Mukherjee et al., 2012) that belong to the meiotic subfamily of AAA ATPases (McNally & Roll-Mecak, 2018); (3) microtubule nucleators as the microtubule polymerases of the XMAP215 family and suppressors of microtubule dynamics (Roostalu & Surrey, 2017); (4) end-binding proteins that specifically associate with plus- or minus-ends of microtubules, such as EB family (Galjart, 2010; Nehlig et al., 2017) or CAMSAP/Patronin/Nezha Family Proteins that specifically recognize microtubule ends and control their dynamics (Akhmanova & Hoogenraad, 2015); (5) the

structural MAPs, a heterogenous group of proteins that bind, and thus stabilize microtubules, such as MAP1 (Borisy et al., 1974) and MAP2 (Sloboda et al., 1975).

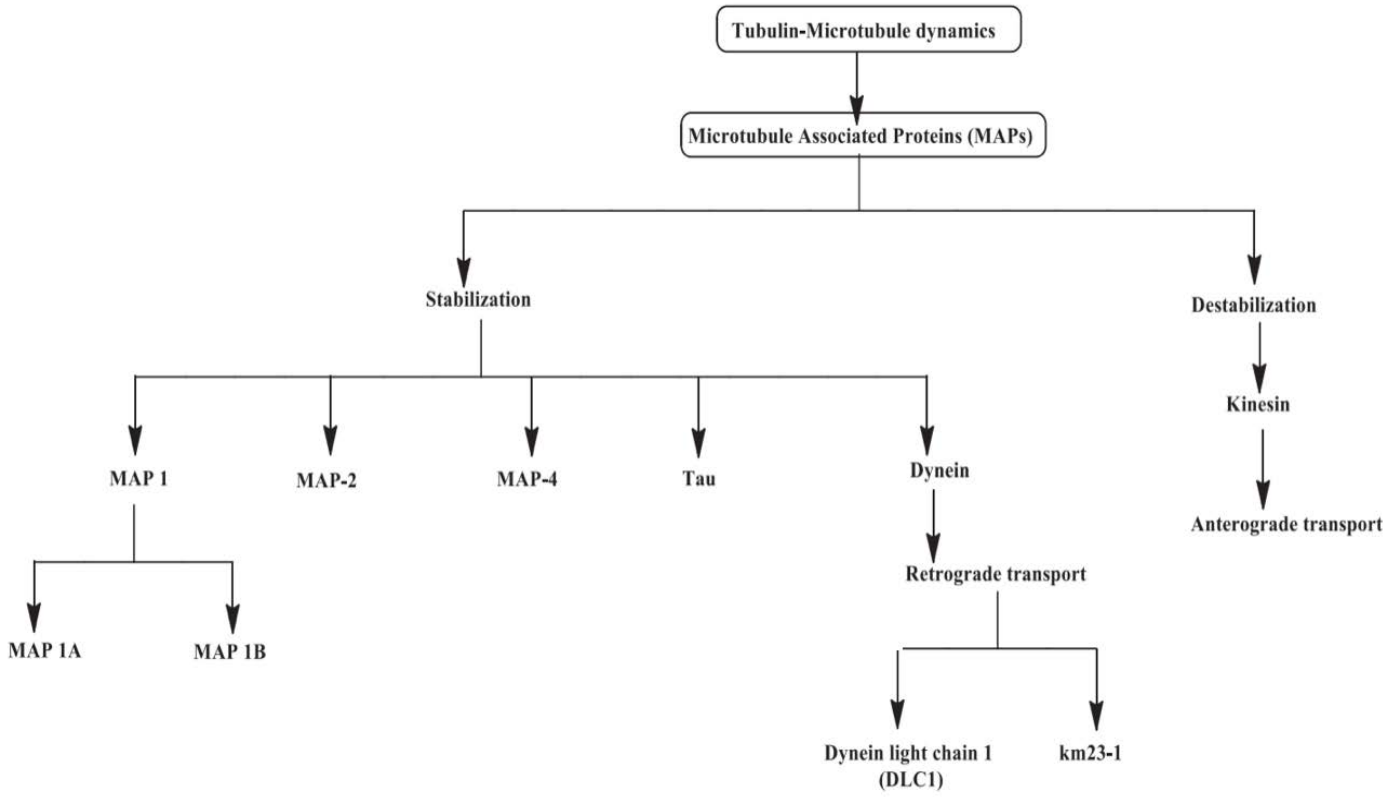

Figure 17. The classification of microtubule-associated proteins (MAPs). *All the MAPs mainly stabilize tubulin-MT dynamics except kinesin. (from* (Khwaja et al., 2021)*.*

Kinesin

Kinesin belongs to the family of motor proteins that use ATP hydrolysis to generate movement and transport organelles and vesicles along MTs. Most, albeit not all kinesins are in charge of cargo movements towards the plus end of the MT (anterograde transport) and also towards the cell periphery. The most studied kinesin member, kinesin-1, was first isolated from squid neurons in 1985. There are up to 45 kinesin genes in the human genome in 14 kinesin families (Wordeman, 2010). The classical kinesin motor consists of two heavy chain kinesins and two light chains kinesis that ensure cargo specificity (**Figure 18B**).

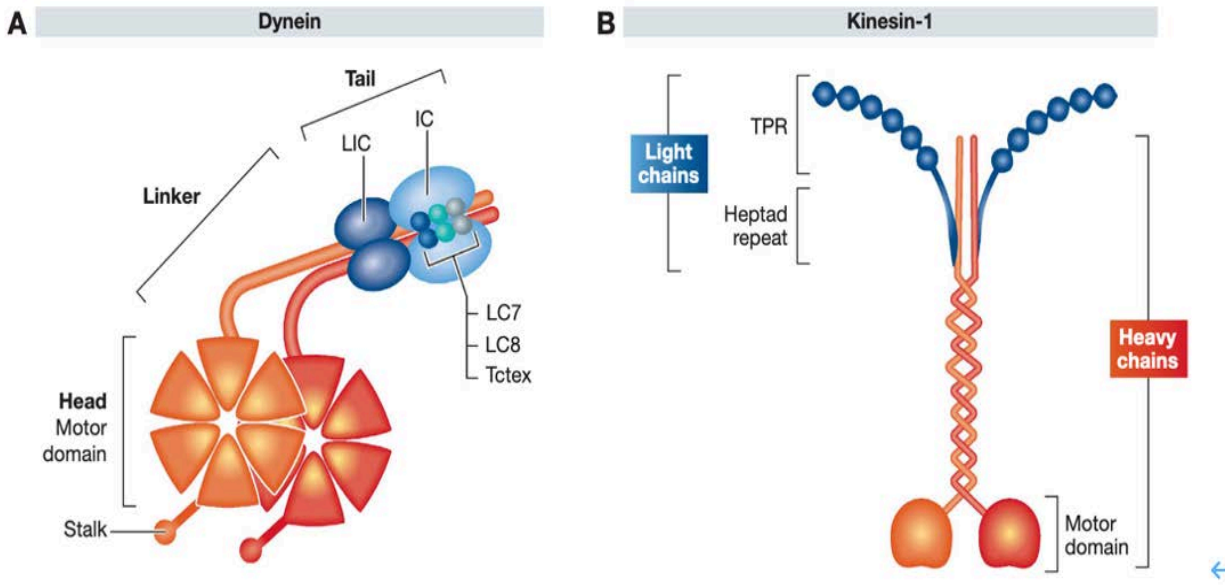

Figure 18. Schematic structure of dynein and kinesin-1. *A.Dynein composed of six AAA ATPase domains (orange) arranged in a hexameric ring from which a microtubule binding stalk projects. The N-terminal tail of the heavy chain mediates its dimerization and contains the binding sites for two intermediate chains (ICs) and two light intermediate chains (LICs). The two intermediate chains (ICs) also interact with three pairs of light chains: Tctex, LC7 and LC8. B. Kinesin-1 is a heterotetramer composed of two motor containing heavy chains (orange) and two light chains (blue). The microtubule binding motor domain is found in the N-terminus of the heavy chain. The light chains associate with the heavy chains via heptad repeat regions in their N-terminus. The C-terminal half of the light chains is composed of six tetratricopeptide repeats (TPR), which represent cargo binding domains. (from* (Dodding & Way, 2011).

Dynein

Dynein are the second class of motors sliding along microtubules this time from the cell periphery to the minus end of microtubules (Gibbons & Rowe, 1965). Dyneins can be divided into two classes: axonemal and cytoplasmic. Axonemal dyneins regulate microtubule sliding in the axonemes of cilia and flagellas, coordinating for example to produce waveforms that drive the swimming of single cells eukaryotes such as the algae Chlamydomonas (Sweeney et al., 2016), whereas cytoplasmic dynein, facilitate the movement of organelles, vesicles, or even virion complexes inside the cell. The dynein complex is composed of two dynein heavy chains (DHCs), two dynein intermediate chains (DICs), several dynein light intermediate chains (DLICs) and a series of dynein light chains (DLCs) such as LC8 (Döhner et al., 2005; Vallee et al., 2004) that are used as cargo adaptors (**Figure 18A**).

The functionalities of these motors is heavily regulated and is highly responses to external stimuli as shown for huntingtin and huntingtin-associated protein 1 (Caviston et al., 2007) that according to their Akt-mediated phosphorylation status can either promote anterograde transport through kinesin-1, or dynein dependent retrograde transport if dephosphorylated (Taran et al., 2020) (**Figure 19**).

Other kinases are likely involved in the regulation of dynein activity as two cyclin dependent kinases, CDK-5 and PCT-1, the cyclin CCY-1 that negatively regulate dynein in the nematode (Holzbaur, 2010), or the JNK kinase pathway (Mercer & D'Armiento, 2006).

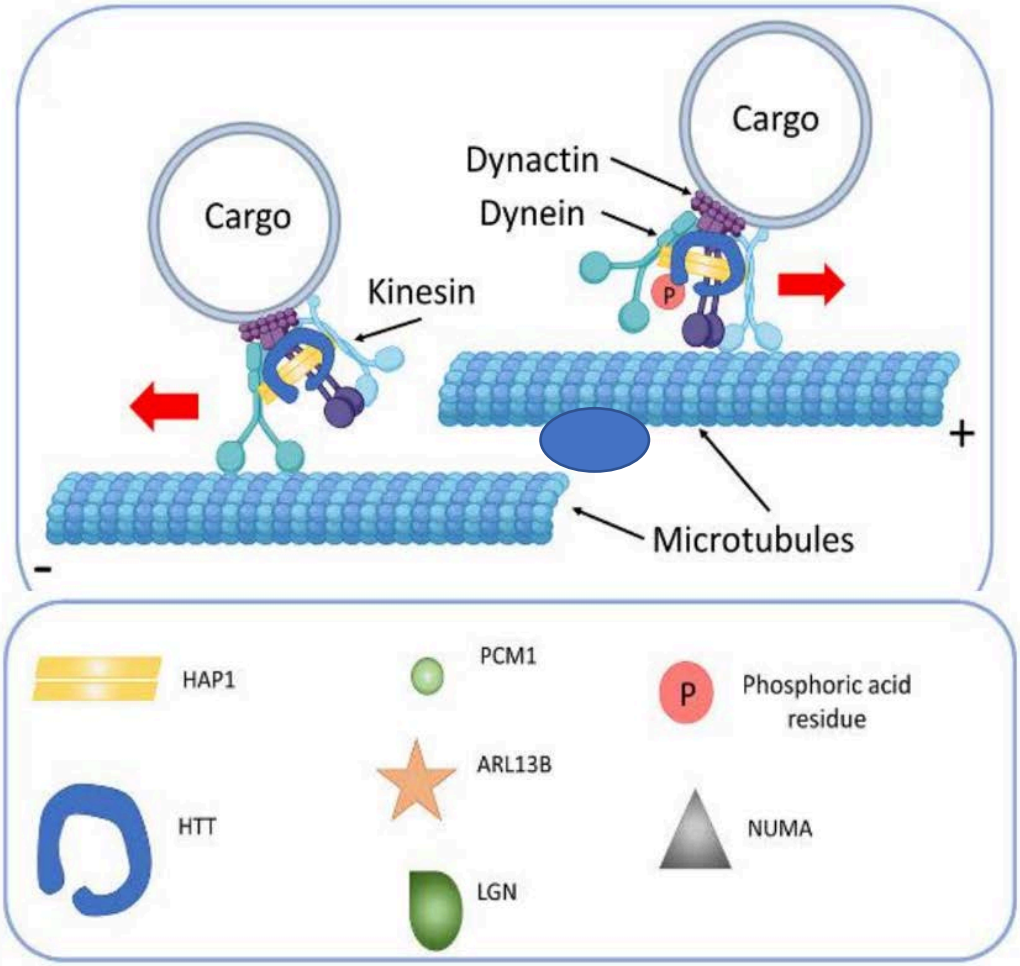

Figure 19. Correlation between microtubules and microtubule-associated proteins. *Kinesin and dynein motors attach the cargo to the microtubule via motor adaptors. HTT functions as a scaffold for the dynein-dynactin complex. The phosphorylation of HTT determines the movement direction of the vesicles to the plus or minus end of the MT (from* (Taran et al., 2020)*.*

6.3 Tubulin isotypes

There are almost ten alpha-tubulin isotypes and ten beta-tubulin ones overall in mammals (9 each in humans) (**Table 2**) whereas other organisms, such as Tetrahymena thermophila, or the yeasts *Saccharomyces cerevisiae* and *Schizosaccharomyces pombe*, contain only one to two (Janke & Chloë Bulinski, 2011). These isotypes exhibit subtle differences particularly in the C-terminal tails, which sticks out from the MT lattice and is therefore important for possible subfunctions of specific microtubules (Kapitein & Hoogenraad, 2015). For instance, TUBA4 A/B (tubulin alpha isotype 4 A/B), TUBA8 (tubulin alpha isotype 8), and TUBAL3 (tubulin alpha L3) do not contain the final tyrosine present in the other alpha-tubulin isotypes (Gu et al., 1988), that is important in the tyrosination–detyrosination cycle in the cell (Gadadhar et al., 2017), see below. For the most part however, these subtle changes have not been fully characterized functionally.

Genes	C-terminal aminoacid chain	Tissue expression
Alpha-tubulin isotypes		
TUBAL3	RDYEEVAQSF	Intestine, colon, oocyte, mucosa
TUBA1A	GEGEEEGEEY	Fetal brain, embryo, bone marrow
TUBA1B	GEGEEEGEEY	Brain, respiratory system, embryo
TUB1C	ADGEDEGEEY	Respiratory system, oocyte, embryo, spinal cord
TUBA3C	EAEAEEGEEY	Testis, sperm, oocyte, brain, respiratory system
TUBA3D	EAEAEEGEEY	Testis, platelet, oocyte, brain, liver, uterus
TUBA3E	EAEAEEGEAY	Testis, heart, placenta, oocyte
TUBA4A	SYEDEDEGEE	Brain, skeletal muscle, platelets
TUBA4B	MPALSLPTRW	Oocyte, respiratory system, oviduct
TUBA8	FEEENEGEEF	Platelet, heart, bone marrow
Beta-tubulin isotypes		
TUBB	DFGEEAEEEA	Respiratory system, brain, embryo, placenta
TUBB1	AEMEPEDKGH	Blood, leukocytes, muscle, liver
TUBB2A	FEEEEGEDEA	Brain, liver, hair follicle
TUBB2B	FEEEEGEDEA	Brain, embryo, testis
TUBB3	EEESEAQGPK	Respiratory system, nervous system
TUBB4A	FEEEAEEEVA	Brain, testis, ovary, heart, colon
TUBB4B	FEEEAEEEVA	Respiratory system, testis, brain, oocyte
TUBB6	FEDEEEEIDG	Breast, respiratory system, muscle, placenta
TUBB8	DEEYAEEEVA	Oocyte, blood system

Table 2. Alpha and beta tubulin isotypes coded in human. *TUBA: Alpha-tubulin, TUBB: Beta-tubulin. A: Alanine, D: Aspartic Acid, E: Glutamic Acid, F: Phenylalanine, G: Glycine, L:*

Leucine, K: Lysine, M: Methionine, N: Asparagine, P: Proline, Q: Glutamine, R: Arginine, S: Serine, T: Threonine, V: Valine, W: Tryptophan, Y: Tyrosine.(from (Amargant et al., 2019)

6.4 Tubulin Post Translational Modifications

There are many different post-translational modifications (PTMs) that have been reported to occur on both of tubulin subunits. The most extensively characterized are: acetylation/deacetylation of lysine (K) residues; the removal and re-addition of the last tyrosine residue (known as detyrosination/tyrosination cycle), polyglutamylation, and polyglycylation (Magiera et al., 2018) (**Figure 20**). All these PTMs occur at the divergent, highly charged C-terminal end of α- and β-tubulin except for the acetylation of α-tubulin that occurs on an internal lysine in position 40. Additional and less studied modifications include phosphorylation, ubiquitination, sumoylation and palmitoylation.

These modifications are highly dynamic and can be reversed by numerous enzymes that will be detailed below.

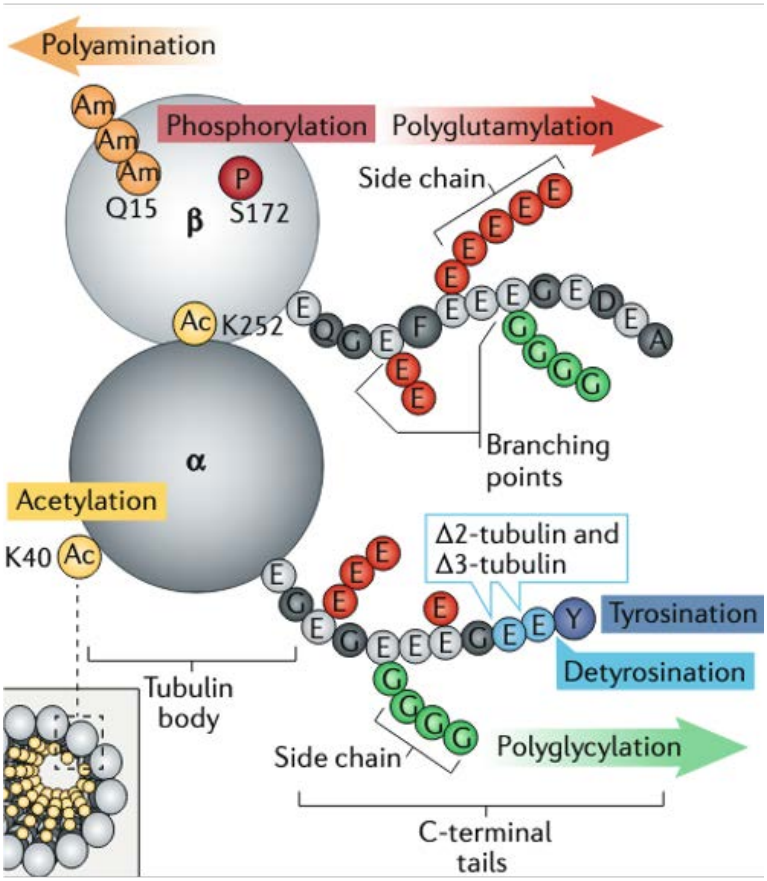

Figure 20. **Post translation modifications of tubulin.** *Tubulin is subjected to a large number of PTM. (such as acetylation (Ac), phosphorylation (P) and polyamination (Am), or at the unstructured C-terminal tails of tubulin (such as, glutamylation, glycylation, tyrosination, detyrosination and removal of glutamate residues to produce Δ2-tubulin and Δ3-tubulin). (from* (Janke & Magiera, 2020)*.*

Acetylation of K40 on α-tubulin and detyrosination

Highly conserved acetylation of the Σ-amino group of residue K40 of α-tubulin (LeDizet & Piperno, 1987; L'Hernault & Rosenbaum, 1985) is catalyzed by the tubulin acetyl transferase (αTAT1) (Bance et al., 2019; Marcaurelle et al., 2010). This modification can be removed by the histone deacetylase 6 (HDAC6) (Matsuyama et al., 2002) as well as by the deacetylase Sirtuin 2 (SIRT2) (Kyrylenko et al., 2003). The acetylation of residue K40 is different from other tubulin PTMs in that it is the only that occurs on an amino acid moiety that extends inside the microtubule lumen (Chau et al., 1998). The acetyl-K40 mark is an established mark of stable

microtubules as it appears with a delay after microtubule assembly and is seen as a marker of polymer age (S. Liu et al., 2004). Injection experiments have allowed the conclusion that acetylation of residue K40 is not responsible for microtubule stabilization, or at least not by itself.

A recent study suggested the possibility that K40 acetylation could regulate the overall levels of tubulin by targeting it through degradation through ubiquitylation, presumably following the disassembly of acetylated microtubules (Solinger et al., 2010). The acetyl-K40-mediated tubulin degradation could involve HDAC6, because this protein binds to acetyl-K40 α-tubulin and also interacts with proteins that mediate ubiquitylation (Boyault et al., 2007; Nishida et al., 2002).

Most α-tubulin genes are expressed with a gene-encoded C-terminal tyrosine residue which can be reversibly removed by process of detyrosination first described in 1973 (Barra et al., 1973). Detyrosination occurs after incorporation of tubulin subunits into the microtubule lattice (Kumar & Flavin, 1981) and is often referred to as Glu-tubulin, a mark of stable microtubules (Gundersen et al., 1984).

Tubulin detyrosination and subsequent tyrosination is a cyclic event driven by enzymes (Hallak et al., 1977), and is involved in various biological processes such as mitosis, neuronal differentiation, and cardiomyocyte contraction (Lopes & Maiato, 2020). The enzymes that remove it are tubulin carboxypeptidases (TCPs): the recently identified Vasohibin 1 (VASH1) and Vasohibin 2 (VASH2) complexes with their associated Small Vasohibin-Binding Protein (SVBP) (Aillaud et al., 2017; X. Liu et al., 2019; Nieuwenhuis et al., 2017). When microtubules

depolymerize, soluble detyrosinated α-tubulin can be retyrosinated by a highly specific tubulin tyrosine ligase (TTL) that closes the cycle (Ersfeld et al., 1993; Schröder et al., 1985). In some cases after detyrosination, α-tubulin C-terminal tails may also be subject to the removal of the penultimate and antepenultimate glutamates by cytosolic carboxypeptidases (CCPs) (Rogowski et al., 2010; Tort et al., 2014), leading to formation of the non-tyrosinatable Δ2- and Δ3-tubulin, respectively (Aillaud et al., 2016; Paturle-Lafanechère et al., 1991). Found so far in the brain, the exact function of these forms remains unclear.

Other post translational modifications

Glutamylation and glycylation (Redeker et al., 1991) are two related PTMs that are generated by the enzymatic addition of one or more the γ-carboxyl group of glutamate or glycine residues as branched peptide chains to the C-terminal tails (CTT) domain of α- and/or β-tubulin (Redeker et al., 1991). Due to their polymeric nature, glycylation and glutamylation are referred to as 'polymodifications'. The side chains branch off multiple glutamic acids within the CTT of α- and β-tubulin. Tubulin glutamylation is abundant on microtubules of axonemes, centrioles and basal bodies, and on some cytoplasmic and spindle microtubules (Bré et al., 1994), while tubulin glycylation is mostly restricted to ciliated cell types and is enriched on axonemes and basal bodies (Iomini et al., 1998). Polymodifications are catalyzed by enzymes that have homology with tyrosine-tubulin ligases (TTL-like proteins, TTLLs, (Janke et al., 2005; Mukai et al., 2009; Wloga et al., 2008). Owing to this intrinsic complexity and the presence of multiple potential modification sites on α- and β-tubulins, polymodifications generate non-binary and often complex and heterogeneous signals.

Additional PTMs on tubulin have been described, including phosphorylation, polyamination, palmitoylation, arginylation, ubiquitylation, glycosylation, sumoylation (reviewed in (Janke & Chloë Bulinski, 2011) and methylation (Park et al., 2016), which remain however far less studied. For instance, phosphorylation on serine 172 of β-tubulins, which is catalyzed by the cyclin-dependent kinase Cdk1, has been shown to affect MT assembly (Fourest-Lieuvin et al., 2006). The recently discovered of methylation on the K40 residue (Park et al., 2016) is highly intriguing, as it provides a PTM that competes with the well-known acetylation of this site.

7. Viral trafficking of viral nucleoprotein complexes on microtubules

Related to my project, below are the studies that implicate microtubules in the life cycle of the different viruses and in particular in the migration of viral nucleoprotein complexes that we believe to be the key target of inhibition of TRIM69.

1) HIV-1

Imaging studies of HIV-1 virions indicated that viral capsids do associate to microtubules and use them to move towards the nucleus (Das et al., 2006) (**Figure 21**). In line with this observation several microtubule binding proteins have been proposed over the years to associate to viral capsids of HIV-1 (dynein, kinesin1, Fez1 etc, (Malikov et al., 2015). More recently, HIV-1 infection was associated to the rapid stimulation of stable microtubules, a specific subset of microtubules (Mitra et al., 2020; Sabo et al., 2013). The possibility that viral infection could result in a modification of the host cytoskeleton is of high interest as it suggests

that the virus could stimulate the creation of an environment that is more favorable to its retrograde transport into the nucleus. However, for the moment these observations have been generated by a single laboratory and it is unclear whether the stimulation of stable microtubule formation is a cause or a consequence in infection. Indeed, in these studies at least 2-3 hours are needed to visualize this stabilization, which is very long with respect to the kinetics of entry and approach to the nucleus measured in cell lines (which is of the same order of magnitude). As such, the relationship between stable microtubule formation and subsequent steps of infection remains unclear.

Several studies showed that HIV-1 induces the rapid formation of post-translationally modified stable MTs and identify key roles for EB1 and its binding partner, Kif4, in regulating MT stability and early post-entry stages of infection. Although treating with nocodazole to depolymerize MT resulted in lower levels of dynamic MTs, infection was indeed minimally affected suggesting that stable MTs are indeed important for HIV infection (Sabo et al., 2013; Naghavi et al., 2013; Jovasevic et al., 2015; Delaney et al., 2017). It is important to remember that the rapid induction of stable MTs in the case of HIV-1 has been described so far by a single group. In the model proposed by this group and validated so far essentially in neuronal cells which present a convoluted microtubular network, HIV exploits a number of specialized microtubule (MT) plus-end tracking proteins (commonly known as +TIPs) to slide towards the nucleus and indeed, several other proteins have been shown to be important for HIV-1 infection as Diaphanous 1 and 2, FEZ1, CLASPs, as well as MAP1 (Akhmanova et al., 2001; Delaney et al., 2017; Efimov et al., 2007; Fernandez et al., 2015, 2015; Malikov et al., 2015; Mitra et al., 2020).

In line with the nature of intricately intertwined processes during early infection by HIV-1 cores, it is possible that incoming capsids take advantage of various co-factors to both slide on MTs towards the nucleus as well as to coordinate the timing of their disassembly (uncoating) (Naghavi, 2021).

However, in light of the results that will be presented in this thesis, MTs stabilization following HIV-1 infection could be regarded also as an IFN response rather than an HIV-1 specifically induced program and this has not been considered in previous studies. As such, the importance and effects of stable MTs in respect to HIV-1 infection remains to be fully elucidated.

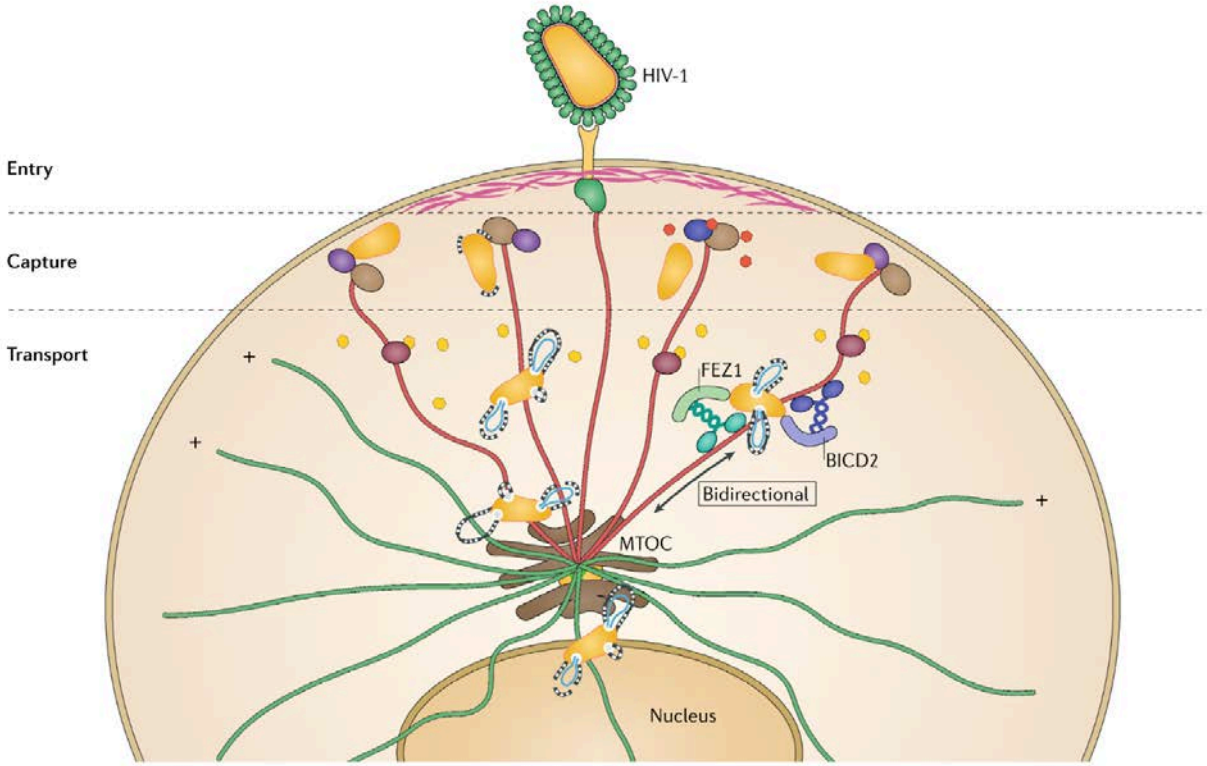

Figure 21. HIV-1 interactions with the host cell cytoskeleton during early infection*. After entry, HIV-1 induces microtubule (MT) stabilization (shown as red filaments), which is regulated in part by actin-MT cross-linking proteins (green). Capture. Fusion of HIV-1 into the cytosol releases matrix (MA) protein (orange) that is captured by a complex of MT plus-end tracking proteins (+TIPs) consisting of the MT end-binding protein (EB1) (light brown) and Kif4 (dark blue) at the tip of MTs (+) to induce MT stabilization. The incoming conical capsid (yellow) is also captured with the EB1-associated actin-MT crosslinkers Dia1/2 (purple) to induce additional MT stabilization. The SxIP containing EB1-associated +TIPs CLIP170 and CLASP2 (dashed lines around the capsid) bind to and stabilize capsid, perhaps via recognition of local capsid lattice ruptures induced by the onset of reverse transcription, to upload the incoming cores from cortical actin onto stable MTs. Transport. The capsid binds MT motor adaptors BICD2 and FEZ1 to bridge viral particles to dynein (dark blue) and kinesin-1 (green) motors, respectively, to mediate their long-range bidirectional transport on stable MTs towards the nucleus. As the conical capsid moving along stable MTs loses small patches of CA to accommodate the outgrowing reverse transcribing viral genome (blue), CA protein release likely further increases MT stabilization over time via interactions with MT associated proteins MAP1A/S (dark red). Incoming cores accumulate at the perinuclear MT organizing center (MTOC) prior to nuclear entry by an as-yet unknown transport mechanism. (from* (Naghavi, 2021)*.*

2) VSV

For the moment, aside from the interaction between the P protein of several *Rhabdoviridae* and LC8 a component of the dynein complex, the importance of microtubules for the migration of viral nucleoprotein complexes remains unclear Disruption of microtubules leads to smaller Negri bodies but does not inhibit viral replication. Instead, using nocodazale inhibition and visualization of intracellular transport of fluorescent VSV a few studies indicate that the transport and release of infectious viruses may occur through microtubules (Das et al., 2006; Hill et al., 1986; Yacovone et al., 2016). This process is associated to MAP 1 and 2 (Hill & Summers, 1990), that bind to and stimulate the polymerization of tubulin (Vallee, 1986). As such it is unclear at which step microtubules come into play during the viral replication cycle. Interestingly, MAPs extract from cells stimulate viral RNA synthesis in vitro, suggesting that a connection could exist between viral RNA replication and microtubules.

3) Sars-cov-2 and Coronaviruses

A solid evidence of involvement of microtubules in the trafficking of Coronaviruses comes from the Porcine Epidemic Dhiarrea Coronaviruses that was described to slide in a dynein dependent manner after entry towards a perinuclear region (Hou et al. 2020) as well as from the mimicry between the JHM virus N protein and the protein Tau in terms of microtubule binding in neuronal cells (Pasick et al., 1994). Instead, microtubules do not seem involved in

the formation of double membrane vesicles (DMVs) that are generated from ER-membranes and in which viral RNA is replicated (Hagemeijer et al., 2010).

Objectives

The laboratory had carried out a previous shRNA screen to identified novel modulators of HIV-1 infection in a macrophage-like cell line (THP-1 differentiated in PMA) stimulated with type I interferons (IFN-I). Among the factors of interest, the laboratory identified TRIM69 and in light of the scarcity of information existing on it at the time, my thesis project was to characterize its mechanism of action. Overall, my objective was to determine whether TRIM69 could affect viral infection in a broad manner on retroviruses as well as on negative- or positive-strand RNAs.

I performed all the experiments described here apart the phylogenetic analyses that were performed by Lucie Etienne and Léa Picard. I received help from Xuan-Nhi Nguyen, IE in the lab, for the qPCRs on Trim69 levels in different cell types, the analysis of HIV-1 viral DNA levels in cells expressing Trim69 by qPCR and the generation of CRISPR/Cas9 KO cells.

The results obtained in this thesis indicate that TRIM69 is a novel modulator of microtubule dynamics and that its effects can broadly target different classes of virus, indicating microtubule dynamics regulation as well as TRIM69 as important checkpoint during viral infection.

In addition to this main project, I was also involved in experiments on an unrelated project: the exploration of the effects of IFITM3 (another broad antiviral factor studied in the laboratory) on the secretory pathway using confocal microscopy techniques. The results I helped obtain, highlight a novel role of IFITM3 as modulator of the functionalities of the secretory pathway and suggest that the functions of this and related IFITM proteins may extend well beyond viral infection.

Results

A three-layer genetic screen to identify novel mediators of the negative effects of IFN-I during the early phases of HIV-1 infection in macrophage-like cells. The early phases of HIV-1 infection are inhibited by type 1 interferons and more potently so in cells of the myeloid lineage. To identify novel effectors of this antiviral response, we individually silenced >400 ISGs described in the *Interferome* database by lentiviral-mediated shRNA transduction in THP-1 cells that were split in two then differentiated into a macrophage-like state with PMA. We then examined the susceptibility of these cells to HIV-1 in the presence or absence of IFNα, using single-round of infection competent viruses coding a Firefly Luciferase reporter. IFNα modulators were defined as silenced genes that modulated the no IFNα/IFNα infectivity ratio (referred to here as the IFN defect) when normalized to the library average value (scheme of **Figure 22A**). To exclude modulators of IFNα signaling rather than of HIV-1 infection *per se,* a secondary screen was carried out on primary IFNα hits, by measuring the effects of gene silencing on the production of IP10, a well-described ISG, in THP-1-PMA cells stimulated with IFNα. A tertiary evolutionary analysis was then performed on remaining hits to prioritize them according to their evolutionary history and their potential roles in host-pathogen evolutionary genetic conflicts, using the DGINN pipeline (Detection of Genetic Innovation)(Picard et al., 2020, p.).

Under these conditions, the primary functional screen yielded 22 genes with significant impact on HIV-1 infection in the presence of IFNα (2.5-fold changes, **Figure 22B** and **Figure 23** for individual values). Given that the IFN defect ratio can also be influenced by the susceptibility to infection of non-stimulated cells (due for instance to different basal levels of expression of the different

genes), candidate genes were recategorized as anti- or pro-viral factors, according to the behavior of silenced THP-1-PMA cells during HIV-1 infection in the absence of IFN (**Figure 23**). Given that silencing of AIM2, TOP1, IGF2BP3 and ABTB2 led to higher HIV-1 infection of unstimulated THP-1-PMA cells, these proteins were recategorized as antiviral factors. Conversely, silencing of AKAP2 and TNPO3, a well-known HIV cofactor (Brass et al., 2008; Zhou et al., 2011) that is not IFN-stimulated but that was introduced in our screen to serve as a sentinel gene, led to lower infection rates in unstimulated cells, so that these proteins were recategorized as pro-viral factors. The remaining genes did not exhibit significant changes in infectivity in unstimulated cells and were thus not recategorized. Overall, this analysis led to the identification of 5 pro- and 17 anti-viral modulators (that were then analyzed for their ability to interfere with IP10 secretion upon IFNα stimulation (**Figure 22C**). Under these conditions, silencing of STAT2, IRF9 as well as of the CBP/p300-interacting transactivator with glutamic acid/aspartic acid-rich carboxyl-terminal domain 2 (CITED2) and the lysophosphatidic acid receptor 1 (LPAR1) significantly decreased IP10 secretion (**Figure 22C**). While the results obtained with STAT2 and IRF9 were expected (Mogensen, 2019), our results highlight a novel role for CITED2 and LPAR1 in the establishment of an IFN state. For the purpose of this study, the four above-mentioned genes were discarded from subsequent analyses.

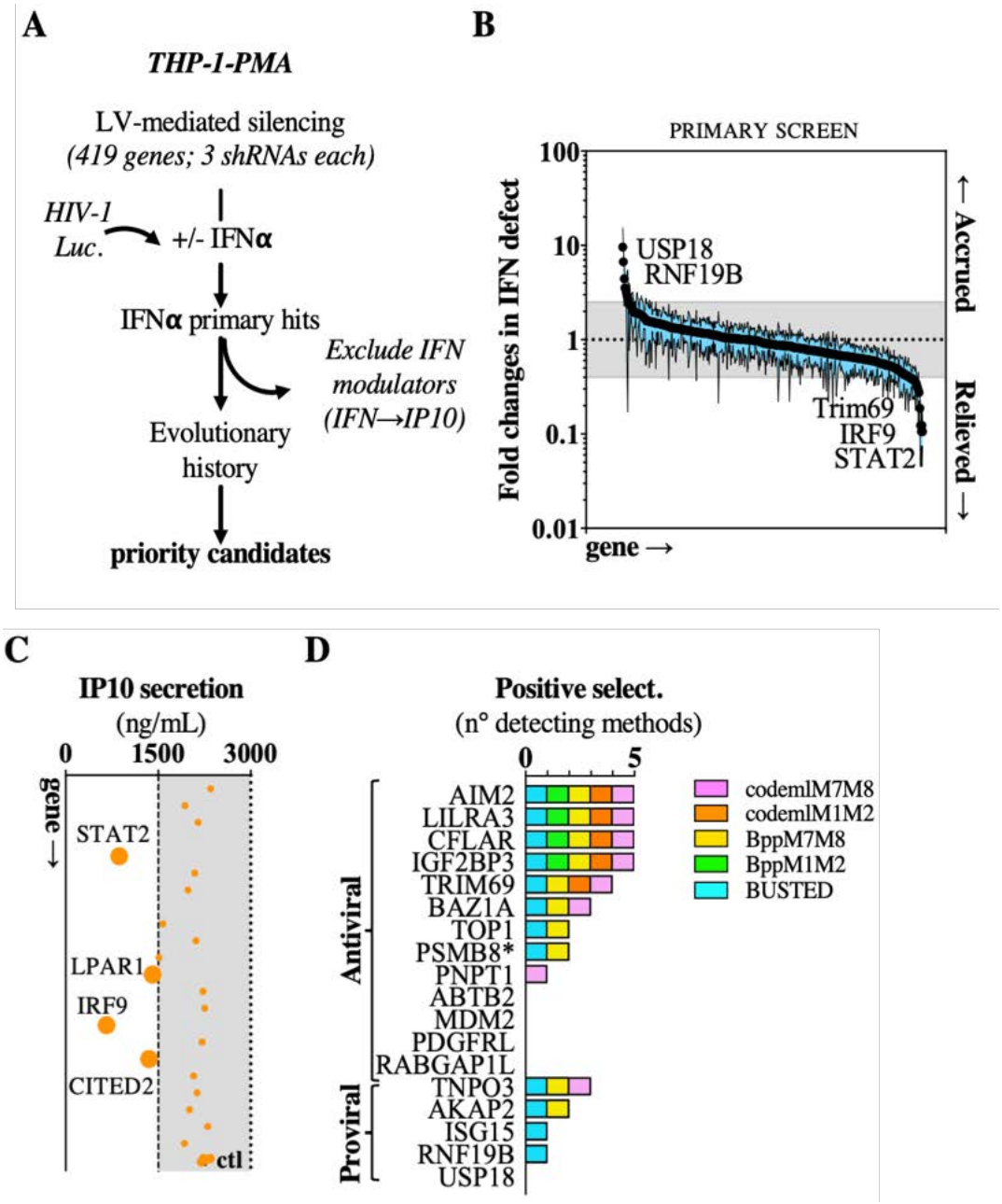

Figure 22. A three-layer genetic screen for IFN modulators of macrophage infection by HIV-1. *A) Schematic approach used here. To identify IFN modulators of the early phases of HIV-1 infection in macrophages, 419 ISGs were individually silenced in THP-1 cells by lentiviral-mediated transfer. Cells were then divided in two, differentiated into a macrophages-like status with PMA, treated or not with 1.000U/mL of IFNα2 for twenty-four hours prior to viral challenge with a VSVg-pseudotyped HIV-1 virus coding for a Firefly Luciferase reporter. A secondary screen was carried out on primary hits to exclude genes that interfered with IFN signaling and a tertiary evolutionary screen was carried out on remaining candidate genes to focus on those most likely involved in an evolutionary-arms race. B) An IFN defect was calculated for each gene as a ratio between the luciferase activities obtained in the no IFN/IFN conditions that was normalized to the average value of the entire library. The graph presents AVG and SEM obtained. A threshold of 2.5 was chosen (outside the grey area) with values >2.5 that indicate accrued IFN defect and values <2.5 that highlight a relieved one. C) Cells silenced*

for the hits retrieved in B were stimulated with 1.000U/mL of IFNα2 and IP10 was measured by ELISA, one day later. Statistically significant differences in IP10 secretion following a one-way Anova test Dunnett's multiple comparison test are represented with larger dots. D) DGINN-mediated positive selection analysis of hits retained after the secondary screen. The graph presents the number of methods that detect positive selection and proteins are separated according to the anti and pro-viral recategorization provided in Figure 23B.

Most antiviral restriction factors are engaged into molecular evolutionary arms-races with pathogens (Daugherty & Malik, 2012; Duggal & Emerman, 2012). They therefore present signatures of these conflicts that can be identified by studying the evolution of their orthologs in host sequences (Sironi et al., 2015). To identify the candidate genes that present such genetic innovations during primate evolution, we screened the functionally retrieved hits with the DGINN pipeline (Picard et al., 2020), which automatically reconstructs multiple sequence alignments and phylogenies and that identifies events of gene duplication, recombination as well as marks of positive selection based on a coding sequence (**Figure 22D**). Automated or manually-retrieved sequences of primary hits were used as query for DGINN. We performed analyses in two steps: (1) phylogenetic analyses and (2) positive selection analyses that combine five methods from PAML Codeml, HYPHY BUSTED and bpp packages (see methods). We found five genes with evidence of strong positive selection in primates, detected by at least four methods (**Figure 22D**): Absent in Melanoma 2 (AIM2), the leukocyte immunoglobulin like receptor LILRA3, the CASP8- and FADD-like apoptosis regulator (CFLAR), the 6-methylated adenosine (m6A) reader IGF2BP3, and the tripartite motif protein 69 (Trim69), a poorly studied member of the TRIM family. Five additional genes exhibited some evidence of positive selection, detected by 2-3 methods: the Bromodomain Adjacent to Zinc Finger Domain 1A (BAZ1A), the DNA Topoisomerase I (TOP1), the A-Kinase Anchoring Protein

2 (AKAP2), the Proteasome subunit beta type-8 (PSMB8) and Transportin 3 (TNPO3) (**Figure 22D**).

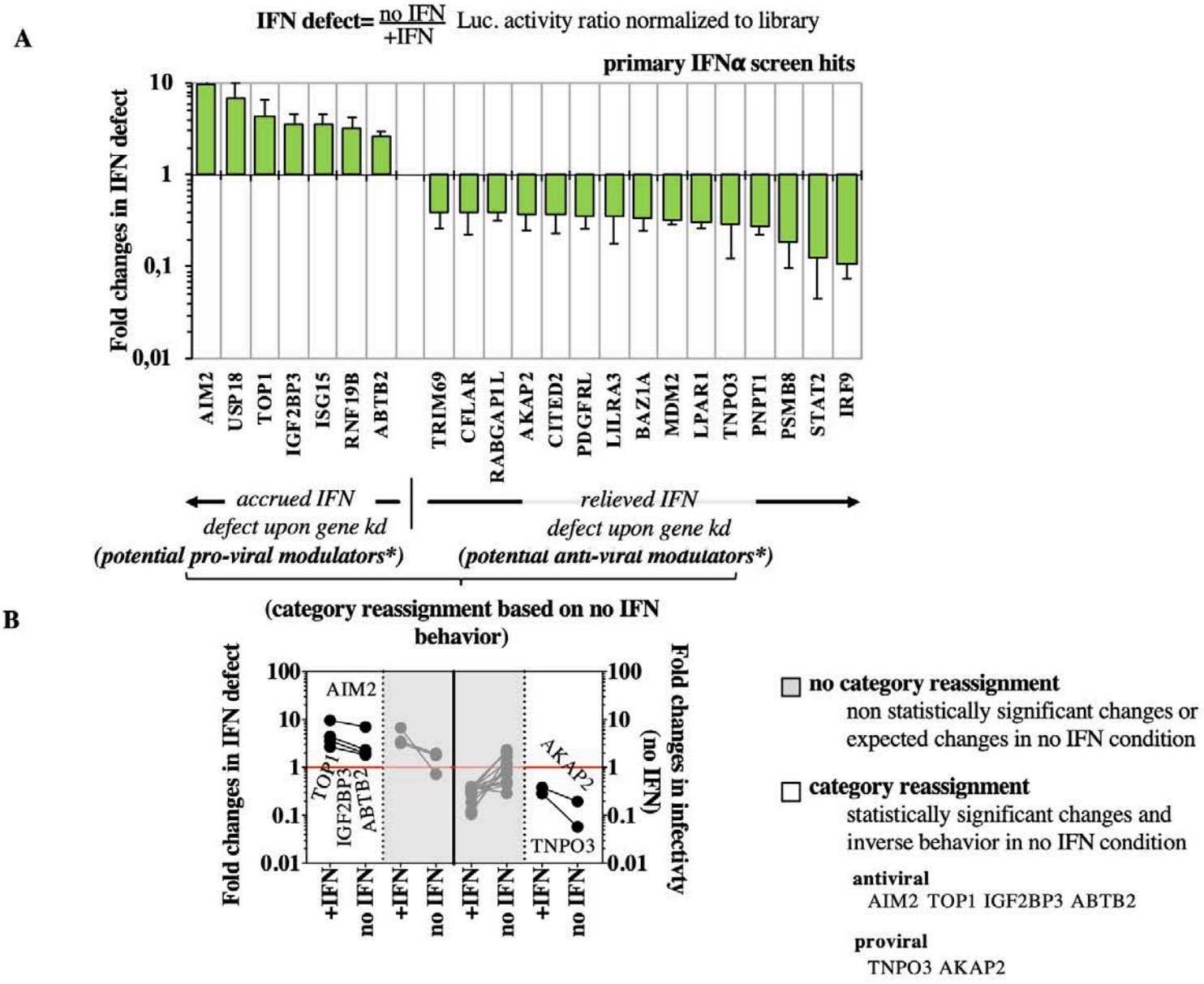

Figure 23. Zoom on the infectivity results and recategorization of functionally retrieved hits. *A) Primary IFNα screen hits were defined as genes that when silenced modulated the normalized IFN defect above or below the chosen threshold value (2.5 fold), in a statistically significant manner when compared to the shRNA control sample, following an unpaired Student t test. Given that the IFN defect ratio is also influenced by the extent of infection in untreated cells (no IFN condition), which is itself dependent on the relative gene silencing efficiency and differential gene expression between basal and IFN conditions, the IFN defect cannot be used directly to categorize primary hits as pro- or anti-viral factors. To do so, the infectivities obtained upon gene silencing in the absence of IFN was used to categories primary*

hits as pro- or anti-viral modulators of infection (B). Genes that upon silencing relieved infection in the absence of IFN in a statistically significant manner were thus recategorized as antiviral (AIM2, TOP1, IGF2BP2 and ABTB2), while on the contrary, genes that upon silencing decreased the extent of infection in unstimulated cells were classified as pro-viral (TNPO3 and AKAP2). Remaining genes did not exhibit statistically significant changes among the two conditions and were not recategorized.

Trim69 is a novel broad inhibitor of viral infection. Among the top hits, we focused on Trim69, a prototypical member of the C-IV subfamily of Trims (Yang et al. 2020), which includes Trim5α which is a well-established antiviral factor against primate lentiviruses. Trim69 possesses a RING, B-box and Coiled-coil (CC) domains followed by a PRY-SPRY domain. Trim69 bears 48% and 44% identity with Trim67 and Trim52/Trim47 following a Blast analysis, while its SPRY domain is closer to Trim39 and Trim21 (46 and 45% identity, respectively, **Figure 24A**). Comparison between the in silico modeled SPRY domains of Trim69 and Trim5α indicates that Trim69 lacks the protruding variable loops (V1, V2 and V3) with which Trim5α contacts specifically retroviral capsids, suggesting an altogether different method of action (**Figure 24B**).

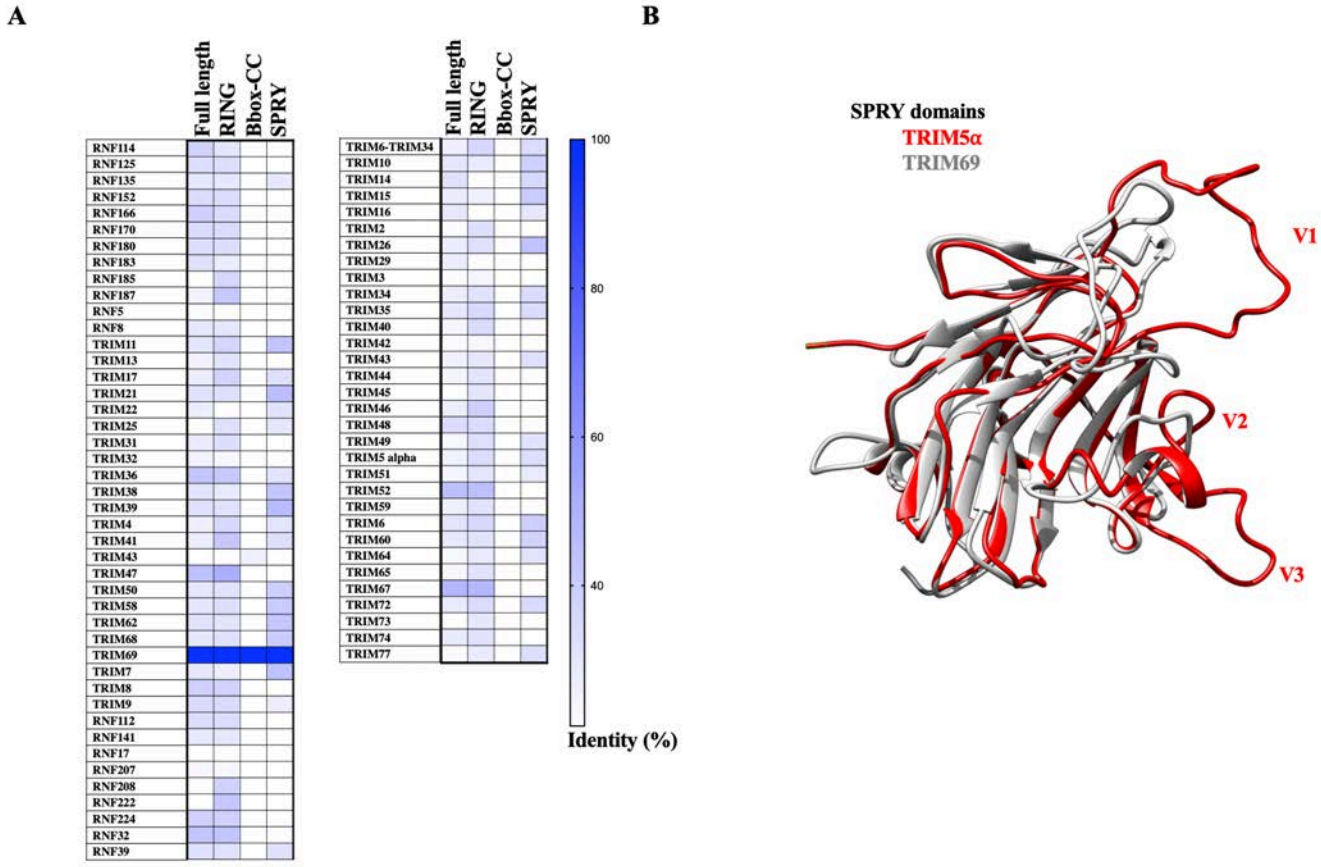

Figure 24. ***Homologies between Trim69 and other members of the Trim family.*** *A) Trim69 amino acid sequences were used as query for a protein Basic Local Alignment Search Tool (BLAST) analysis. Blue hit map depicting percentage identities between the indicated Trim members using either the entire protein, or its individual domains. B) Overlay between the modeled 3D structures of the PRY-SPRY domains of human Trim5α and Trim69 (in red and grey respectively, RaptorX). V1 to V3 indicate variable loops known to be important for Trim5α target recognition.*

Despite having being first identified as a spermatids-specific gene (Shyu et al., 2001), Trim69 exhibits a heterogeneous pattern of expression in different cell lines and primary blood cell types tested (**Figure 25A**). In THP-1-PMA cells, Trim69 is expressed already at basal levels and is extremely sensitive to IFN-I (α/ β) stimulation, similarly to primary macrophages. To first

validate the results obtained in our screen, we generated Trim69 knockout THP-1 cells (KO) by Crispr/Cas9 mediated gene deletion (**Figure 25B** for cell viability).

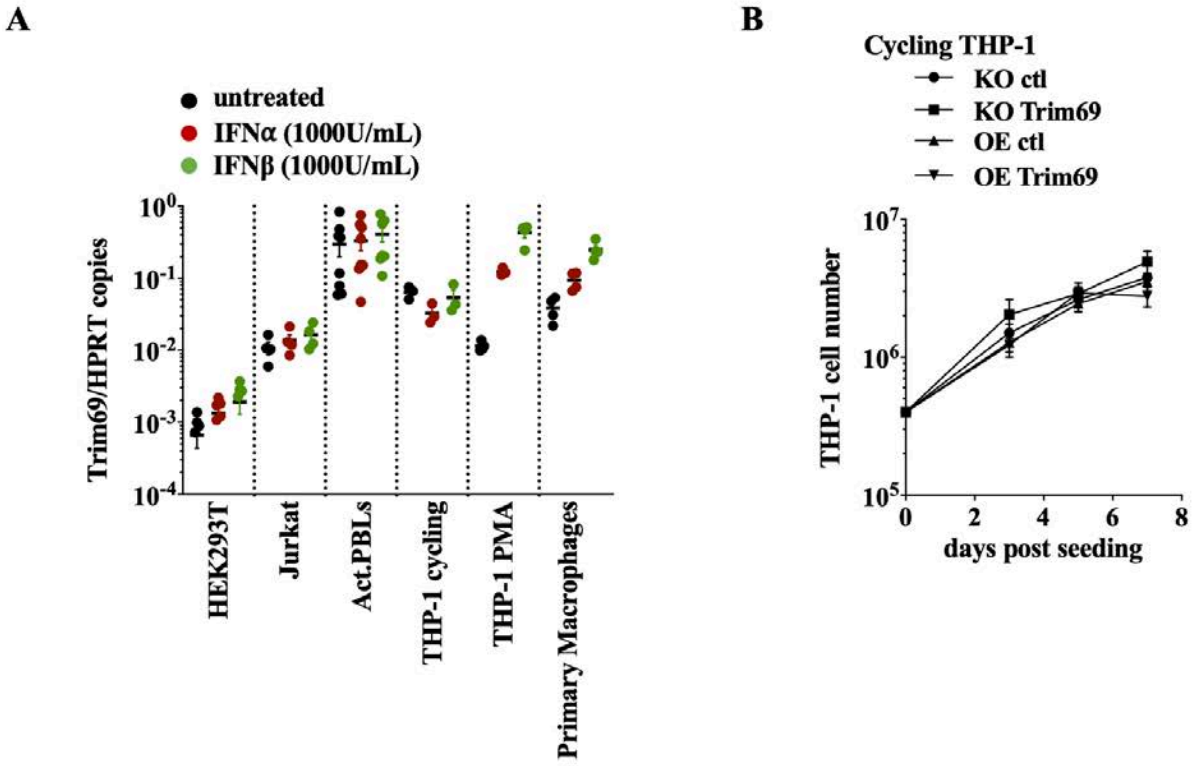

Figure 25. Trim69 cell expression pattern and effects of stable overexpression/knock out of Trim69 on cell division. *A) The indicated cells were stimulated with 1.000 U/mL of IFNα or with 500 U/mL of IFNβ for twenty-four hours, prior to RNA extraction. The levels of expression of Trim69 were determined by RT-qPCR (Avg and SEM of > 3 independent experiments/donors). Primary macrophages were differentiated from blood monocytes with M-CSF, while PBLs were activated for 24 hours with PHA/IL2. B) THP-1 cells either expressing Trim69 under the control of doxycycline (OE), or knocked out for Trim69 (KO) were induced with 1 μg/mL of dox. and then plated at equal density. Cell division was measured at the indicated time. The graph presents values obtained in three independent experiments.*

Cells were then challenged macrophage-differentiated cells with HIV-1, HIV-2 or SIV_{MAC} lentiviruses in the presence or absence of IFNα. Under these conditions, removal of Trim69 increased the susceptibility of target cells to the three primate lentiviruses in the presence, but also in the absence of IFNα (from 2.25 to 3.35 on average), in line with its expression pattern (**Figure 26A**).

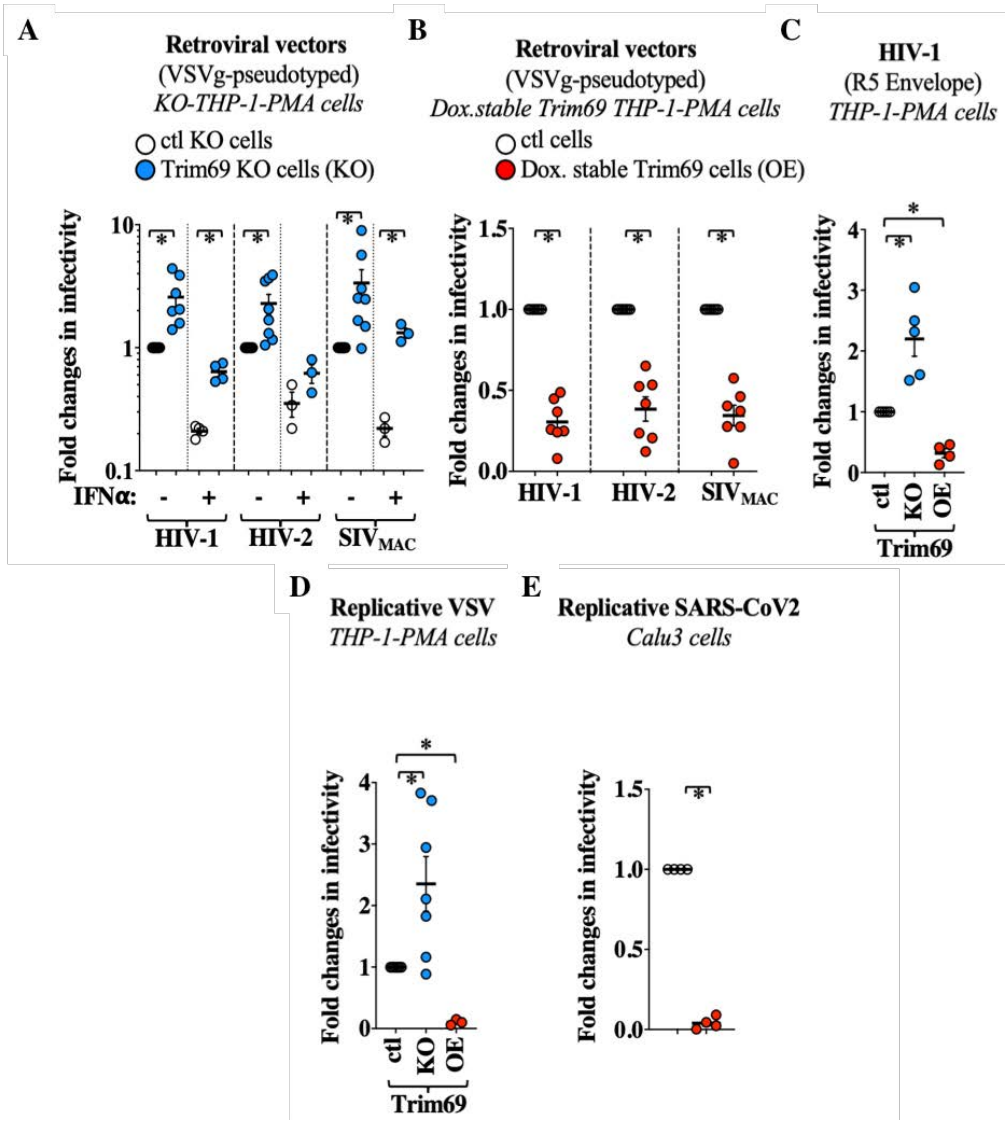

Figure 26. Trim69 is a broad antiviral inhibitor. *A-E) Stable THP-1 cells either ablated for Trim69 (KO) or overexpressing (OE) Trim69 under the control of a doxycycline promoter were generated by lentiviral-mediated gene transfer and selection. Cell pools were then challenged with the indicated single round of infection viruses expressing a GFP reporter at multiplicities of infection (MOIs) comprised between 2 and 4. The extent of infection was then measured two-three days later by flow cytometry. H-I) Replicative VSV and SARS-CoV2 viruses bearing respectively a GFP and mNeonGreen reporter were used to infect either THP-1-PMA cells or*

*epithelial lung Calu-3 cells expressing Trim69 stably at MOIs comprised between 0.1 and 0.5. The extent of infection was measured either 16 hours or two days later by flow cytometry. All panels presented AVG and SEM of 3 to 8 independent experiments after normalization. When indicated, IFNα was used at 1.000 U/mL for 24 hours prior to infection. *, indicates statistically significant differences between the relevant conditions, according to a two-tailed Student t test.*

Conversely and as expected for an antiviral factor, the susceptibility of THP-1 PMA cells stably expressing TRIM69 under the control of doxycycline (OE, was decreased to the same extent during infection with these retroviruses (**Figure 26B**). Given that in this set of experiments viruses were pseudotyped with the pantropic envelope VSVg, Trim69 KO and OE cells were also challenged with an HIV-1 virus bearing the R5-tropic HIV-1 envelope JR-FL and similar results were obtained, indicating that the antiviral effects of Trim69 were envelope independent (**Figure 26C**).

In agreement with two previous reports (Kueck et al., 2019; Rihn et al., 2019), Trim69 also potently modulated replication of the negative-strand RNA virus, VSV (**Figure 26D**). Next, we examined the ability of Trim69 to interfere with the replication of SARS-CoV2, a positive-strand RNA Coronavirus, in epithelial lung Calu-3 cells. Under these conditions, Calu3 expressing Trim69 were strongly protected from SARS-CoV2 infection (**Figure 26E**), overall indicating that Trim69 is able to interfere with a broad range of RNA viruses that extends from retroviruses to positive- and negative-strand RNA viruses.

Of note, Trim69 overexpression did not inhibit lentivirus infection in HEK293T cells, in agreement with one previous report (Rihn et al., 2019). Inhibition of VSV replication occurred

in these cells, albeit to a lower magnitude with respect to what observed in the case of THP-1-PMA cells (**Figure 27**), suggesting that the extent of the effects of Trim69 may be governed by a combination of both virus and cell type specific features.

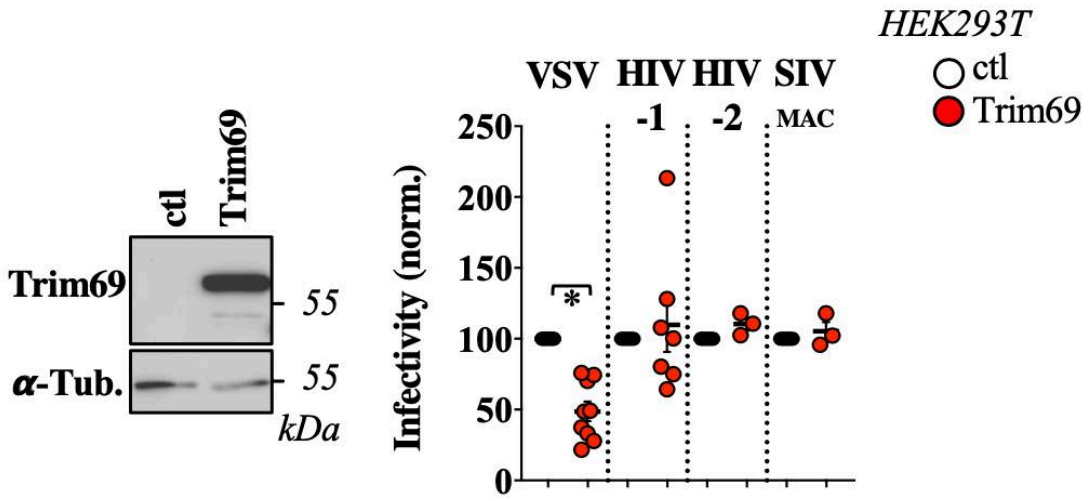

Figure 27. The extent of viral inhibition by Trim69 is cell-type dependent. *Trim69 was transiently expressed in HEK293T cells upon calcium phosphate DNA transfection and cells were then challenged with the indicated virus at an MOI comprised between 0.1 and 0.5 prior to flow cytometry analysis 18 hours (VSV) or 3 days later (Lentiviruses). The graph present Avg and SEM obtained in 3 to 9 independent experiments. * indicates p<0.05 following a two-tailed Student t test between the indicated conditions.*

Trim69 inhibits HIV-1 reverse transcription and the early phases of VSV and SARS-CoV2 infection. To identify the step/s at which Trim69 interfered with virus replication, Trim69-overexpressing THP-1-PMA or Calu3 cells were challenged with the different viruses and the early phases specific to each one was analyzed (schematically resumed in **Figures 28A-C**). In the case of Lentiviruses, THP-1-PMA OE cells were challenged with R5-HIV-1 and virus entry into the cell was measured using the EURT assay (Entry/ Uncoating assay based on core-packaged RNA availability and Translation (Da Silva Santos et al., 2016), which is based on the direct translation of a Luciferase-bearing HIV-1 mini-genome incorporated into virion particles (**Figure 28A**). Under these conditions, Trim69 did not affect HIV-1 entry. On the contrary, Trim69 impaired the accumulation of all HIV-1 viral DNA intermediates tested (2.7 fold for MSSS to 5.3 for 2LTRs), indicating that this protein inhibits reverse transcription rapidly after the entry of viral capsids in target cells.

VSV is a negative-strand RNA virus and, as such, it undergoes an obligate round of primary transcription after cell entry that is required for the translation of P, N and L proteins that in turn ignite viral RNA replication (for a review see (Dietzgen et al., 2017) (**Figure 28B**). Given that translation from primary transcripts is required for viral RNA replication, the translation inhibitor cycloheximide (CHX) can be used to distinguish primary transcription from overall RNA replication. Contrarily to what was observed for HIV-1, TRIM69 exerted a measurable defect in VSV entry into the cell (2.9 fold) and this defect increased during primary transcription (6.5-fold) and overall RNA replication levels (34 fold). Thus, in the case of VSV, Trim69 imparts successive cumulative antiviral effects.

SARS-CoV2 is a positive-strand RNA virus and as such its genome can be directly translated in viral proteins that ignite RNA replication (for a review see (V'kovski et al., 2021).

When Calu-3 cells overexpressing Trim69 were challenged with SARS-CoV2, no major defects were observed at entry, but a defect in RNA replication was clearly observable by six hours post infection (**Figure 28C**, 3.6 fold, in line with the replication defect observed).

Overall, these results indicate that Trim69 inhibits the early steps of viral replication of different viruses at slightly distinct steps: at a post entry step that affects the efficiency of reverse transcription and of viral RNA replication in the case of lentiviruses and of the SARS-CoV2 Coronavirus, and at both entry and post entry events in the case of VSV. In the latter, the efficiency of virus entry in cells expressing Trim69 exhibits a small but detectable defect, together with a more apparent defect in primary transcription.

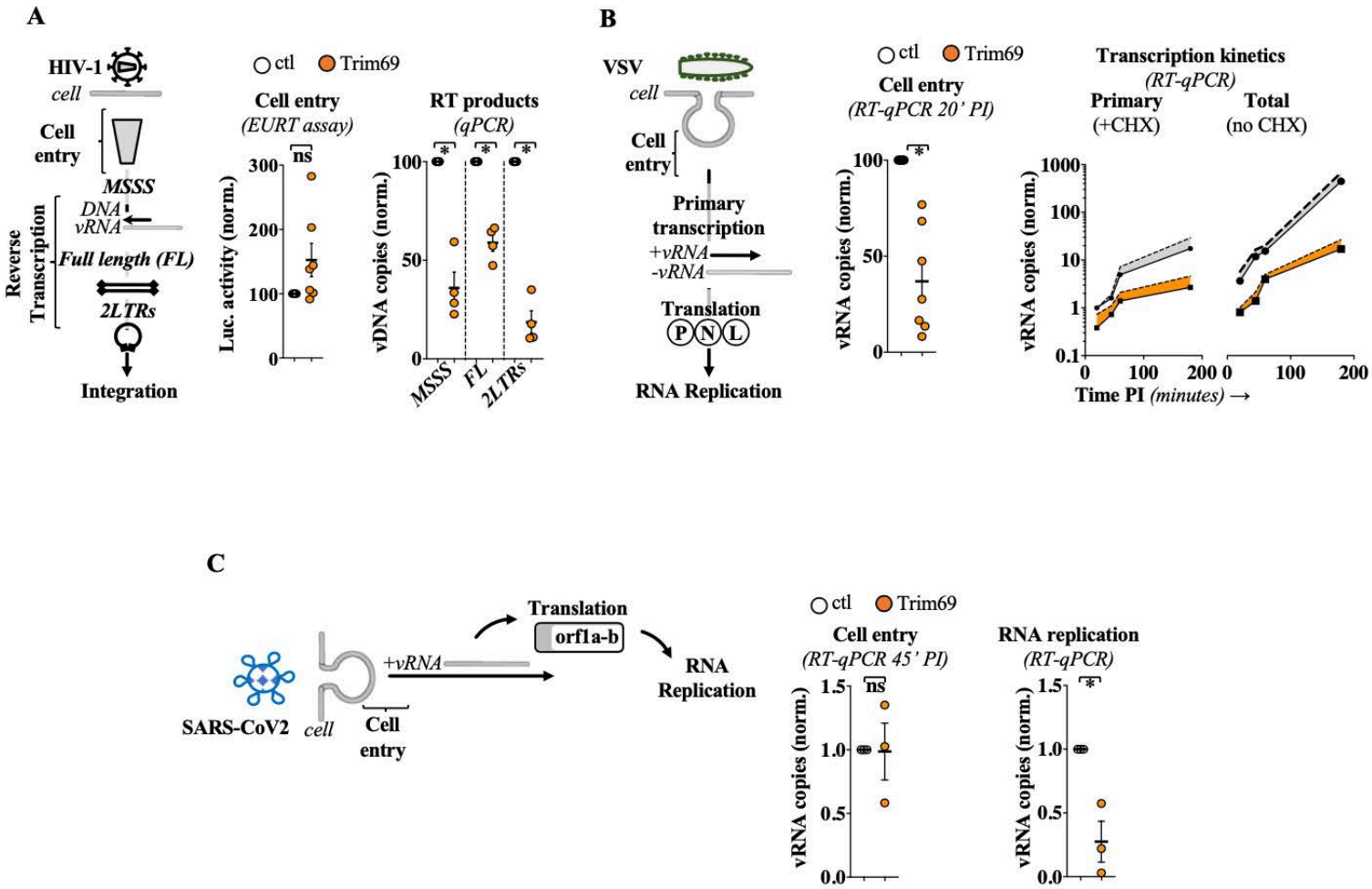

Figure 28. Trim69 inhibits the early phases of infection of different viruses. *A) Virus entry into target cells and accumulation of viral reverse transcription DNA intermediates were measured in THP-1-PMA cells overexpressing or not Trim69, obtained upon lentiviral-mediated gene transfer and selection, upon challenge with an R5-tropic Env HIV-1. Minus-strand strong stop (MSSS) is the first reverse transcription intermediate before the formation of full length double-stranded DNA genomes, FL, that are then imported in the nucleus. Viral DNA ends can then either be integrated in the cell genome or ligated on themselves, yielding 2 LTRs circles used as measure of nuclear entry of viral DNA. Cell entry was tested by the EURT assay, an HIV-1-based cell entry assay based on the direct translation of an HIV genome mimic carrying the Firefly Luciferase. To ensure complete exposure of viral RNA, infections were carried out with 10 μM of PF74, prior to luciferase measurement 18 hours post viral challenge. B) VSV cell entry and RNA transcription steps were similarly tested in THP-1-PMA cells. Cell entry was quantified by measuring the levels of viral RNA that entered cells 20 min after viral challenge and trypsin treatment of target cells to remove unbound virus. Pioneer and whole RNA replication were discriminated by performing infections at an MOI of 1 +/- 100 μg/mL of CHX. C) As in B for SARS-CoV2. Infection was determined in Calu3 cells +/- Trim69 at 45 minutes post infection and after a trypsin treatment to remove non-internalized viruses. Viral RNA replication was then determined by RT-qPCR at six hours post infection to focus on early events. Graphs present Avg and SEM of 3 to 7 individual experiments. ns and *, non-significant and p<0.05 following a two-tailed Student t test between the indicated conditions.*

Trim69 is a novel regulator of stable microtubule dynamics. As a first step to decorticate the functions of Trim69, its intracellular distribution was determined by confocal microscopy along with a selection of markers available in the lab. Exploratory analyses indicated that Trim69 exhibited little to no colocalization with a series of cellular markers in HEK293T cells (actin, ATG-3, ER, or CLIP170), with the exception of α-Tubulin (**Figure 29**).

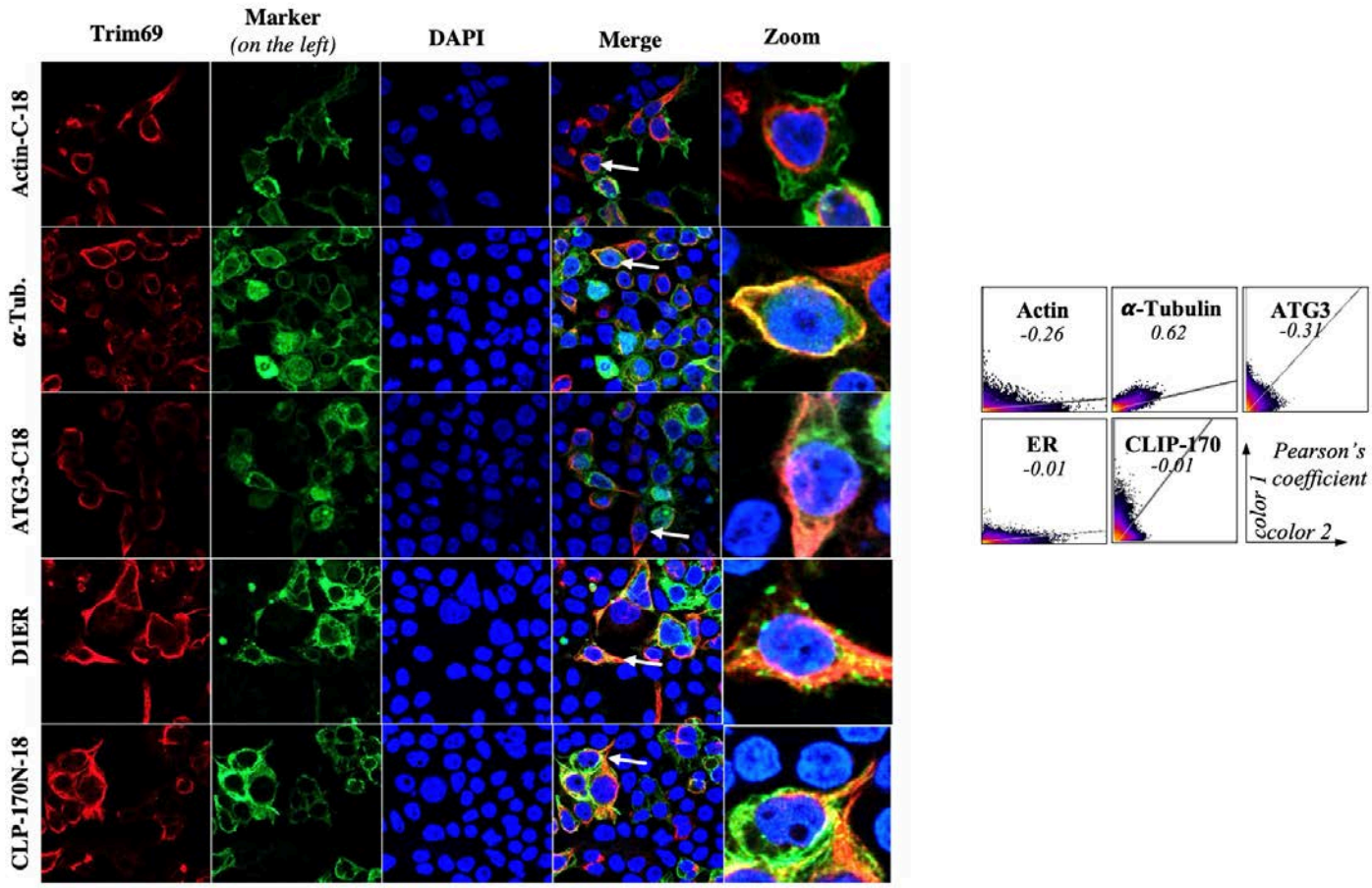

Figure 29. Qualitative confocal microscopy assessment of the colocalization of Trim69 with known cellular markers. *HEK293T cells were transiently transfected with DNAs coding TRIM69 along with the indicated fluorescent cellular markers (all colored or pseudo-colored in green for simplicity), prior to confocal microscopy analyses. The right panels present typical Pearson's correlation coefficients between Trim69 and the indicated marker, as indicated.*

In agreement with a previous report (Kueck et al., 2019), Trim69 adopts a filamentous distribution in the cell cytoplasm which is particularly marked in THP-1-PMA cells (**Figure 30A**).

Indeed, Trim69 colocalized strongly in all cell tested with stable microtubules (defined here as either acetylated, or detyrosinated) which represent a subset of MTs (**Figure 30B, 30E**). Interestingly, Trim69-expressing cells exhibited higher levels of stable microtubules which was also confirmed by WB, suggesting that this protein could promote their formation.

Taxol is a compound that also leads to the accumulation of stable MTs in cells. To determine whether the program of MTs stabilization induced by Trim69 was specific or similar to the one induced by Taxol, control or Trim69 overexpressing THP-1-PMA cells were incubated for twenty-four hours with either Taxol, or Nocodazole that instead depolymerizes MTs, and then cells were either analyzed by confocal microscopy or challenged with VSV prior to flow cytometry (Figure 30 F). Under these conditions, Taxol exerted a slightly positive effect on VSV infectivity in control cells, while Nocodazole led to a specular decrease, in line with previous reports (McDonald et al., 2002; Naghavi, 2014). However, neither Taxol nor Nocodazole modified the extent of virus inhibition driven by Trim69, strongly supporting the notion that Trim69 drives a specific program of MTs stabilization that is distinct from the one induced by Taxol. Of interest, confocal microscopy analysis revealed differences in the arrangement of stable microtubules that accumulate in the presence of Taxol or Trim69 (Figure 30F, compare the arrangement of stable microtubules in the zoomed control cell treated with Taxol or in the Trim69 overexpressing one), further corroborating the notion of specificity in the action of Trim69. Finally, Trim69 induced MTs resisted Nocodazole which further strengthen the contention that they are stable structures.

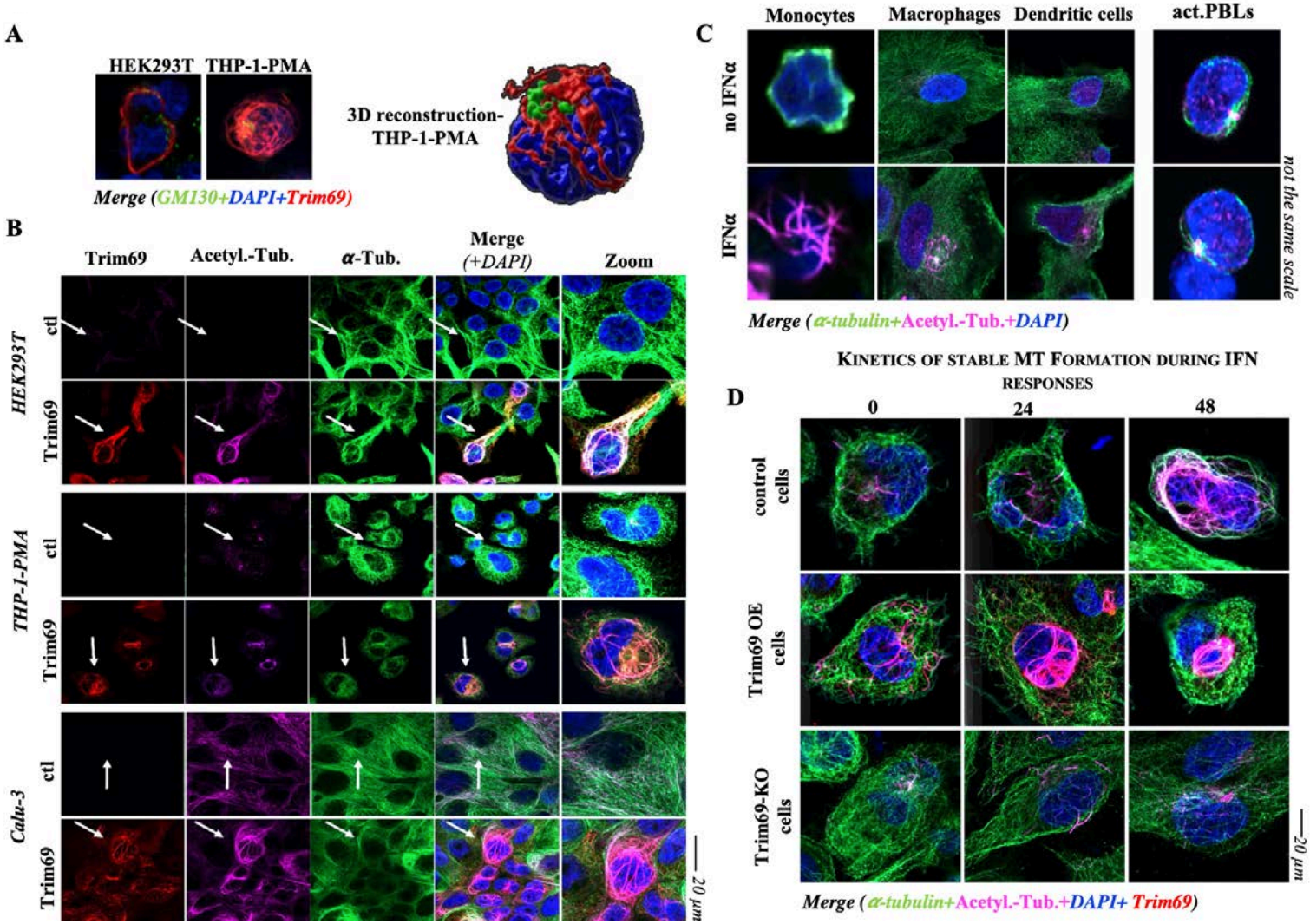
A
HEK293T
THP-1-PMA
3D reconstruction-
THP-1-PMA
Merge (GM130+DAPI+Trim69)
B
Trim69
Acetyl.-Tub.
α-Tub.
Merge
(+DAPI)
Zoom
HEK293T
THP-1-PMA
Calu-3
ctl
Trim69
20 μm
C
Monocytes
Macrophages
Dendritic cells
act.PBLs
no IFNα
IFNα
not the same scale
Merge (α-tubulin+Acetyl.-Tub.+DAPI)
D
KINETICS OF STABLE MT FORMATION DURING IFN RESPONSES
0
24
48
control cells
Trim69 OE cells
Trim69-KO cells
20 μm
Merge (α-tubulin+Acetyl.-Tub.+DAPI+ Trim69)

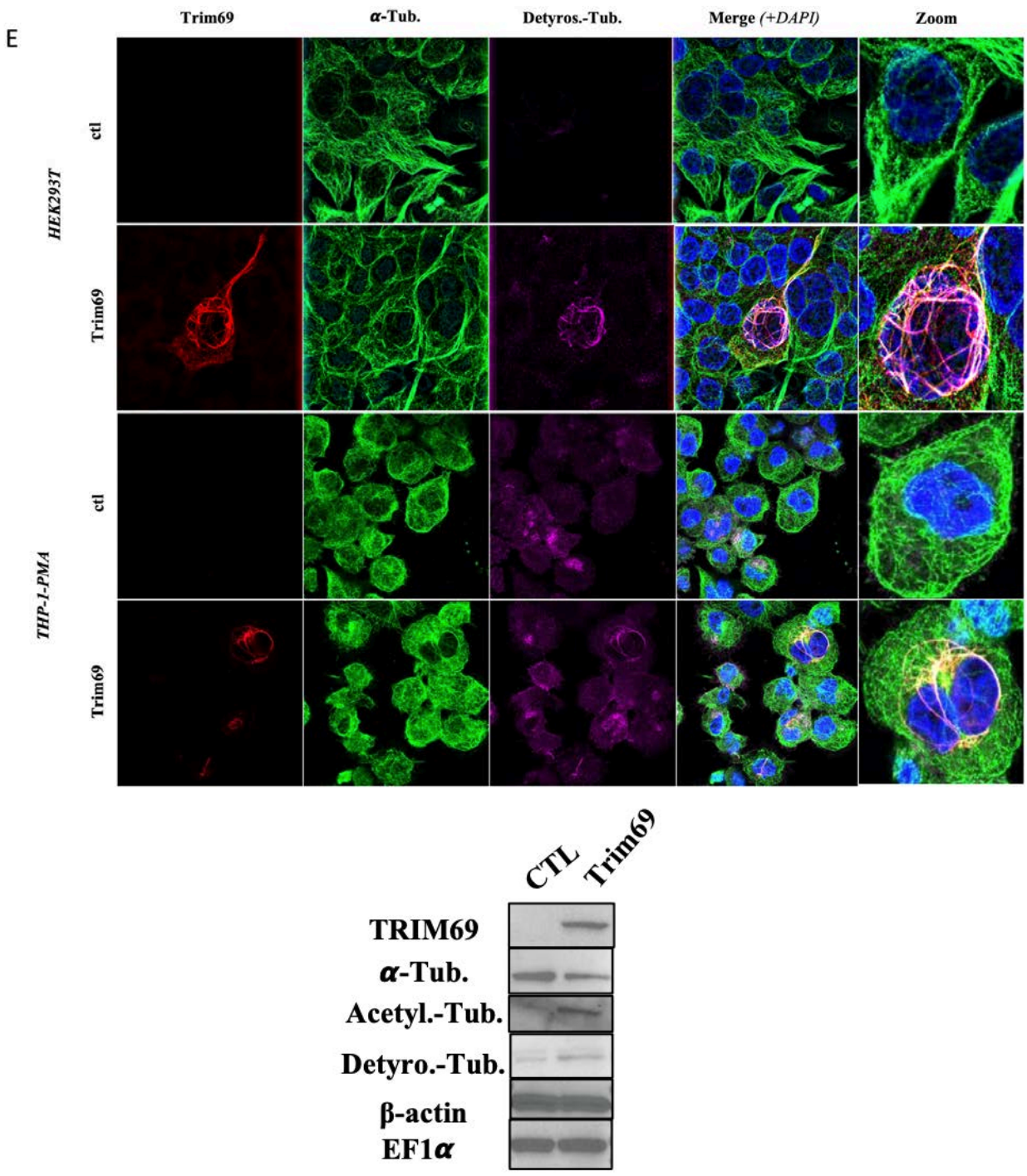
E
Trim69
α-Tub.
Detyros.-Tub.
Merge (+DAPI)
Zoom
HEK293T
ctl
Trim69
THP-1-PMA
ctl
Trim69
CTL
Trim69
TRIM69
α-Tub.
Acetyl.-Tub.
Detyro.-Tub.
β-actin
EF1α

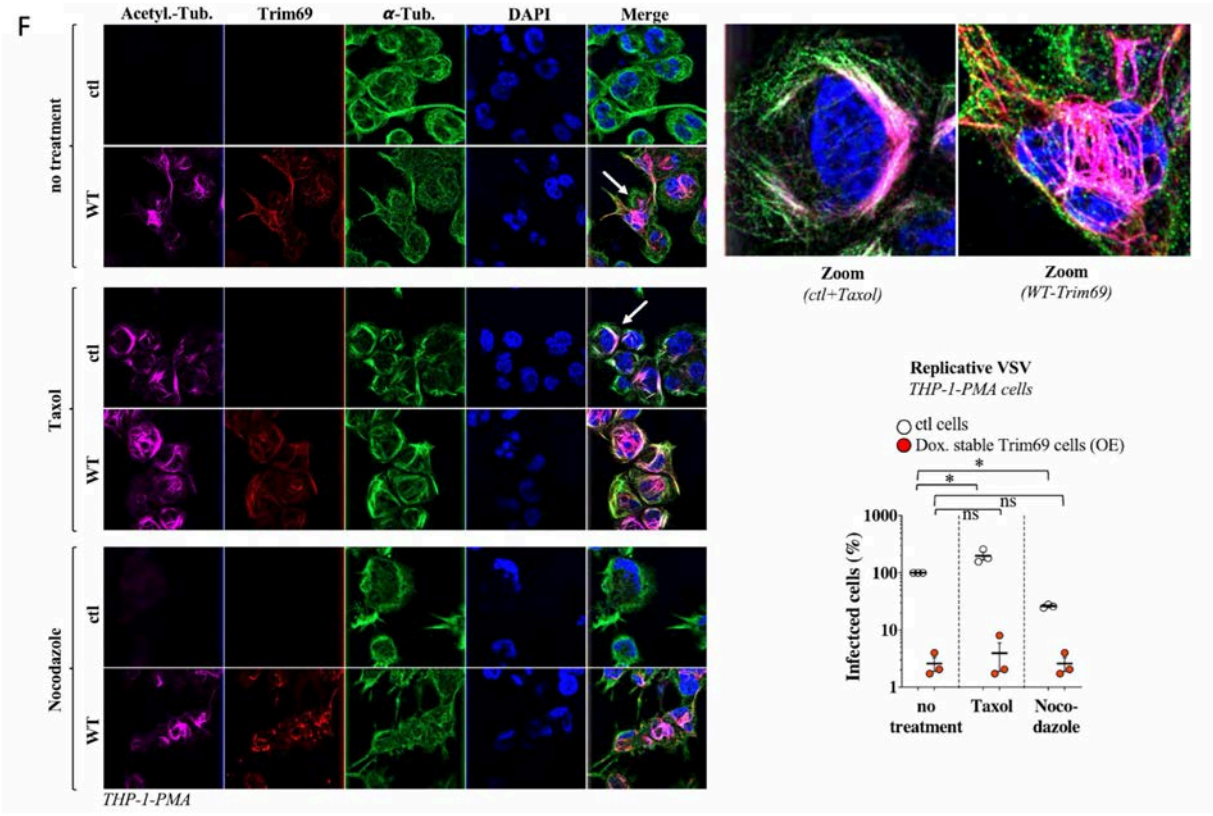

Figure 30. Trim69 is a novel and key mediator of IFN-I induced microtubule stabilization. *A) Representative confocal microscopy pictures and 3D reconstruction of the intracellular distribution of Trim69 in HEK293T and THP-1-PMA cells expressing Trim69 either upon transient DNA transfection (HEK293T) or upon lentiviral-mediated gene transduction (THP-1 and Calu-3). B) Distribution of Trim69 with antibodies recognizing endogenous α-tubulin or its acetylated form in the indicated cell types. Arrows indicates the cell zoomed on the right panels. C) Primary blood monocytes, macrophages, dendritic cells (DCs) as well as PH1/IL2 activated PBLs were stimulated or not with 1.000U/mL of IFNα for twenty-four and forty-eight hours prior to fixation and confocal microscopy analysis. Representative cells at 24 or 48 hours are presented here. Given the large differences in cell size, the pictures do not use the same scale. D) as in B in THP-1-PMA cells either control (wild-type) or in which Trim69 was either overexpressed or knocked out (OE and KO, respectively). Pictures present typical results obtained in >3 independent experiments in over 50 cells examined per condition. E) Distribution of Trim69 with antibodies recognizing endogenous α-tubulin or its detyrosined form in the indicated cell types and WB analysis of acetylation and detyrosination. F) Effects of Taxol and Nocodazole on the phenotypes driven by Trim69. THP-1-PMA cells expressing or not Trim69 stably were treated for twenty-four hours prior to infection with Taxol or Nocodazole (20 and 33 μM, respectively), prior to either confocal microscopy or VSV viral challenge and flow cytometry analysis. The panels present typical results obtained with a particular zoom on cells relevant here to determine whether Taxol and Trim69 exert similar or distinct programs of MTs stabilization. The graph presents Avg and SEM of three independent experiments. * and ns; statistically significant, or non-significant differences between the indicated conditions, following an ordinary one-way Anova with Tukey's multiple comparisons test.*

To put this observation in the context of IFN-I responses, we determined whether microtubule stabilization could be observed in response to IFN-I in different primary blood cells (**Figure 30C**). Stimulation of primary blood monocytes as well as of monocyte-derived macrophages and dendritic cells (DCs) led to a pronounced upregulation of stable microtubules within 24-48 hours (monocytes>macrophages>DCs). In contrast, such accumulation was not observed in activated primary lymphocytes. Overall, these results indicate that IFN leads to a program of microtubule stabilization that may be particularly important for antiviral responses in cells of myeloid origins.

To determine the role that Trim69 may play in this program, we used THP-1, cells of myeloid origins more amenable to genetic manipulation. In control cells, stable MTs were present at low levels in the absence of IFN stimulation, but they increased over time following IFNα stimulation similarly to what was observed in primary macrophages (**Figure 30D**). As expected from our previous observations, expression of Trim69 (OE) increased the basal levels of stable microtubules accumulation and this was further stimulated by IFNα. However, the accumulation of stable microtubules was severely diminished in Trim69 KO cells stimulated with IFNα, indicating for the first time that the accumulation of stable microtubules is an integral part of the antiviral IFN response and that Trim69 plays an instrumental role in this program. Quantification of stable MTs was carried out on a per cell basis and is provided in **Figure 31**.

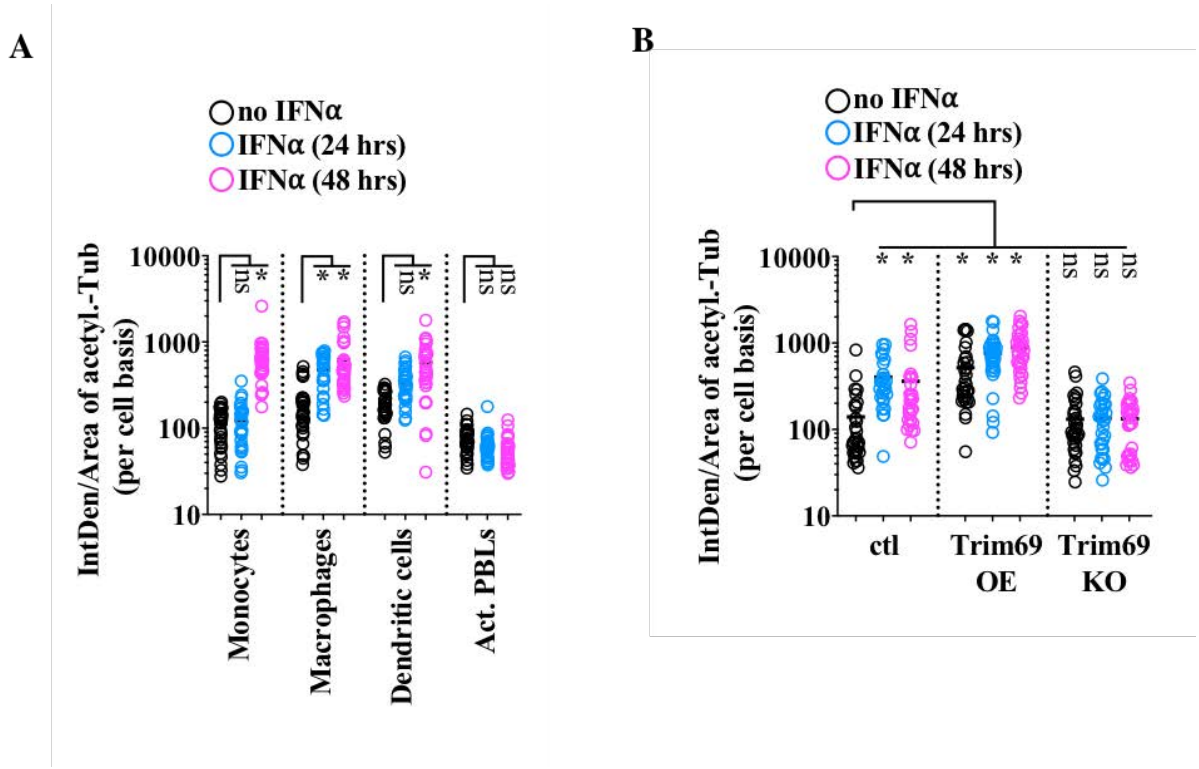

Figure 31. Per cell stable MTs quantification of the samples presented in Figure 30. *The graph presents the quantification of the amount of stable tubulin on a per cell basis (Integrated Density weighted for area, IntDen/area) calculated on 30 cells per condition/time point. * and ns, indicates statistically significant, or non-significant, following an ordinary one-way Anova with Tukey's multiple comparisons test, as indicated.*

Trim69 directly associates to microtubules. To determine whether Trim69 could physically associate to microtubules, a microtubule polymerization/sedimentation assay (Schweiger et al., 1999) was performed on THP-1 cell lysates expressing or not Trim69. In this assay, tubulin is induced into polymerization upon incubation with GTP and Taxol and stabilized microtubules are then purified by ultracentrifugation, along with associated cellular proteins (scheme of **Figure 32A**). Accordingly, a large fraction of microtubules sedimented in the pellet fraction upon Taxol stabilization and, when present, Trim69 was also present in this fraction, indicating that Trim69 was indeed physically associated to microtubules (**Figure 32A**, fraction

P). To determine whether this association was direct, Trim69 was purified from bacteria as a fusion protein with the glutathione-S-transferase protein (GST). Commercially available and pure tubulin was then incubated in the presence of GTP and Taxol before binding to either GST or GST-Trim69 (**Figure 32B**). Under these conditions, Trim69 interacts with microtubules, indicating that Trim69 interacts directly with microtubules.

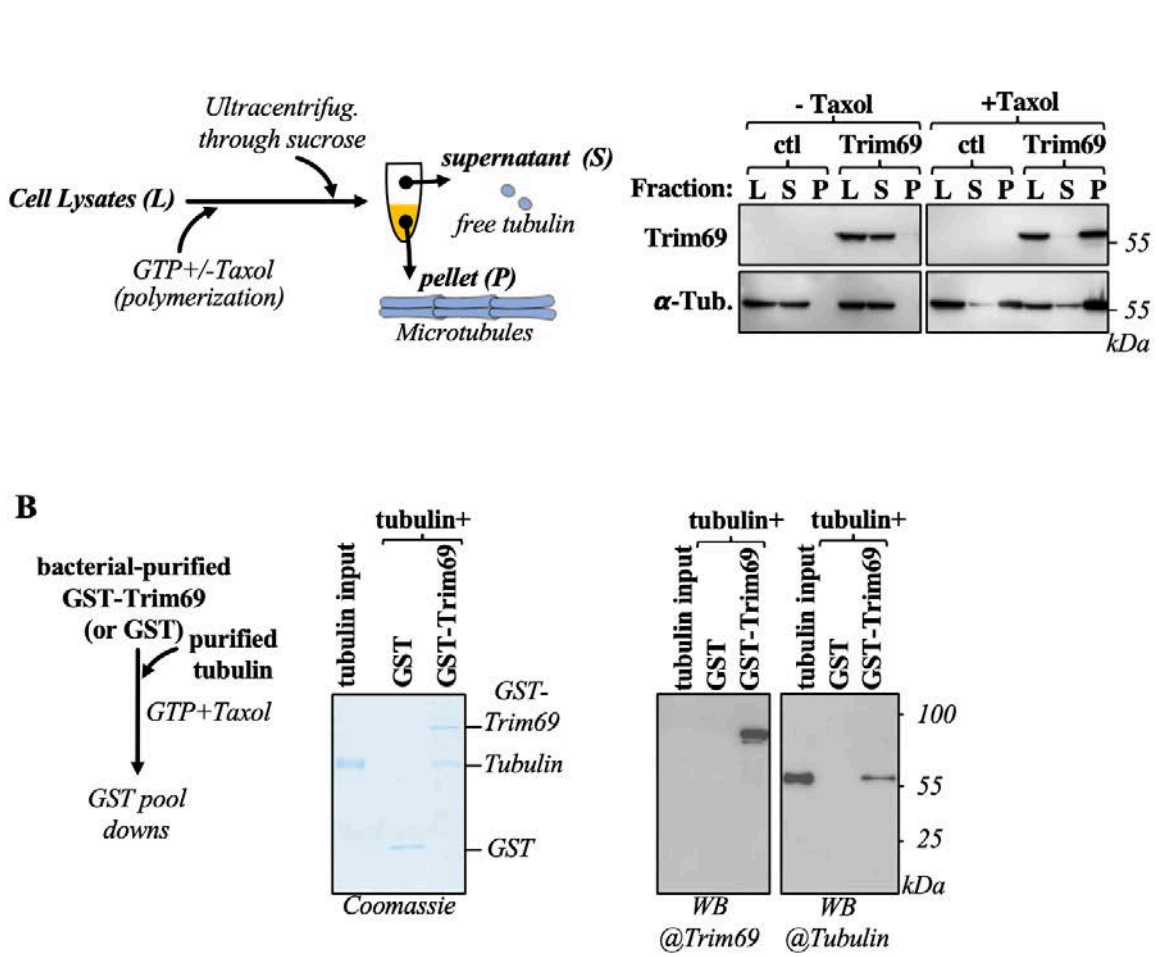

Figure 32. Trim69 associates directly to microtubules. *A) Schematic representation of the microtubule sedimentation assay used. Briefly, the cytosolic fraction of THP-1-PMA cells stably expressing or not Trim69 was harvested and free cellular tubulin polymerization and stabilization was induced by incubation with GTP and Taxol. Microtubules and associated cellular proteins were then purified through a sucrose gradient prior to WB analysis. B) Direct binding between tubulin and Trim69, was assessed by using commercially available pure tubulin and GST-Trim69 purified from bacteria. The Coomassie and WB panels are representative of 3 independent experiments.*

Stable microtubule formation is key to the antiviral effects of Trim69. Five different isoforms issued from alternative splicing have been recently described for *trim69* (from the *wild-type* A to E) that contain extensive deletion in domains that are normally important for Trim family members functions. These isoforms were therefore expressed in THP-1-PMA cells prior to confocal microscopy analysis, or viral challenge with VSV (**Figure 33A** and **33B** and **Figure 34** for WB analysis and separated IF channels). Under these conditions, isoforms B to E lost their ability to stimulate stable MTs and to protect target cells from viral challenge. Two additional mutations were then introduced in Trim69: mutations in two key cysteine residues that destabilize the RING domain (C61A/C64A), in addition to the deletion of the PRY-SPRY domain that in certain Trim members represents the domain of interaction with cellular partners (ΔP-SPRY, **Figure 33A** and **33B** and **Figure 34,** as above). Similarly, to what was observed with the Trim69 isoforms, both mutants lost their ability to drive stable MT accumulation and both were unable to prevent viral infection. To gather further insights on the ability of the different mutants not only to stimulate stable microtubules, but also to co-localize with α-Tubulin, the Pearson's coefficients between these two markers were determined (**Figure 33A)**. Co-localization with α-Tubulin was lost for all mutants, suggesting that they have likely lost their ability to associate to microtubules in the first place.

Overall, these results indicate that the antiviral effects of Trim69 are intimately linked to its ability to drive the accumulation of stable MTs.

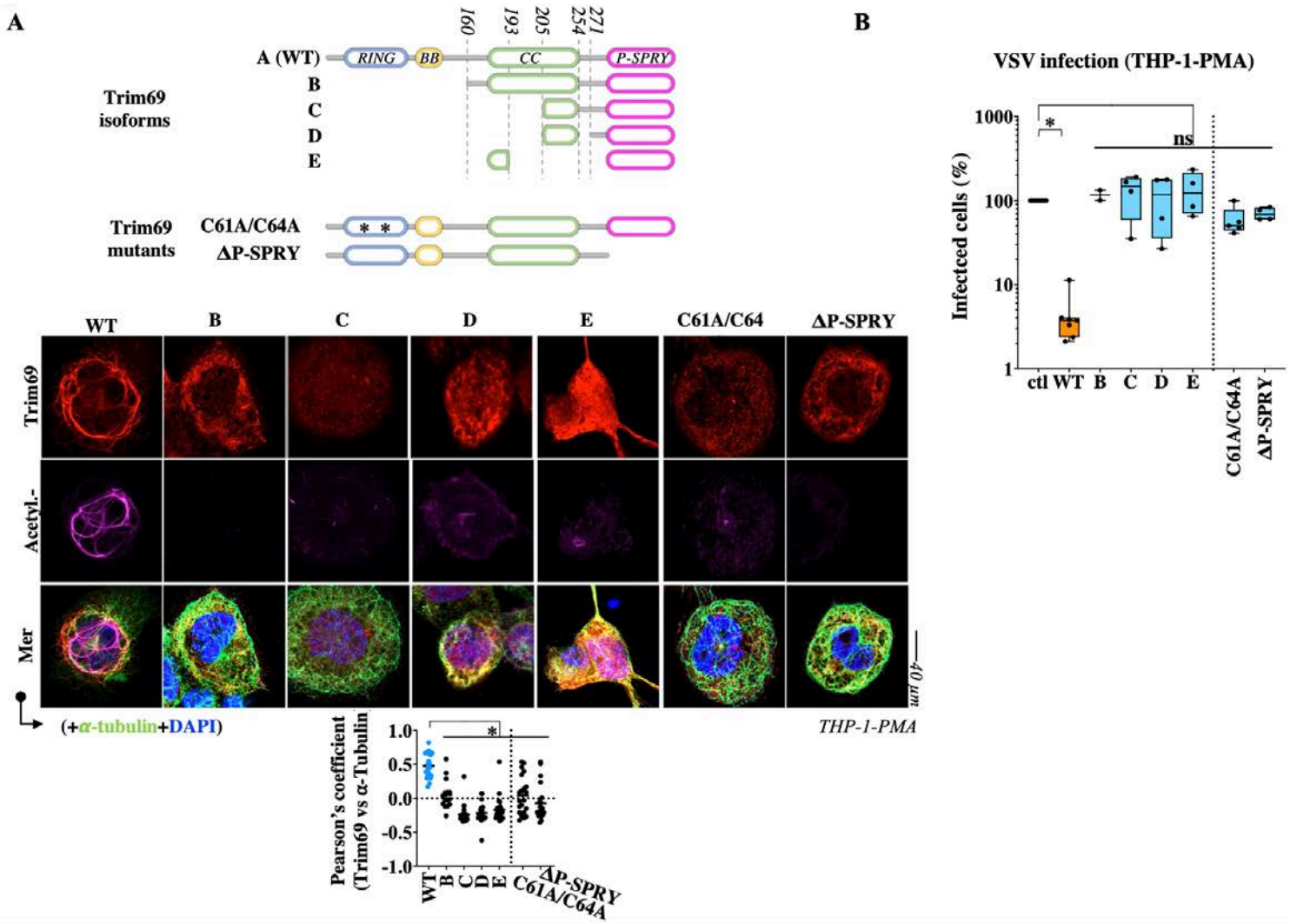

Figure 33. The ability of Trim69 to stimulate stable MTs is intimately linked to its antiviral abilities. *A) Schematic presentation of Trim69 domains, isoforms and mutants used here. Mutants were evaluated for their ability to stimulate stable MTs formation in THP-PMA cells stably expressing them after lentiviral-mediated gene transduction and pool selection by confocal microscopy. The graph presents Pearson's coefficients calculated between Trim69 mutants and α-Tubulin in 24 to 15 cells. *, indicates statistical significant differences between each mutant and WT, following an ordinary one-way Anova with Dunnett's multiple comparison test. Representative WB panels of the different mutants in THP-1-PMA cells is provided in the extended data Figure 10. B) Cells were also challenged with an MOI of 0.1 of VSV, prior to flow cytometry analysis eighteen hours later. Pictures display representative patterns obtained and the box and whiskers presents data obtained from 2 to 4 independent experiments. Ns and *, respectively non significant and p=0.0005 following an ordinary one-way Anova with Dunnett's multiple comparison test of the indicated samples over control.*

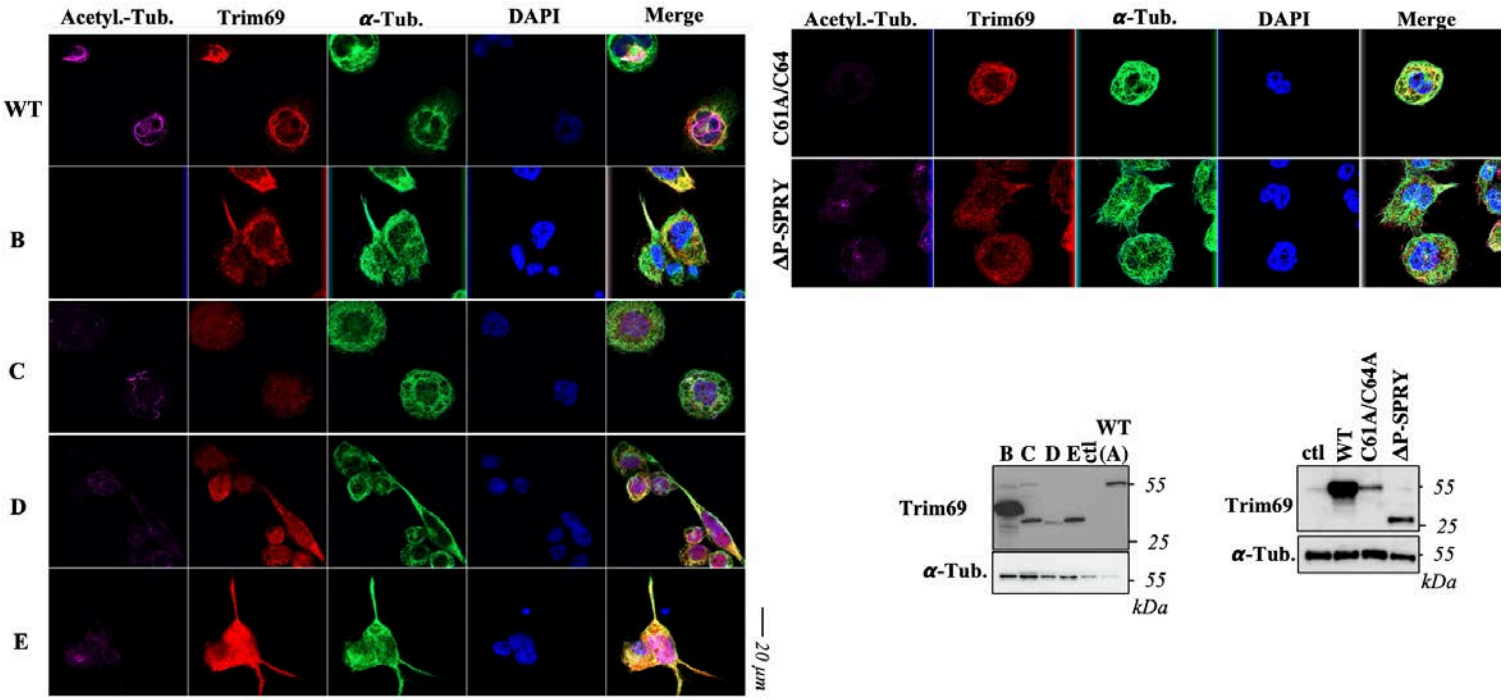

Figure 34. Complete confocal microscopy panels of the analysis presented in Figure 33 and WB of the different Trim69 mutants. *Separated channel panels, not presented in the main figure for lack of space, are presented here along with representative WB analysis of the different mutants*.

Induction of stable MTs, as well as antiviral functions are conserved in a non-human divergent primate Trim69 ortholog. To increase the primate sequences available for phylogenetic analyses and to obtain a more complete evolutionary perspective of the selective pressure on Trim69 (Malfavon-Borja et al., 2013; Rihn et al., 2019), we *de novo* sequenced Trim69 from two additional monkey species, L'Hoest's monkey (*Cercopithecus l'hoesti*) and Cotton-headed tamarin (*Saguinus oedipus*) (**Figure 35A**), and we determined the evolutionary history of Trim69 inferred from 26 primate species and 22 simian species (**Figure 35A, 35B** and **Figure 36**). Additional species sequences and multiple methods to detect positive selection allowed us to confirm that Trim69 has been under adaptative evolution. The site-by-site analyses on the simian alignment allowed us to identify eight sites under positive selection distributed through the protein domains, with residues 158, 246 and 299 identified by several methods (**Figure 35A-C** and **Figure 36**). Because the soTrim69 was one of the most divergent simian sequences from hTrim69 (88.6% identity; **Figure 35B**) and differed at 7/8 sites under positive selection, we cloned the soTrim69 gene to determine whether it exhibited distinct, or conserved, functionalities compared to its human counterpart. Stable THP-1-PMA cells expressing each of them were challenged with the indicated viruses prior to analysis by WB, confocal microscopy and flow cytometry to quantify the extent of infection (**Figure 35D**). Under these conditions, soTrim69 was capable of strong induction of stable microtubule formation and exhibited equivalent antiviral properties than hTrim69 upon challenge with VSV or distinct retroviruses. Overall, these results indicate that the main functional properties are maintained in the soTrim69 orthologue underscoring their importance in the antiviral

properties of Trim69. Our data also indicate that retroviruses are unlikely to have driven positive selection in Trim69.

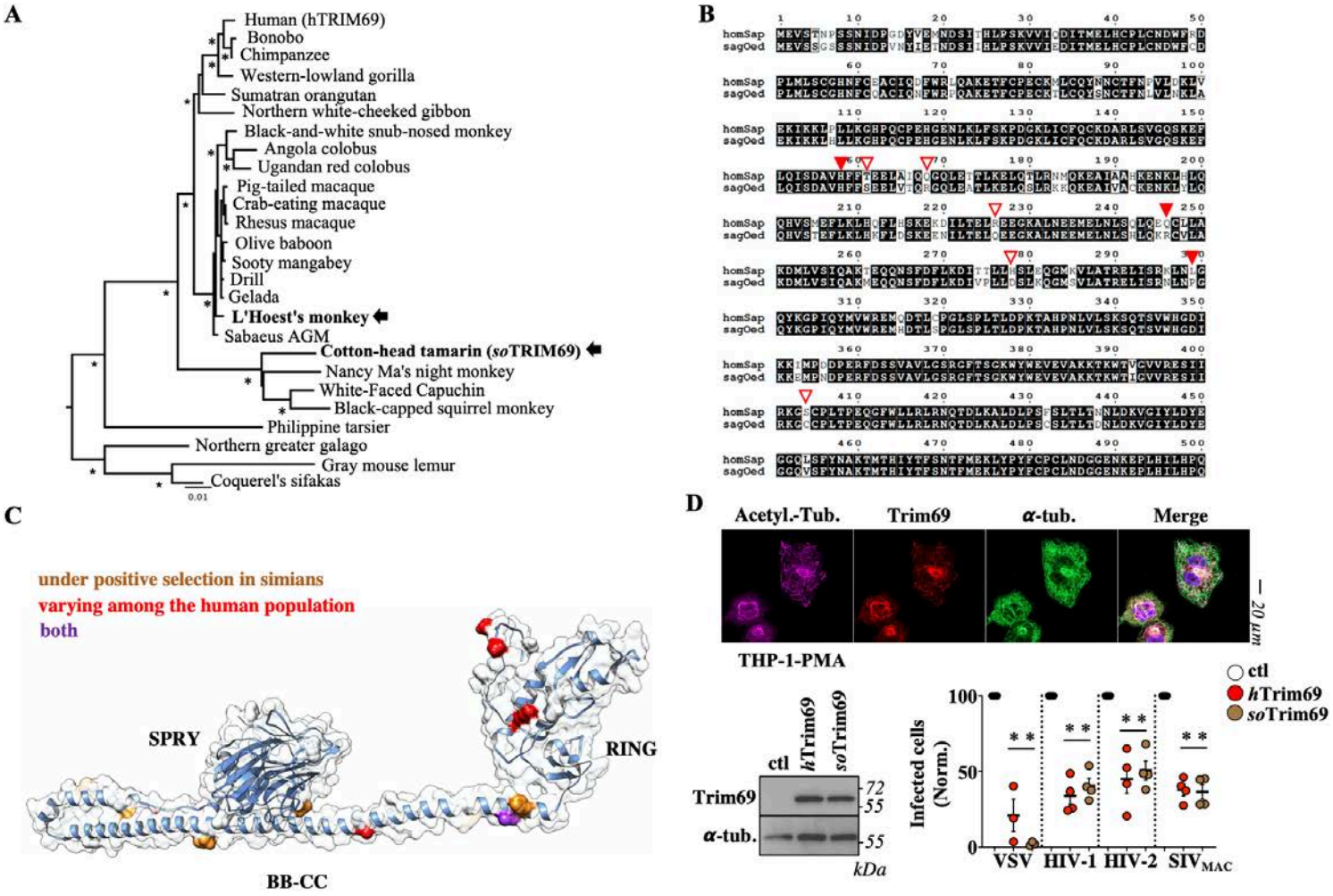

Figure 35. Trim69 exhibits signatures of positive selection during primate evolution and the divergent Trim69 orthologue from Saguinus oedipus (soTrim69) also inhibits viral infection and drives microtubule changes. *A) Phylogenetic tree of primate Trim69, including two newly sequenced orthologs from L'hoest's monkey and Cotton-head tamarin (arrows). PhyML was run with GTR+I+G model and 1,000 bootstrap replicates for node statistical supports (asterisks represent values above 700/1000). Sequence references are shown in Figure 36A. B) Amino acid alignment of human and cotton-headed tamarin Trim69 (88.6% identity). Representation with ESPript*(Robert & Gouet, 2014). *Sites under positive selection are highlighted with red triangles (plain triangles, sites identified by >2 methods; open triangles, sites identified by one method). C) Amino acid positions undergoing positive selection or allelic variations in the human population are presented in the modeled 3D structure of human Trim69. D) Functional equivalency of the soTrim69 orthologue with respect to the induction of stable microtubule formation and to antiviral activities against VSV (n=3) and primate lentiviruses (n=4). Experiments present Avg and SEM. *, p<0.05 following a two-tailed Student t test between Trim69 proteins and respective controls.*

A

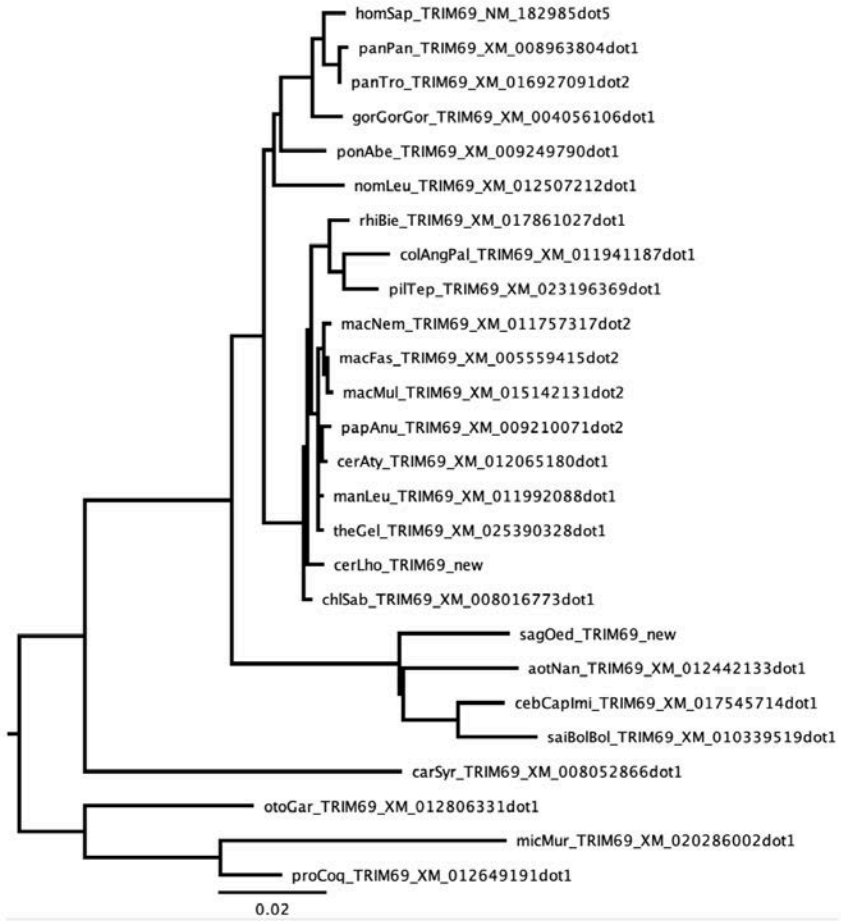

B

Sequence alignment				BUSTED		MEME (p<0.1)	FUBAR (PP>0.9)	Bpp M1vsM2				Bpp M7vsM8				Codeml M1vsM2			Codeml M7vsM8		
Gene	Order	Size	n sp.	PS?	p value	PSS	PSS	PS?	p value	ω (PS)	PSS	PS?	p value	ω (PS)	PSS	PS?	p value	PSS	PS?	p value	PSS
TRIM69	primates	511	26	Y	0.0487	188, 274, 278, 288, 316, 332, 333, 364, 365, 437	-	N	0.1783	2.08	**246**	N	0.0796	3.12	**246**	Y	0,0119	-	Y	0.0116	**246**
TRIM69	simians	500	22	N	0.5	**158, 246**, 278	161, 169, **158**, 226, **246**	N	1	1.002	-	N	0.991	0	-	Y	0,0002	**158, 246, 299**	Y	0.0002	**158, 246, 299**, 404

Figure 36. ***Trim69 evolutionary analyses.*** *A) Phylogenetic tree of primate Trim69 corresponding to Figure 34A, with the NCBI reference of the sequences and the species nomenclature (three first letters from genus and three first letters from species). The tree includes the two newly sequenced orthologs from L'hoest's monkey and Cotton-head tamarin ("new"). B) Results of the comprehensive positive selection analyses of primate (top row) and simian (bottom) TRIM69 sequences: BUSTED, MEME, FUBAR from HYPHY/Datamonkey.com, M1vsM2 and M7vsM8 from Bpp and PAML Codeml. Legend details: Size, length of the codon alignment; n. sp., number of species in the alignment; PS?, if the gene is under positive selection: Y, yes, N, no; p value, supporting a model under positive selection; PSS, positive selection sites; -, no site identified; omega (PS) in bpp, corresponds to the omega value in the positive selection class (dN/dS>1).*

Discussion

Thanks to the laboratory's previous efforts in a complex genetic screen to identify novel mediators of the negative effects of IFN-I against HIV-1 in macrophage-like cells an interesting set of genes has been retrieved. After preliminary validation, the main body of my thesis consisted in focusing on Trim69. Very little was known at the time on Trim69 which a first study documented to inhibit Dengue virus (Wang et al. 2018). This work was contradicted by following studies that however described Trim69 as a potent antiviral factor against VSV (Rihn et al. 2019; Kueck et al. 2019). Fortunately, the mechanism of inhibition was not described. In my work, I found that Trim69 is first of all a broad virus inhibitor as it inhibits not only lentiviruses, but also VSV and SARS-CoV2 which represent negative and positive polarity RNA virus models. The magnitude of inhibition varies according to the combination between virus and cell type which is not surprising. In primate lentiviruses, viral inhibition is observed in THP-1 cells differentiated into macrophage-like cells, also in agreement with the fact that the original screen that led to Trim69 was carried out to identify genes that modulate HIV infection in myeloid cells. This is not unprecedented as other cellular factors inhibit HIV-1 in a cell type specific manner (for example SAMHD1, or APOBEC3A (Berger, Durand, Fargier, et al., 2011; Laguette et al., 2011).

Viral inhibition occurs during the early phases of the different viruses' life cycle, albeit with slight differences. In the case of HIV-1, inhibition occurs at reverse transcription, after entry of viral complexes into the cell and SARS-Cov2 seems to follow the same inhibitory path, with no measurable defects in virus entry, but an early defect in viral RNA replication. Instead, in the case of VSV a small but non negligible defect can be observed at the step of entry, which

is followed by a first major detectable defect occurs during pioneer transcription, in line with a previous report (Kueck et al., 2019).

VSV is a negative-strand RNA virus, and undergoes an obligate round of primary transcription after cell entry that is required for the translation of P, N and L proteins that in turn ignite viral RNA replication (Dietzgen et al., 2017). Given that translation from primary transcripts is required for viral RNA replication, using the translation inhibitor cycloheximide (CHX) allow to distinguish primary transcription from overall RNA replication. Contrarily to what was observed for HIV-1, TRIM69 effect both of entry and pioneer transcription. While in SARS-CoV2, a positive-strand RNA virus and as such its genome can be directly translated in viral proteins (V'kovski et al., 2021) and in this case no major defects are observed at entry, but post entry by six hours post infection. Overall, Trim69 inhibits the early steps of viral replication of different viruses at slightly distinct steps: at a post entry step that affects the efficiency of reverse transcription and of viral RNA replication in the case of lentiviruses and of the SARS-CoV2 Coronavirus, and at both entry and post entry events in the case of VSV.

Although it remains formally possible that Trim69 targets viral components, the very diversity of viruses examined here lends support to the hypothesis that Trim69 modifies the cellular environment in a manner that is preclusive to viral infection. The hypothesis we privilege is that Trim69 interferes with the movements of viral complexes along microtubules. Indeed, HIV-1 viral cores have been visualized as sliding along microtubules with inward rates of 1 μm/sec consistent with Dynein-dependent movement (Arhel et al., 2006; McDonald et al., 2002) and adaptor proteins of this complex have been involved in this association (for example the Bicaudal D2 adaptor, BICD2 (Carnes et al., 2018; Dharan et al., 2017). Interestingly,

interference with dynein-dependent movement has been associated to an early reverse transcription defect (Pawlica & Berthoux, 2014) which is consistent with the defects observed here for Trim69. In the case of *Rhabdoviridae*, the phosphoprotein P, which is part of the viral nucleoprotein complex along with the nucleocapsid protein (N) and the RNA polymerase (L), does interact with the dynein light chain 8 (LC8) (Jacob et al. 2000; Tan et al. 2007; Mebatsion et al. 2001) and Coronaviruses accumulation in the perinuclear region that evolves in double membrane vesicles (DMVs) is also influenced by dynein (Hou et al., 2020; Hagemeijer et al. 2010; Pasick, Kalicharran, and Dales 1994). It is thus possible that dynein transport is inhibited in the presence of stable microtubules that are decorated with Trim69.

One possibility to test this hypothesis would be to carry out infections in the presence or absence of dynein specific inhibitors as Ciliobrevin, often used to this effect, as well as through genetically using silencing of dynein components. If the effects of Trim69 pass through the inhibition of Dynein, we could expect that the drug will reproduce the infectivity defects of Trim69.

Importantly, I found that expression of Trim69 induces the formation (or drastic accumulation) of stable microtubules, which are distinct from the more dynamic pool of MTs and acquire distinguishing posttranslational modifications, notably detyrosination and acetylation. The presence of Trim69 leads to the accumulation of MTs that accumulate both modifications and we have used often one or the other in our confocal microscopy experiments. Acting as specialized tracks for vesicle and macromolecular transport, their formation is regulated by the end-binding protein, EB1, which recruits proteins that stabilize MTs (Gurland & Gundersen, 1995).

The fact that an antiviral factor acts by stabilizing MTs may seem in contradiction with reports indicating that viral infection can also lead to the induction of stable MTs. Indeed, several viruses have been described to induce stable MTs formation: Herpesviruses (Elliott & O'Hare, 1998; Frampton et al., 2010; Naranatt et al., 2005); Influenza virus (Husain & Harrod, 2011); Hepatitis E virus (Kannan et al., 2009); Adenovirus (Warren & Cassimeris, 2007; Yea et al., 2007) as well as HIV-1 (Mitra et al., 2020; Sabo et al., 2013; Santos da Silva et al., 2020).

However, first some studies describe the accumulation of stable MTs in cells supporting active viral spread and infected for prolonged periods of time. Second, in other studies the functional importance of stable MT formation remains unclear. Thus, MT stabilization can be induced by viruses for a number of purposes and at different time during viral replication not directly related to the early phases during the virus life cycle I describe here. In addition, according to our data this could even represent a cellular IFN response to viral infection, which is often not controlled.

However, there are cases in which MT stabilization is associated to a pro-viral functionality. This seems to be the case for HIV-1 in which viral capsids that enter target cells induce prompt MT stabilization and mimic cellular cap-loading proteins to promote their loading onto MTs and their dynein-dependent transport towards the nucleus (Mitra et al., 2020; Sabo et al., 2013; Santos da Silva et al., 2020).

It is therefore counterintuitive that IFN may induce a program of MT stabilization via Trim69, as this particular pool of MTs exhibit higher stability and higher cargo trafficking propensity with respect to the dynamic pool of MTs (Janke and Chloë Bulinski 2011; Li and Gundersen 2008).

In my mind, this dichotomy is however only apparent. First, while it is true that stable MTs can be preferentially used for cargo transport, the initial step of cargo loading is instead highly inefficient when it occurs on microtubules that are already detyrosinated (i.e. stable) (McKenney et al., 2016). As such, it is easy to envision that according to the timing at which microtubules become stabilized with respect to virus entry, MT stabilization can lead to either pro- or anti-viral outcomes.

Second, while stable MTs are often considered as a single homogeneous entity, the existence of several post-translational modifications on MTs, as well as the existence of numerous MT-bound factors, is likely to result in a far more complex functional heterogeneity of microtubules. In line with this contention, our study indicates that as part of an antiviral response, Trim69 starts a program of microtubule stabilization that leads to structures whose functionality is markedly antiviral.

Trim69 binds directly to MTs, but contrarily to other members of the Trim family we could not identify a C-terminal subgroup one signature (COS domain), a 60 amino acid stretch that mediates MT binding in certain Trim family members (Short & Cox, 2006b). I then show that both its RING and PRY-SPRY domains are required for the antiviral activities of Trim69, as well as for microtubule stabilization. A most plausible model would therefore be that Trim69 associates to microtubules and that contacts relevant substrates via its PRY-SPRY domain leading to their degradation. However, mutations in the RING domain can also interfere with Trim homodimerization and the importance of the E3-ubiquitin ligase activity in the functions of Trim69 is debated (Wang et al. 2018; Kueck et al. 2019).

Trim69 could lead to the accumulation of stable microtubules in different manners. First, it could inhibit their depolymerization rather than promote their accumulation. This remains possible, although in our experiments the effects of Trim69 are much stronger than Taxol which is a known MTs stabilizing agent. As such we believe that Trim69 really works by leading to a true de novo accumulation of stable microtubules. How will be the subject of following studies. We can hypothesize that Trim69 can simply multimerize on MTs and by this stabilize them enough time so that key markers of stable MTs accumulate on them. Alternatively, we can imagine that Trim69 binds MTs and through its domains interact with cellular proteins that in turn act normally on MTs dynamics. Acetylation and detyrosination are modifications that involve αTAT1 and the VASH1 complex which are in turn regulated in manners not completely understood. One possibility is that Trim69 acts on proteins that regulate αTAT1 and VASH1 and leads to their accumulation. Given that Trim69 is an Ubiquitin ligase it is possible that Trim69 induces the degradation of such proteins. As such, one possibility would be to determine whether the protein levels of αTAT1 and VASH1 are increased in the presence of Trim69. Alternatively, proteomic studies should be carried out to identify more directly Trim69 co-factors. Certainly, how Trim69 leads to MT stabilization will be the next question to address for the lab.

Finally, three studies including the present one have accumulated evidence of ongoing genetic conflict in primate Trim69 (Malfavon-Borja et al., 2013; Rihn et al., 2019), as well as of polymorphism in the human population. Using a very divergent simian Trim69, our results seem to exclude Lentiviruses that have invaded primates as main drivers of this selective pressure. However, Trim69 has been described to physically interact with the P protein of VSV

and with the NS3 protein of Dengue virus (Wang et al. 2018; Rihn et al. 2019; Kueck et al. 2019), suggesting that viral antagonists of these or of other viral families that remain to be discovered may have exerted a genetic pressure on Trim69.

Overall, in a panorama filled with positive cofactors at the level of cytoskeleton, Trim69 represents for the moment the first antiviral factor that opposes viral infection by regulating microtubule dynamics. Given the fact that these structures influence several aspects of the cellular physiology, these findings may bear implications that extend beyond viral infection.

Methods and materials

Cells

Human embryonic kidney HEK293T cells (ATCC cat. CRL-3216), monocytic THP-1 cells (ATCC cat. Cat# TIB-202) and epithelial lung Calu-3 cells (ATCC cat. HTB-55) were respectively maintained in complete DMEM, RPMI-1640 or MEM media and 10% Fetal Calf Serum (FCS, Sigma cat. F7524). THP-1 cells media was also supplemented with 0.05 mM β-mercaptoethanol (Euromedex, cat. 4227-A) and 10 mM HEPES (Sigma, cat. H0887) and macrophage-like differentiation was induced upon a twenty-four hours treatment with 100ng/ml of phorbol 12-myristate 13-acetate (PMA) (Sigma cat. P1585). Calu-3 cells media was instead supplemented with a 1x final concentration of non-essential amino-acids (Sigma cat. M7145) and sodium pyruvate (Gibco cat. 11360-039).

Primary blood monocytes and lymphocytes were purified from blood leukopacks of healthy and anonymous donors, as described (Berger et al. 2011). White leukocytes were first separated through a Ficoll gradient and then monocytes and lymphocytes enriched fractions were harvested at the interface and bottom of a Percoll gradient, respectively. Monocytes were further purified by negative depletion (monocyte isolation kit II, catalogue n° 130-091-153, Miltenyi; purity ≥ 90%) and when indicated, they were differentiated in either macrophages or dendritic cells (DCs) upon incubation for 4 to 6 days in complete RPMI-1640+ 10%FCS with either human Macrophage-Colony Stimulating Factor (M-CSF at 100 ng/mL; Eurobio, cat. 01-A0220-0050), or with Granulocyte-Macrophage-Colony Stimulating Factor and interleukin 4 (Berger, Durand, Goujon, et al., 2011) (GM-CSF and IL4, at 100 ng/mL each; Eurobio, cat. PCYT-221 and PCYT-211). PBLs were instead used without further purification. In

this case, cell stimulation was carried out for twenty-four hours with 1 μg/mL of phytohemagglutinin (PHA, Sigma) plus 150U/mL of interleukin 2 (Eurobio, cat. PCYT-209). Unless otherwise specified, cells were incubated for twenty-four hours with 1,000 U/mL of human IFNα2 prior to use (Tebu Bio, cat. 11100–1). IFNβ was similarly used at 500 U/mL (R&D systems cat. 8499-IF-010).

Antibodies

The following primary antibodies were used for WB, or confocal microscopy: mouse monoclonal antibodies; anti-α-Tubulin, anti-Flag (Sigma cat. T5168, cat. F3165, respectively) and anti-GM130 (BD biosciences cat. 556019 and cat. 610823); rabbit polyclonal antibodies: anti-GM130 (Abcam cat. Ab52649); anti-detyrosinated tubulin (Millipore cat. Ab3201) and anti-acetyl (K40)-α-tubulin (Abcam cat. ab179484) that were used interchangeably to label stable microtubules; goat anti-Flag polyclonal antibody (Biotechne cat. NB600-344). The following secondary antibodies were used for WB: anti-mouse, anti-rabbit IgG-Peroxidase conjugated (Sigma, cat. A9044 and cat. AP188P); while the following ones were used for confocal microscopy: donkey anti-rabbit IgG–Alexa Fluor 594 conjugate and donkey anti-mouse IgG–Alexa Fluor 488 conjugate (Life Technologies, cat. A-21207 and cat. A-21202) donkey anti-rabbit IgG–Alexa Fluor 555 conjugate (Life Technologies, cat. A32794); donkey anti-rabbit IgG–Alexa Fluor 647 conjugate (Life Technologies, cat. A-21447); donkey anti-goat IgG–Alexa Fluor 546 conjugate (Life Technologies, cat. A-11035).

Plasmid DNAs, retroviral vectors and viruses

Full length Trim69 (gene ID: 140691, isoform A) was obtained by gene synthesis and codon optimization (Genewiz) and it was cloned with an N-terminal Flag- tag in pRetroX-tight, a murine leukemia virus (MLV)-based retroviral vector that can be used for the generation of stable cells in which the expression of the gene of interest is under the control of doxycycline (dox. Ozyme, cat. 631311). Trim69 mutants were generated by standard molecular biology techniques. DNAs coding for several cellular markers were obtained through Addgene and in particular: mCherry-Actin-C-18, mEmerald-CLIP170-N-18 and mCherry-ATG3-C-18 were gifts from Michael Davidson (Addgene cat. 54967, 54044 and 54993) (Rizzo et al., 2009) *;* mCh-alpha-tubulin was a gift from Gia Voeltz (Addgene cat. 49149), while pcDNA-D1ER was a gift from Amy Palmer & Roger Tsien (Addgene cat. 36325). For presentation simplicity, the cellular markers cited above and Trim69 were pseudocolored in green and red, respectively, in the qualitative colocalization analysis presented in **Figure 28**.

Single round of infection competent HIV-1, HIV-2 and SIV_{MAC} lentiviruses have been described before (Goujon et al., 2007). Briefly, viruses were generated upon transient transfection of HEK293T cells with DNAs coding three components: the structural Gag-Pro-Pol protein of the virus of interest, the envelope protein (in our case either the G protein of the Vesicular Stomatitis Virus, VSVg, or the HIV-1 R5 Envelope, JR-FL) and a mini-viral genome containing a reporter gene expression cassette (CMV-GFP and for the HIV-1 screening the Firefly luciferase (obtained from Didier Negre, CIRI-Lyon, France). An MLV- or an HIV-1-based vector system were used for the generation of stable cell lines overexpressing Trim69 under the control of

doxycycline (OE), or to generate *trim69* knockout cells (KO) by CRISPR/Cas9-mediated gene targeting, respectively.

Replicative VSV virus (Indiana serotype) bearing a GFP reporter transcription unit inserted between M and G have been described before (Ostertag et al., 2007). Replicative SARS-CoV2 virus (Wuhan strain, (Xie et al., 2020)) bearing the mNeonGreen reporter inserted into the ORF7 was obtained from Pei-Yong Shi from the University of Texas Medical Branch, Galveston, TX, USA.

De novo sequencing of cotton-headed tamarin (Saguinus oedipus) and L'Hoest monkey (Cercopithecus l'hoesti) Trim69. First, simian peripheral blood mononuclear cells (PBMCs) were isolated using Histopaque 1077 from leftover blood samples (approximately 1 ml, from blood drawn for health purposes) from a L'Hoest monkey (Old World monkey *Cercopithecus l'hoesti*) hosted at the Zoo de Lyon, France (Guillaume Douay). Second, B92a cells (a gift from Branka Horvat, CIRI Lyon) from cotton-headed tamarin (New World monkey *Saguinus oedipus* were maintained in Dulbecco's modified Eagle's medium (DMEM) supplemented with 10% fetal calf serum. Total RNA was extracted from cells following the manufacturer's instructions (Macherey-Nagel NucleoSpin RNA cat. 740956). Reverse transcription was performed using SuperScript III reverse transcriptase (Thermo Fisher cat. 18080) with random hexamers and oligo(dT). Single-round PCR was performed using Q5 high-fidelity DNA polymerase (NEB; M0491) following the manufacturer's instructions, with primers targeting the UTRs: T69-F1: 5'- TCATGCTCTGAGYYCATTCC, and T69-R1: 5'- TCAATACCTCTTTAATAWCACTCTG. The sequences of the TRIM69 gene from cotton-headed monkey (soTrim69) and from L'Hoest

monkey (cerLhoTrim69) are available at Genbank under accession numbers ON745601 and ON745600, respectively. The coding region of soTRIM69 was subsequently cloned in the pRetroX-tight using standard molecular biology techniques.

Viruses production and infections

Single round of infection competent HIV-1, SIV_{MAC} or HIV-2 viruses were produced by calcium phosphate DNA transfection of HEK293T cells (Gag-Pro-Pol packaging construct, mini-viral genome and pantropic VSVg envelope: ratio of 8:8:4, for a total of 20 μg per 10cm dish). In the case of HIV-1 viruses bearing the HIV-1 JR-FL envelope, the ratio used was: 8:8:2: plus 0.5 of HIV-1 Rev to stimulate Env production). Supernatants were collected at forty-eight hours post transfection, syringe-filtered to remove cellular debris and virions were purified through a 25(w/v) sucrose cushion for 1h15min at 28.000 rpm. The number of infectious viral particles was determined by infecting HeLa cells with virus dilutions and by quantifying the number of green fluorescent protein (GFP)-positive cells obtained two-three days after by flow cytometry. The infectious titer equivalent of non-GFP coding viruses was determined against standards of known infectivity by exo-RT or p24 ELISA (Goujon et al., 2007).

VSV and SARS-CoV2 viral stocks were produced by infecting HEK293T cells (10cm plates) or VeroE6 cells (T125 flasks) and by harvesting cell supernatants obtained 18 to 36 hours later. Infectious titers were measured by limiting dilutions infections followed by flow cytometry analysis 18 hours post infection.

Infections were carried out with multiplicities of infection (MOIs) comprised between 0,1 and 5 depending on the viruses, as specified in the Figure legends. The percentage of infected cells

was determined at different times post infection, depending on the virus: retroviruses (two days); VSV (eighteen hours); SARS-Cov2 (two days). In all cases, infected cells were fixed and analyzed by flow cytometry on a FACSCantoII (Becton Dickinson, USA).

Generation of stable cell lines

Doxycycline-inducible stable cells overexpressing Trim69 were generated using the pRetroX-Tight system (Clontech), a murine leukemia virus (MLV) retroviral -based gene transduction system, as described earlier (Wu et al., 2019). Briefly, MLV retroviral vectors were produced by calcium phosphate DNA transfection of HEK293T cells with plasmids coding MLV Gag-Pro-Pol, the VSVg envelope and two pRetro-X based mini-viral genomes, the first bearing Trim69 under the control of the dox-inducible promoter and the second coding the transcriptional transactivator rtTA (ratio 8:4:4:4 for a total of 20 μg per 10cm dish). Virion particles in the cell supernatant were directly used for cell transduction followed by selection of cell pools thanks to the Puromycin (Sigma, cat. P8833) and G418 (Sigma, cat. G8168) resistance genes carried by the two constructs. Stable cell lines were freshly generated every two-weeks maximum.
CRISPR/Cas9 *trim69* KO pools of stable cells were generated by two successive rounds of gene transduction with Cas9 and CRISPR-bearing vectors (gift of Feng Zhang, obtained from Addgene cat. 52963 and cat. 52962). In this case, selection of pool cells was carried out thanks to the Blasticidin (Invivogen cat. ant-bl-1) and Puromycin (Sigma cat. P8833) resistance genes carried by the two vectors. Two guides were used as described in (Rihn et al., 2019). Two guides were cloned into the BsmBI site of LentiGuide-Puro by annealing/ligation of two overlapping oligonucleotides (up and down, respectively): Guide 1, nt 276-295 of coding

sequence, CACCGCAACCCTGTACTGGACAAGT and AAACACTTGTCCAGTACAGGGTTGC; Guide 2, nt 311-329 of coding sequence, CACCGAAGAAGTTACCCTTACTCAA and AAACTTGAGTAAGGGTAACTTCTTC. Effective gene editing was determined by PCR on genomic DNA using primers CACTTTCAAAGGAGAGATTATGTGC and GAGCAGTCTGGGCTTTCTAAT, cloning of the corresponding PCR fragment and sequencing of 10 individual clones.

Library details and screening procedure

The shRNA library originated from the Broad institute Genetic Perturbation platform and individual shRNA clones were purchased from Sigma in an pLKO or pLKO_TRC005 context (3 shRNA per genes for a total of 419 genes, list provided in the supplementary file). shRNA coding HIV-1 vectors were prepared in 96 well plates by ectopic transfection of HEK293T cells by calcium phosphate DNA transfection of 80 ng of Gag-Pro-Pol, 80 ng of the pool of the 3 shRNA coding constructs, plus 40 ng VSVg. Cycling THP-1 cells were transduced with three rounds of HIV-1 coding LVs preparations (daily), prior to puromycin selection (at 2.5 μg/mL). Cells were then counted, split in two and then differentiated for 24 hours with PMA prior to an additional 24 hours incubation period with or without 1.000 U/mL of IFNα. Cells were then challenged with an MOI equivalent of 0.5 of VSVg-pseudotyped HIV-1 virus coding the Firefly Luciferase reporter, prior to cell lysis and Luc analysis forty-eight hours later (Promega cat. E4530, according to the manufacturers' instructions). An IFN defect was calculated for each gene as a ratio of the Luc. activities measured in the no IFNα/+IFNα conditions, normalized to the average value obtained for all genes together. Retained changes were below/above 2.5, with a statistically significant Student t test value over control. Retrieved hits that led to either

a relieved or increased IFN defect were then recategorized as pro- or anti-viral proteins, according to their behavior in the no IFNα condition, as the IFN defect ratio is also influenced by this parameter. CD40 and TNPO3 were added as sentinel samples for routine control of silencing efficiency and effect under library screening conditions.

A secondary screen was performed to exclude primary hits whose silencing was likely to alter HIV-1 infection indirectly, by modulating IFN signaling. To this end, shRNA stable cells were differentiated with PMA and stimulated with 1.000 U/mL of IFNα. IP10 secretion in the supernatant was measured by ELISA, according to the manufacturer's instructions (R&D cat. DY266).

Phylogenetic and positive selection screen using DGINN

The Consensus CoDing Sequences (CCDS) were downloaded from the CCDS database (https://www.ncbi.nlm.nih.gov/CCDS/) using the CCDSQuery script provided with DGINN, with the exception of LILRA3 for which the coding sequence was manually retrieved from the NCBI databases (human sequence NM_006865) as no CCDS existed. In cases where multiple CCDS were referenced for one gene, the longest one was kept. We used the DGINN pipeline (Picard et al., 2020); available at: http://bioweb.me/DGINN-github) for the analyses in a two-step fashion. For the primate homologous sequence retrieval and phylogenetic analyses, we used the NCBI nr database limited to primate species, with otherwise default parameters (blastn e-value 10-4, identity 70% and coverage 50%, at least eight species for separation of orthologous groups). Alignments and phylogenetic trees produced during this first step were then used for positive selection analyses, according to different packages: BUSTED and MEME

from the Hyphy package (Pond et al., 2005); Codeml from PAML (Z. Yang, 2007) and Bio++ (Guéguen et al., 2013), all running codon substitution M1, M7 and M2, M8 models that do not and do allow codons to evolve under positive selection, respectively. BUSTED and MEME from the Hyphy package (Pond et al., 2005) to look for gene-wide and site-specific episodic positive selection. Genes were considered under positive selection for a BUSTED p-value < 0.05 and sites for a MEME p-value < 0.05. Codeml from PAML (Z. Yang, 2007) and Bio++ (Guéguen et al., 2013), were used to run codon substitution models M1, M2, M7 and M8. M1 and M7 are neutral models not allowing for positive selection and M2 and M8 are their pendant with a class allowing codons to evolve under positive selection. P-values derived from the likelihood ratio tests between the two models (M1 vs M2, M7 vs M8) were used to determine which model is a better fit for the data. Genes were considered under positive selection for $p < 0.05$ and sites for posterior probabilities (PP) > 0.95 (in the Bayes empirical bayes BEB test for Codeml M2 and M8, and in the PP test for bio++ M2NS and M8NS).

Phylogenetic and positive selection analyses of primate and simian TRIM69. The codon alignment of primate TRIM69 from the DGINN screen was retrieved, and new sequences from NCBI databases and from de novo sequencing were added. Codon alignments of primate TRIM69 sequences and simian-only TRIM69 sequences were performed using MUSCLE (Edgar, 2004) and manually edited, resulting in 26 and 22 included species, respectively. Phylogenetic analyses were performed with PhyML with a GTR+I+G model and 1,000 bootstrap replicates (Guindon et al., 2010). Positive selection analyses were performed in DGINN using the new codon alignments, as previously described. Additionally, FUBAR and MEME were run in

Datamonkey (Weaver et al., 2018) and sites with PP>0.9 and p<0.1 were considered under positive selection, respectively.

Analyses of the virus life cycle steps affected by Trim69

HIV-1 entry (Entry/ Uncoating assay based on core-packaged RNA availability and Translation system, EURT). This assay is based on the direct translation of a Luciferase-bearing HIV-1 genome mimic that can be directly translated, yielding a precise measure of virus entry into the cell cytoplasm (Da Silva Santos et al., 2016, p.). Single round of infection R5 Env HIV-1 virus incorporating this reporter (EU-repRNA) were produced by transient transfection of HEK293T cells, as described above. Infections were carried out overnight in THP-1-PMA cells expressing or not Trim69, with a MOI-equivalent of 2, prior to cell lysis and Luciferase activity quantification (Promega, cat. E2620, according to the manufacturers' instructions). To increase the levels of capsid opening, the capsid destabilizing compound PF74 was added for the assay at 10 μg/mL (Sigma, cat. SML0835-5).

HIV-1 reverse transcription. The quantification of revere transcription vDNA intermediates was performed as described earlier (Cordeil et al., 2013). Briefly, cells were infected with DNase-treated R5-HIV-1 virus preparations at an MOI of 2 to 4 and lysed 24h post infection, and extracted DNA was used to amplify the different vDNA forms with specific primers (from 5' to 3'): minus-strand strong stop (MSSS), TGGGAGCTCTCTGCTAACT and ACCAGAGTCACACAACAGACG; full- length (FL-GFP), GAACGGCATCAAGGTGAACT and TGCTCAGGTAGTGGTTGTCG; HIV-1 2LTR, TCGTTGGGAGTGAATTAGCC and

CCCACTGCTTAAGCCTCAAT. Cellular HPRT or 18S RNA were used for sample normalization: TGACCTTGATTTATTTTGCATACC and CGAGCAAGACGTTCAGTCCT, or GTGGAGCGATTTGTCTGGTT and CGCTGAGCCAGTCAGTGTAG, respectively.

VSV entry and RNA replication. VSV entry was measured by quantifying the levels of viral RNA in cells 20 min after infection by RT-qPCR. Prior to cell lysis, cells were extensively washed and treated for 10 minutes at 37°C with trypsin to remove non-internalized virions. Pioneer and overall RNA replication levels were measured by performing infections at a MOI of 0,1 to 0,5 for different times points in the presence or absence of 100 μg/mL of chycloheximide (CHX, Sigma, cat. 4859). This compound blocks the translation of viral proteins from positive strand viral RNAs, preventing the accumulation of proteins required for the full replication cycle of RNA. It thus allows the distinction between pioneer transcription and full RNA replication. Primers amplified the GFP gene inserted into the viral genome: GAACGGCATCAAGGTGAACT and TGCTCAGGTAGTGGTTGTCG.

SARS-CoV-2 entry and RNA replication. SARS-CoV-2 entry was measured as described above by measuring the amount of viral RNA inside cells 45 min after infection. Variations in the amount of viral RNA were then assessed at an early time point after infection by RT-qPCR (6 hours), as pilot experiments indicated defects in viral RNA replication in the presence of Trim69 already at early time points. Primers amplified the Neongreen gene inserted into Orf7 were: GAGCTGCATATCTTCGGATCCATCAACG and CAGGTCTCCCTTGGTACTCTTCAGGTTC.

RNA extractions and RT-qPCR. Total cellular RNA was extracted according to the manufacturer's instructions (Macherey-Nagel NucleoSpin RNA cat. 740956) and reverse transcription was performed using random hexamers and oligo (dT) with the SuperScript III reverse transcriptase (Thermo Fisher cat.18080) also following the manufacturers' instructions. qPCRs were performed on a StepOne Plus real-time PCR system (Applied Biosystems) using the FastStart universal SYBR green master mix (Roche Diagnostics, cat. 4913914001). For the quantification of the levels of Trim69 mRNA levels, the PCR primers used were as published (P. Wang et al., 2018) (TCTGTGGGGCAGTCTAAGGA and CCATGGACACATGTTGCTGC) and HPRT1 (see above) was used to normalize samples.

Microtubule binding assays

Microtubule sedimentation in THP-1-PMA cell lysates. The protocol was adapted from (Schweiger et al., 1999). Briefly, THP-1-PMA cells in which expression of Trim69 had been induced for forty-eight hours with 0.5μg/ml dox were lysed in PEM buffer (80 mM PIPES pH 6.8, 1mM EGTA, 1mM $MgCl_2$, 0.5mM DTT,150mM NaCl,1% IGEPAL) supplemented with protease inhibitors (Sigma, cat. 4693159001), at 4°C for 1 hour. Cell lysates were then depleted of insoluble material by four consecutive rounds of centrifugation (610g for 10 min; 10.000g for 10 min; 21.000g for 20 min and last at 100.000g for 1 hour all at 4°C). The resulting cell lysate (L) was then supplemented with 2 mM GTP +/- 40 μM Taxol (Life technologies, cat. R0461 and P3456) and incubated at 37°C for 30 min to induce the polymerization of free tubulin into microtubules. Samples were then layered over a 15% (w/v) sucrose cushion and centrifuged at 30.000 g for 30 min at 30°C to sediment polymerized microtubules (P) and

associated proteins from unpolymerized tubulin (S). All samples were then equalized in sample buffer prior to immunoblot analysis.

***In vitro* binding experiments.** Flag-Trim69 was cloned downstream of a gluthathione-S-transferase (GST) in the pTKPL vector (an in-house derivative of the vector pGEXTK, Promega) and purified from bacterial lysates on glutathione agarose beads (Sigma, cat. 17-0756-01). Equal amounts of GST or GST-Trim69 proteins were then bound to 10 μg of pure porcine brain tubulin (purchased from Euromedex, cat. CS-T240-A) in a total volume of 40 μl of PEM buffer supplemented with 40 μM of Taxol and 1mM GTP. Samples were first incubated for 45 min at 37°C and then incubated for 1 hour at 4°C to induce microtubule polymerization first and Trim69 binding, respectively. Beads were washed three times in the same buffer prior to analysis.

Confocal microscopy

Cells were plated on 0.01% poly-L-lysine-coated coverslips (Sigma, cat. P4832) and analyzed 24 hours after ectopic DNA transfection (unless otherwise specified, Lipofectamine 3000 cat. L3000008, ThermoFisher, according to the manufacturer's instructions). Cells were washed three times with PBS 1x, fixed with 4% paraformaldehyde (Euromedex, cat. 15713), quenched with 50 mM NH_4Cl (Sigma cat. A4514) and permeabilized with PBS–0.5% Triton X-100 (Sigma, cat. X100) (the timing of these steps was 10, 10 and 5 minutes each). After a blocking step in PBS–5% milk, cells were incubated with primary antibodies for 1 hour at room temperature (dilution 1:100), washed and then incubated with fluorescent secondary antibodies (dilution 1:100). A 4'-5-diamidina-2-phenylindole (DAPI)- containing mounting medium was used

(ThermoFisher, cat. 62248). Images were acquired using a spectral Zeiss LSM800 confocal microscope or Confocal Zeiss LSM980 - AiryScan and analyzed with Fiji software (version 2.0.0). Colocalisations were quantified using the Pearson's overlap coefficient, and intensities of stable tubulin were quantified by measuring the pixels Integrated Density function weighted for the area in each cell (Fiji software).

Softwares

Confocal microscopy: Fiji software (version 2.0.0), Zen (version 2.3, Zeiss) and Imaris 9.2.0 software (Oxford Instruments Group). WB: Image Lab Touch Software (version 2.0.0.27, Chemidoc Imaging System from Bio-Rad). Flow cytometry: FlowJo (version X, BD). Protein structure modeling: RaptorX (http://raptorx.uchicago.edu/)(Källberg et al., 2012).

Statistics and graphs: Graphpad Prism8 (8.4.3, Graphpad software, LLC) and Excel (16.16.3, Microsoft).

Statistical analyses

Statistical analyses were calculated with the Graphpad Prism8, or Excel softwares: Student t tests (unpaired, two-tailed), one-way Anova tests with either Tukey's or Dunnett's multiple comparisons, as indicated.

References

1. Abdelmageed, M. I., Abdelmoneim, A. H., Mustafa, M. I., Elfadol, N. M., Murshed, N. S., Shantier, S. W., & Makhawi, A. M. (2020). Design of a Multiepitope-Based Peptide Vaccine against the E Protein of Human COVID-19: An Immunoinformatics Approach. *BioMed Research International*, *2020*, 1–12. https://doi.org/10.1155/2020/2683286
2. Ahmed, M., & Lyles, D. S. (1998). Effect of Vesicular Stomatitis Virus Matrix Protein on Transcription Directed by Host RNA Polymerases I, II, and III. *Journal of Virology*, *72*(10), 8413–8419.
3. Ahmed, M., McKenzie, M. O., Puckett, S., Hojnacki, M., Poliquin, L., & Lyles, D. S. (2003). Ability of the matrix protein of vesicular stomatitis virus to suppress beta interferon gene expression is genetically correlated with the inhibition of host RNA and protein synthesis. *Journal of Virology*, *77*(8), 4646–4657. https://doi.org/10.1128/jvi.77.8.4646-4657.2003
4. Aillaud, C., Bosc, C., Peris, L., Bosson, A., Heemeryck, P., Van Dijk, J., Le Friec, J., Boulan, B., Vossier, F., Sanman, L. E., Syed, S., Amara, N., Couté, Y., Lafanechère, L., Denarier, E., Delphin, C., Pelletier, L., Humbert, S., Bogyo, M., … Moutin, M.-J. (2017). Vasohibins/SVBP are tubulin carboxypeptidases (TCPs) that regulate neuron differentiation. *Science (New York, N.Y.)*, *358*(6369), 1448–1453. https://doi.org/10.1126/science.aao4165
5. Aillaud, C., Bosc, C., Saoudi, Y., Denarier, E., Peris, L., Sago, L., Taulet, N., Cieren, A., Tort, O., Magiera, M. M., Janke, C., Redeker, V., Andrieux, A., & Moutin, M.-J. (2016). Evidence for new C-terminally truncated variants of α- and β-tubulins. *Molecular Biology of the Cell*, *27*(4), 640–653. https://doi.org/10.1091/mbc.E15-03-0137
6. Akhmanova, A., & Hoogenraad, C. C. (2015). Microtubule Minus-End-Targeting Proteins. *Current Biology*, *25*(4), R162–R171. https://doi.org/10.1016/j.cub.2014.12.027
7. Akhmanova, A., Hoogenraad, C. C., Drabek, K., Stepanova, T., Dortland, B., Verkerk, T., Vermeulen, W., Burgering, B. M., De Zeeuw, C. I., Grosveld, F., & Galjart, N. (2001). Clasps are CLIP-115 and -170 associating proteins involved in the regional regulation of microtubule dynamics in motile fibroblasts. *Cell*, *104*(6), 923–935. https://doi.org/10.1016/s0092-8674(01)00288-4
8. Akhmanova, A., & Steinmetz, M. O. (2015). Control of microtubule organization and dynamics: Two ends in the limelight. *Nature Reviews Molecular Cell Biology*, *16*(12), 711–726. https://doi.org/10.1038/nrm4084
9. Albertini, A. A., Mérigoux, C., Libersou, S., Madiona, K., Bressanelli, S., Roche, S., Lepault, J., Melki, R., Vachette, P., & Gaudin, Y. (2012). Characterization of monomeric intermediates during VSV glycoprotein structural transition. *PLoS Pathogens*, *8*(2), e1002556. https://doi.org/10.1371/journal.ppat.1002556
10. Albertini, A. A. V., Baquero, E., Ferlin, A., & Gaudin, Y. (2012). Molecular and Cellular Aspects of Rhabdovirus Entry. *Viruses*, *4*(1), 117–139. https://doi.org/10.3390/v4010117
11. Alushin, G. M., Lander, G. C., Kellogg, E. H., Zhang, R., Baker, D., & Nogales, E. (2014). High-Resolution Microtubule Structures Reveal the Structural Transitions in αβ-Tubulin upon GTP Hydrolysis. *Cell*, *157*(5), 1117–1129. https://doi.org/10.1016/j.cell.2014.03.053

12. Amargant, F., Barragan, M., Vassena, R., & Vernos, I. (2019). Insights of the tubulin code in gametes and embryos: From basic research to potential clinical applications in humans†. *Biology of Reproduction*, *100*(3), 575–589. https://doi.org/10.1093/biolre/ioy203
13. Anderson, S. L., Carton, J. M., Lou, J., Xing, L., & Rubin, B. Y. (1999). Interferon-induced guanylate binding protein-1 (GBP-1) mediates an antiviral effect against vesicular stomatitis virus and encephalomyocarditis virus. *Virology*, *256*(1), 8–14. https://doi.org/10.1006/viro.1999.9614
14. Arhel, N., Genovesio, A., Kim, K.-A., Miko, S., Perret, E., Olivo-Marin, J.-C., Shorte, S., & Charneau, P. (2006). Quantitative four-dimensional tracking of cytoplasmic and nuclear HIV-1 complexes. *Nature Methods*, *3*(10), 817–824. https://doi.org/10.1038/nmeth928
15. Arya, R., Kumari, S., Pandey, B., Mistry, H., Bihani, S. C., Das, A., Prashar, V., Gupta, G. D., Panicker, L., & Kumar, M. (2021). Structural insights into SARS-CoV-2 proteins. *Journal of Molecular Biology*, *433*(2), 166725. https://doi.org/10.1016/j.jmb.2020.11.024
16. Asmi, F. E., Brantis-de-Carvalho, C. E., Blondel, D., & Chelbi-Alix, M. K. (2018). Rhabdoviruses, Antiviral Defense, and SUMO Pathway. *Viruses*, *10*(12), 686. https://doi.org/10.3390/v10120686
17. Baldini, R., Mascaro, M., & Meroni, G. (2020). The MID1 gene product in physiology and disease. *Gene*, *747*, 144655. https://doi.org/10.1016/j.gene.2020.144655
18. Baltzis, D., Qu, L.-K., Papadopoulou, S., Blais, J. D., Bell, J. C., Sonenberg, N., & Koromilas, A. E. (2004). Resistance to vesicular stomatitis virus infection requires a functional cross talk between the eukaryotic translation initiation factor 2alpha kinases PERK and PKR. *Journal of Virology*, *78*(23), 12747–12761. https://doi.org/10.1128/JVI.78.23.12747-12761.2004
19. Bance, B., Seetharaman, S., Leduc, C., Boëda, B., & Etienne-Manneville, S. (2019). Microtubule acetylation but not detyrosination promotes focal adhesion dynamics and astrocyte migration. *Journal of Cell Science*, *132*(7), jcs225805. https://doi.org/10.1242/jcs.225805
20. Banerjee, A. K. (1987). The transcription complex of vesicular stomatitis virus. *Cell*, *48*(3), 363–364. https://doi.org/10.1016/0092-8674(87)90184-X
21. Banerjee, A. K., & Barik, S. (1992). Gene expression of vesicular stomatitis virus genome RNA. *Virology*, *188*(2), 417–428. https://doi.org/10.1016/0042-6822(92)90495-B
22. Baquero, E., Albertini, A. A., Raux, H., Buonocore, L., Rose, J. K., Bressanelli, S., & Gaudin, Y. (2015). Structure of the Low pH Conformation of Chandipura Virus G Reveals Important Features in the Evolution of the Vesiculovirus Glycoprotein. *PLOS Pathogens*, *11*(3), e1004756. https://doi.org/10.1371/journal.ppat.1004756
23. Barr, J. N., Whelan, S. P. J., & Wertz, G. W. (2002). Transcriptional control of the RNA-dependent RNA polymerase of vesicular stomatitis virus. *Biochimica et Biophysica Acta (BBA) - Gene Structure and Expression*, *1577*(2), 337–353. https://doi.org/10.1016/S0167-4781(02)00462-1
24. Barra, H. S., Rodriguez, J. A., Arce, C. A., & Caputto, R. (1973). A soluble preparation from rat brain that incorporates into its own proteins (14 C)arginine by a ribonuclease-sensitive system and (14 C)tyrosine by a ribonuclease-insensitive system. *Journal of Neurochemistry*, *20*(1), 97–108. https://doi.org/10.1111/j.1471-4159.1973.tb12108.x

25. Barré-Sinoussi, F., Chermann, J. C., Rey, F., Nugeyre, M. T., Chamaret, S., Gruest, J., Dauguet, C., Axler-Blin, C., Vézinet-Brun, F., Rouzioux, C., Rozenbaum, W., & Montagnier, L. (1983). Isolation of a T-Lymphotropic Retrovirus from a Patient at Risk for Acquired Immune Deficiency Syndrome (AIDS). *Science*, *220*(4599), 868–871. https://doi.org/10.1126/science.6189183
26. Battivelli, E., Migraine, J., Lecossier, D., Matsuoka, S., Perez-Bercoff, D., Saragosti, S., Clavel, F., & Hance, A. J. (2011). Modulation of TRIM5α Activity in Human Cells by Alternatively Spliced TRIM5 Isoforms. *Journal of Virology*, *85*(15), 7828–7835. https://doi.org/10.1128/JVI.00648-11
27. Beck, M., & Hurt, E. (2017). The nuclear pore complex: Understanding its function through structural insight. *Nature Reviews Molecular Cell Biology*, *18*(2), 73–89. https://doi.org/10.1038/nrm.2016.147
28. Beilstein, F., Obiang, L., Raux, H., & Gaudin, Y. (2015). Characterization of the Interaction between the Matrix Protein of Vesicular Stomatitis Virus and the Immunoproteasome Subunit LMP2. *Journal of Virology*, *89*(21), 11019–11029. https://doi.org/10.1128/JVI.01753-15
29. Belot, L., Albertini, A., & Gaudin, Y. (2019). Structural and cellular biology of rhabdovirus entry. In *Advances in Virus Research* (Vol. 104, pp. 147–183). Elsevier. https://doi.org/10.1016/bs.aivir.2019.05.003
30. Ben-Chetrit, E., Chan, E. K., Sullivan, K. F., & Tan, E. M. (1988). A 52-kD protein is a novel component of the SS-A/Ro antigenic particle. *Journal of Experimental Medicine*, *167*(5), 1560–1571. https://doi.org/10.1084/jem.167.5.1560
31. Ben-Chetrit, E., Fox, R. I., & Tan, E. M. (1990). Dissociation of immune responses to the ss-a (ro) 52-kd and 60-kd polypeptides in systemic lupus erythematosus and sjögren's syndrome. *Arthritis & Rheumatism*, *33*(3), 349–355. https://doi.org/10.1002/art.1780330307
32. Berger, G., Durand, S., Fargier, G., Nguyen, X.-N., Cordeil, S., Bouaziz, S., Muriaux, D., Darlix, J.-L., & Cimarelli, A. (2011). APOBEC3A is a specific inhibitor of the early phases of HIV-1 infection in myeloid cells. *PLoS Pathogens*, *7*(9), e1002221. https://doi.org/10.1371/journal.ppat.1002221
33. Berger, G., Durand, S., Goujon, C., Nguyen, X.-N., Cordeil, S., Darlix, J.-L., & Cimarelli, A. (2011). A simple, versatile and efficient method to genetically modify human monocyte-derived dendritic cells with HIV-1-derived lentiviral vectors. *Nature Protocols*, *6*(6), 806–816. https://doi.org/10.1038/nprot.2011.327
34. Bhabha, G., Johnson, G. T., Schroeder, C. M., & Vale, R. D. (2016). How Dynein Moves Along Microtubules. *Trends in Biochemical Sciences*, *41*(1), 94–105. https://doi.org/10.1016/j.tibs.2015.11.004
35. Bhatt, P. N., & Rodrigues, F. M. (1967). Chandipura: A new Arbovirus isolated in India from patients with febrile illness. *The Indian Journal of Medical Research*, *55*(12), 1295–1305.
36. Biris, N., Yang, Y., Taylor, A. B., Tomashevski, A., Guo, M., Hart, P. J., Diaz-Griffero, F., & Ivanov, D. N. (2012). Structure of the rhesus monkey TRIM5α PRYSPRY domain, the HIV capsid recognition module. *Proceedings of the National Academy of Sciences*, *109*(33), 13278–13283. https://doi.org/10.1073/pnas.1203536109

37. Black, L. R., & Aiken, C. (2010). TRIM5α Disrupts the Structure of Assembled HIV-1 Capsid Complexes *In Vitro*. *Journal of Virology*, *84*(13), 6564–6569. https://doi.org/10.1128/JVI.00210-10
38. Blondel, D., Kheddache, S., Lahaye, X., Dianoux, L., & Chelbi-Alix, M. K. (2010). Resistance to rabies virus infection conferred by the PMLIV isoform. *Journal of Virology*, *84*(20), 10719–10726. https://doi.org/10.1128/JVI.01286-10
39. Blondel, D., Maarifi, G., Nisole, S., & Chelbi-Alix, M. (2015). Resistance to Rhabdoviridae Infection and Subversion of Antiviral Responses. *Viruses*, *7*(7), 3675–3702. https://doi.org/10.3390/v7072794
40. Bloor, S., Maelfait, J., Krumbach, R., Beyaert, R., & Randow, F. (2010). Endoplasmic reticulum chaperone gp96 is essential for infection with vesicular stomatitis virus. *Proceedings of the National Academy of Sciences*, *107*(15), 6970–6975. https://doi.org/10.1073/pnas.0908536107
41. Borden, K. L. (1998). RING fingers and B-boxes: Zinc-binding protein-protein interaction domains. *Biochemistry and Cell Biology*, *76*(2–3), 351–358. https://doi.org/10.1139/o98-021
42. Borden, K. L., Lally, J. M., Martin, S. R., O'Reilly, N. J., Etkin, L. D., & Freemont, P. S. (1995). Novel topology of a zinc-binding domain from a protein involved in regulating early Xenopus development. *The EMBO Journal*, *14*(23), 5947–5956.
43. Borisy, G. G., Olmsted, J. B., Marcum, J. M., & Allen, C. (1974). Microtubule assembly in vitro. *Federation Proceedings*, *33*(2), 167–174.
44. Boyault, C., Zhang, Y., Fritah, S., Caron, C., Gilquin, B., Kwon, S. H., Garrido, C., Yao, T.-P., Vourc'h, C., Matthias, P., & Khochbin, S. (2007). HDAC6 controls major cell response pathways to cytotoxic accumulation of protein aggregates. *Genes & Development*, *21*(17), 2172–2181. https://doi.org/10.1101/gad.436407
45. Brass, A. L., Dykxhoorn, D. M., Benita, Y., Yan, N., Engelman, A., Xavier, R. J., Lieberman, J., & Elledge, S. J. (2008). *Identification of Host Proteins Required for HIV Infection Through a Functional Genomic Screen*. *319*, 7.
46. Bré, M. H., de Néchaud, B., Wolff, A., & Fleury, A. (1994). Glutamylated tubulin probed in ciliates with the monoclonal antibody GT335. *Cell Motility and the Cytoskeleton*, *27*(4), 337–349. https://doi.org/10.1002/cm.970270406
47. Cambiaghi, V., Giuliani, V., Lombardi, S., Marinelli, C., Toffalorio, F., & Pelicci, P. G. (2012). TRIM Proteins in Cancer. In G. Meroni (Ed.), *TRIM/RBCC Proteins* (Vol. 770, pp. 77–91). Springer New York. https://doi.org/10.1007/978-1-4614-5398-7_6
48. Campbell, E. M., & Hope, T. J. (2015). HIV-1 capsid: The multifaceted key player in HIV-1 infection. *Nature Reviews Microbiology*, *13*(8), 471–483. https://doi.org/10.1038/nrmicro3503
49. Carnes, S. K., Zhou, J., & Aiken, C. (2018). HIV-1 Engages a Dynein-Dynactin-BICD2 Complex for Infection and Transport to the Nucleus. *Journal of Virology*, *92*(20), e00358-18. https://doi.org/10.1128/JVI.00358-18
50. Cassimeris, L. (2009). Microtubule Associated Proteins in Neurons. In L. R. Squire (Ed.), *Encyclopedia of Neuroscience* (pp. 865–870). Academic Press. https://doi.org/10.1016/B978-008045046-9.00725-7

51. Caviston, J. P., Ross, J. L., Antony, S. M., Tokito, M., & Holzbaur, E. L. F. (2007). Huntingtin facilitates dynein/dynactin-mediated vesicle transport. *Proceedings of the National Academy of Sciences of the United States of America*, *104*(24), 10045–10050. https://doi.org/10.1073/pnas.0610628104
52. Chau, M. F., Radeke, M. J., de Inés, C., Barasoain, I., Kohlstaedt, L. A., & Feinstein, S. C. (1998). The microtubule-associated protein tau cross-links to two distinct sites on each alpha and beta tubulin monomer via separate domains. *Biochemistry*, *37*(51), 17692–17703. https://doi.org/10.1021/bi9812118
53. Coil, D. A., & Miller, A. D. (2004). Phosphatidylserine Is Not the Cell Surface Receptor for Vesicular Stomatitis Virus. *Journal of Virology*, *78*(20), 10920–10926. https://doi.org/10.1128/JVI.78.20.10920-10926.2004
54. Connacher, R. P., & Goldstrohm, A. C. (2021). Molecular and biological functions of TRIM-NHL RNA-BINDING proteins. *WIREs RNA*, *12*(2). https://doi.org/10.1002/wrna.1620
55. Connor, J. H., & Lyles, D. S. (2002). Vesicular stomatitis virus infection alters the eIF4F translation initiation complex and causes dephosphorylation of the eIF4E binding protein 4E-BP1. *Journal of Virology*, *76*(20), 10177–10187. https://doi.org/10.1128/jvi.76.20.10177-10187.2002
56. Cordeil, S., Nguyen, X.-N., Berger, G., Durand, S., Ainouze, M., & Cimarelli, A. (2013). Evidence for a different susceptibility of primate lentiviruses to type I interferons. *Journal of Virology*, *87*(5), 2587–2596. https://doi.org/10.1128/JVI.02553-12
57. Crawford, L. J., Johnston, C. K., & Irvine, A. E. (2018). TRIM proteins in blood cancers. *Journal of Cell Communication and Signaling*, *12*(1), 21–29. https://doi.org/10.1007/s12079-017-0423-5
58. Cureton, D. K., Burdeinick-Kerr, R., & Whelan, S. P. J. (2012). Genetic inactivation of COPI coatomer separately inhibits vesicular stomatitis virus entry and gene expression. *Journal of Virology*, *86*(2), 655–666. https://doi.org/10.1128/JVI.05810-11
59. Cureton, D. K., Massol, R. H., Saffarian, S., Kirchhausen, T. L., & Whelan, S. P. J. (2009). Vesicular Stomatitis Virus Enters Cells through Vesicles Incompletely Coated with Clathrin That Depend upon Actin for Internalization. *PLoS Pathogens*, *5*(4), e1000394. https://doi.org/10.1371/journal.ppat.1000394
60. Cureton, D. K., Massol, R. H., Whelan, S. P. J., & Kirchhausen, T. (2010). The Length of Vesicular Stomatitis Virus Particles Dictates a Need for Actin Assembly during Clathrin-Dependent Endocytosis. *PLOS Pathogens*, *6*(9), e1001127. https://doi.org/10.1371/journal.ppat.1001127
61. Da Silva Santos, C., Tartour, K., & Cimarelli, A. (2016). A Novel Entry/Uncoating Assay Reveals the Presence of at Least Two Species of Viral Capsids During Synchronized HIV-1 Infection. *PLoS Pathogens*, *12*(9), e1005897. https://doi.org/10.1371/journal.ppat.1005897
62. Das, S. C., Nayak, D., Zhou, Y., & Pattnaik, A. K. (2006). Visualization of Intracellular Transport of Vesicular Stomatitis Virus Nucleocapsids in Living Cells. *Journal of Virology*, *80*(13), 6368–6377. https://doi.org/10.1128/JVI.00211-06
63. Daugherty, M. D., & Malik, H. S. (2012). Rules of Engagement: Molecular Insights from Host-Virus Arms Races. *Annual Review of Genetics*, *46*(1), 677–700. https://doi.org/10.1146/annurev-genet-110711-155522

64. D'Cruz, A. A., Babon, J. J., Norton, R. S., Nicola, N. A., & Nicholson, S. E. (2013). Structure and function of the SPRY/B30.2 domain proteins involved in innate immunity. *Protein Science : A Publication of the Protein Society*, *22*(1), 1–10. https://doi.org/10.1002/pro.2185
65. De, B. P., & Banerjee, A. K. (1984). Specific interactions of vesicular stomatitis virus L and NS proteins with heterologous genome ribonucleoprotein template lead to mRNA synthesis in vitro. *Journal of Virology*, *51*(3), 628–634. https://doi.org/10.1128/JVI.51.3.628-634.1984
66. de Haan, C. A. M., Vennema, H., & Rottier, P. J. M. (2000). Assembly of the Coronavirus Envelope: Homotypic Interactions between the M Proteins. *Journal of Virology*, *74*(11), 4967–4978. https://doi.org/10.1128/JVI.74.11.4967-4978.2000
67. Delaney, M. K., Malikov, V., Chai, Q., Zhao, G., & Naghavi, M. H. (2017). Distinct functions of diaphanous-related formins regulate HIV-1 uncoating and transport. *Proceedings of the National Academy of Sciences*, *114*(33). https://doi.org/10.1073/pnas.1700247114
68. Desai, A., & Mitchison, T. J. (1997). MICROTUBULE POLYMERIZATION DYNAMICS. *Annual Review of Cell and Developmental Biology*, *13*(1), 83–117. https://doi.org/10.1146/annurev.cellbio.13.1.83
69. Desforges, M., Despars, G., Bérard, S., Gosselin, M., McKenzie, M. O., Lyles, D. S., Talbot, P. J., & Poliquin, L. (2002). Matrix protein mutations contribute to inefficient induction of apoptosis leading to persistent infection of human neural cells by vesicular stomatitis virus. *Virology*, *295*(1), 63–73. https://doi.org/10.1006/viro.2001.1329
70. Dharan, A., Opp, S., Abdel-Rahim, O., Keceli, S. K., Imam, S., Diaz-Griffero, F., & Campbell, E. M. (2017). Bicaudal D2 facilitates the cytoplasmic trafficking and nuclear import of HIV-1 genomes during infection. *Proceedings of the National Academy of Sciences of the United States of America*, *114*(50), E10707–E10716. https://doi.org/10.1073/pnas.1712033114
71. Diehl, W. E., Stansell, E., Kaiser, S. M., Emerman, M., & Hunter, E. (2008). Identification of Postentry Restrictions to Mason-Pfizer Monkey Virus Infection in New World Monkey Cells. *Journal of Virology*, *82*(22), 11140–11151. https://doi.org/10.1128/JVI.00269-08
72. Dietzgen, R. G., Kondo, H., Goodin, M. M., Kurath, G., & Vasilakis, N. (2017). The family Rhabdoviridae: Mono- and bipartite negative-sense RNA viruses with diverse genome organization and common evolutionary origins. *Virus Research*, *227*, 158–170. https://doi.org/10.1016/j.virusres.2016.10.010
73. Ding, H., Green, T. J., Lu, S., & Luo, M. (2006). Crystal structure of the oligomerization domain of the phosphoprotein of vesicular stomatitis virus. *Journal of Virology*, *80*(6), 2808–2814. https://doi.org/10.1128/JVI.80.6.2808-2814.2006
74. Dinh, P. X., Beura, L. K., Panda, D., Das, A., & Pattnaik, A. K. (2011). Antagonistic effects of cellular poly(C) binding proteins on vesicular stomatitis virus gene expression. *Journal of Virology*, *85*(18), 9459–9471. https://doi.org/10.1128/JVI.05179-11
75. Dodding, M. P., & Way, M. (2011). Coupling viruses to dynein and kinesin-1: Coupling viruses to dynein and kinesin-1. *The EMBO Journal*, *30*(17), 3527–3539. https://doi.org/10.1038/emboj.2011.283

76. Döhner, K., Nagel, C.-H., & Sodeik, B. (2005). Viral stop-and-go along microtubules: Taking a ride with dynein and kinesins. *Trends in Microbiology*, *13*(7), 320–327. https://doi.org/10.1016/j.tim.2005.05.010
77. Dolnik, O., Gerresheim, G. K., & Biedenkopf, N. (2021). New Perspectives on the Biogenesis of Viral Inclusion Bodies in Negative-Sense RNA Virus Infections. *Cells*, *10*(6), 1460. https://doi.org/10.3390/cells10061460
78. Downing, K. H., & Nogales, E. (1998). New insights into microtubule structure and function from the atomic model of tubulin. *European Biophysics Journal*, *27*(5), 431–436. https://doi.org/10.1007/s002490050153
79. Drouin, O., Hepburn, C. M., Farrar, D. S., Baerg, K., Chan, K., Cyr, C., Donner, E. J., Embree, J. E., Farrell, C., Forgie, S., Giroux, R., Kang, K. T., King, M., Laffin, M., Luu, T. M., Orkin, J., Papenburg, J., Pound, C. M., Price, V. E., … pour l'équipe de l'étude sur la COVID-19 du Programme canadien de surveillance pédiatrique. (2021). Caractéristiques des hospitalisations au Canada d'enfants ayant contracté une infection aiguë par le SRAS-CoV-2 en 2020. *Canadian Medical Association Journal*, *193*(46), E1774–E1785. https://doi.org/10.1503/cmaj.210053-f
80. Duggal, N. K., & Emerman, M. (2012). Evolutionary conflicts between viruses and restriction factors shape immunity. *Nature Reviews Immunology*, *12*(10), 687–695. https://doi.org/10.1038/nri3295
81. Ebner, P., Versteeg, G. A., & Ikeda, F. (2017). Ubiquitin enzymes in the regulation of immune responses. *Critical Reviews in Biochemistry and Molecular Biology*, *52*(4), 425–460. https://doi.org/10.1080/10409238.2017.1325829
82. Edgar, R. C. (2004). MUSCLE: A multiple sequence alignment method with reduced time and space complexity. *BMC Bioinformatics*, *5*, 113. https://doi.org/10.1186/1471-2105-5-113
83. Efimov, A., Kharitonov, A., Efimova, N., Loncarek, J., Miller, P. M., Andreyeva, N., Gleeson, P., Galjart, N., Maia, A. R. R., McLeod, I. X., Yates, J. R., Maiato, H., Khodjakov, A., Akhmanova, A., & Kaverina, I. (2007). Asymmetric CLASP-dependent nucleation of noncentrosomal microtubules at the trans-Golgi network. *Developmental Cell*, *12*(6), 917–930. https://doi.org/10.1016/j.devcel.2007.04.002
84. Elliott, G., & O'Hare, P. (1998). Herpes simplex virus type 1 tegument protein VP22 induces the stabilization and hyperacetylation of microtubules. *Journal of Virology*, *72*(8), 6448–6455. https://doi.org/10.1128/JVI.72.8.6448-6455.1998
85. Emerson, S. U., & Yu, Y. (1975). Both NS and L proteins are required for in vitro RNA synthesis by vesicular stomatitis virus. *Journal of Virology*, *15*(6), 1348–1356. https://doi.org/10.1128/JVI.15.6.1348-1356.1975
86. Ersfeld, K., Wehland, J., Plessmann, U., Dodemont, H., Gerke, V., & Weber, K. (1993). Characterization of the tubulin-tyrosine ligase. *The Journal of Cell Biology*, *120*(3), 725–732. https://doi.org/10.1083/jcb.120.3.725
87. Esposito, D., Koliopoulos, M. G., & Rittinger, K. (2017). Structural determinants of TRIM protein function. *Biochemical Society Transactions*, *45*(1), 183–191. https://doi.org/10.1042/BST20160325
88. Fernandez, J., Portilho, D. M., Danckaert, A., Munier, S., Becker, A., Roux, P., Zambo, A., Shorte, S., Jacob, Y., Vidalain, P.-O., Charneau, P., Clavel, F., & Arhel, N. J. (2015).

Microtubule-associated proteins 1 (MAP1) promote human immunodeficiency virus type I (HIV-1) intracytoplasmic routing to the nucleus. *The Journal of Biological Chemistry*, *290*(8), 4631–4646. https://doi.org/10.1074/jbc.M114.613133

89. Finkelshtein, D., Werman, A., Novick, D., Barak, S., & Rubinstein, M. (2013). LDL receptor and its family members serve as the cellular receptors for vesicular stomatitis virus. *Proceedings of the National Academy of Sciences of the United States of America*, *110*(18), 7306–7311. https://doi.org/10.1073/pnas.1214441110
90. Fletcher, A. J., & James, L. C. (2016). Coordinated Neutralization and Immune Activation by the Cytosolic Antibody Receptor TRIM21. *Journal of Virology*, *90*(10), 4856–4859. https://doi.org/10.1128/JVI.00050-16
91. Fletcher, A. J., Mallery, D. L., Watkinson, R. E., Dickson, C. F., & James, L. C. (2015). Sequential ubiquitination and deubiquitination enzymes synchronize the dual sensor and effector functions of TRIM21. *Proceedings of the National Academy of Sciences of the United States of America*, *112*(32), 10014–10019. https://doi.org/10.1073/pnas.1507534112
92. Flood, E. A., & Lyles, D. S. (1999). Assembly of nucleocapsids with cytosolic and membrane-derived matrix proteins of vesicular stomatitis virus. *Virology*, *261*(2), 295–308. https://doi.org/10.1006/viro.1999.9856
93. Flood, E. A., McKenzie, M. O., & Lyles, D. S. (2000). Role of M protein aggregation in defective assembly of temperature-sensitive M protein mutants of vesicular stomatitis virus. *Virology*, *278*(2), 520–533. https://doi.org/10.1006/viro.2000.0675
94. Foss, S., Bottermann, M., Jonsson, A., Sandlie, I., James, L. C., & Andersen, J. T. (2019). TRIM21—From Intracellular Immunity to Therapy. *Frontiers in Immunology*, *10*, 2049. https://doi.org/10.3389/fimmu.2019.02049
95. Fourest-Lieuvin, A., Peris, L., Gache, V., Garcia-Saez, I., Juillan-Binard, C., Lantez, V., & Job, D. (2006). Microtubule regulation in mitosis: Tubulin phosphorylation by the cyclin-dependent kinase Cdk1. *Molecular Biology of the Cell*, *17*(3), 1041–1050. https://doi.org/10.1091/mbc.e05-07-0621
96. Frampton, A. R., Uchida, H., von Einem, J., Goins, W. F., Grandi, P., Cohen, J. B., Osterrieder, N., & Glorioso, J. C. (2010). Equine herpesvirus type 1 (EHV-1) utilizes microtubules, dynein, and ROCK1 to productively infect cells. *Veterinary Microbiology*, *141*(1–2), 12–21. https://doi.org/10.1016/j.vetmic.2009.07.035
97. Frankel, A. D., & Young, J. A. T. (1998). HIV-1: Fifteen Proteins and an RNA. *Annual Review of Biochemistry*, *67*(1), 1–25. https://doi.org/10.1146/annurev.biochem.67.1.1
98. Freemont, P. S. (1993). The RING Finger.: A Novel Protein Sequence Motif Related to the Zinc Finger. *Annals of the New York Academy of Sciences*, *684*(1 Zinc-Finger P), 174–192. https://doi.org/10.1111/j.1749-6632.1993.tb32280.x
99. Freemont, P. S., Hanson, I. M., & Trowsdale, J. (1991). A novel gysteine-rich sequence motif. *Cell*, *64*(3), 483–484. https://doi.org/10.1016/0092-8674(91)90229-R
100. Fujita, T., Onoguchi, K., Onomoto, K., Hirai, R., & Yoneyama, M. (2007). Triggering antiviral response by RIG-I-related RNA helicases. *Biochimie*, *89*(6–7), 754–760. https://doi.org/10.1016/j.biochi.2007.01.013

101. Fultz, P. N., & Holland, J. J. (1985). Differing responses of hamsters to infection by vesicular stomatitis virus Indiana and New Jersey serotypes. *Virus Research*, *3*(2), 129–140. https://doi.org/10.1016/0168-1702(85)90003-6
102. Gadadhar, S., Bodakuntla, S., Natarajan, K., & Janke, C. (2017). The tubulin code at a glance. *Journal of Cell Science*, jcs.199471. https://doi.org/10.1242/jcs.199471
103. Galjart, N. (2010). Plus-End-Tracking Proteins and Their Interactions at Microtubule Ends. *Current Biology*, *20*(12), R528–R537. https://doi.org/10.1016/j.cub.2010.05.022
104. Gallo, R. C., Salahuddin, S. Z., Popovic, M., Shearer, G. M., Kaplan, M., Haynes, B. F., Palker, T. J., Redfield, R., Oleske, J., Safai, B., White, G., Foster, P., & Markham, P. D. (1984). Frequent Detection and Isolation of Cytopathic Retroviruses (HTLV-III) from Patients with AIDS and at Risk for AIDS. *Science*, *224*(4648), 500–503. https://doi.org/10.1126/science.6200936
105. Ganser-Pornillos, B. K., Chandrasekaran, V., Pornillos, O., Sodroski, J. G., Sundquist, W. I., & Yeager, M. (2011). Hexagonal assembly of a restricting TRIM5α protein. *Proceedings of the National Academy of Sciences*, *108*(2), 534–539. https://doi.org/10.1073/pnas.1013426108
106. Ganser-Pornillos, B. K., & Pornillos, O. (2019). Restriction of HIV-1 and other retroviruses by TRIM5. *Nature Reviews Microbiology*, *17*(9), 546–556. https://doi.org/10.1038/s41579-019-0225-2
107. Gaudier, M. (2002). Crystal structure of vesicular stomatitis virus matrix protein. *The EMBO Journal*, *21*(12), 2886–2892. https://doi.org/10.1093/emboj/cdf284
108. Gerard, F. C. A., Ribeiro, E. de A., Albertini, A. A. V., Gutsche, I., Zaccai, G., Ruigrok, R. W. H., & Jamin, M. (2007). Unphosphorylated rhabdoviridae phosphoproteins form elongated dimers in solution. *Biochemistry*, *46*(36), 10328–10338. https://doi.org/10.1021/bi7007799
109. Gibbons, I. R., & Rowe, A. J. (1965). Dynein: A Protein with Adenosine Triphosphatase Activity from Cilia. *Science (New York, N.Y.)*, *149*(3682), 424–426. https://doi.org/10.1126/science.149.3682.424
110. Glodowski, D. R., Petersen, J. M., & Dahlberg, J. E. (2002). Complex nuclear localization signals in the matrix protein of vesicular stomatitis virus. *The Journal of Biological Chemistry*, *277*(49), 46864–46870. https://doi.org/10.1074/jbc.M208576200
111. Goujon, C., Rivière, L., Jarrosson-Wuilleme, L., Bernaud, J., Rigal, D., Darlix, J.-L., & Cimarelli, A. (2007). SIVSM/HIV-2 Vpx proteins promote retroviral escape from a proteasome-dependent restriction pathway present in human dendritic cells. *Retrovirology*, *4*, 2. https://doi.org/10.1186/1742-4690-4-2
112. Grdzelishvili, V. Z., Smallwood, S., Tower, D., Hall, R. L., Hunt, D. M., & Moyer, S. A. (2005). A Single Amino Acid Change in the L-Polymerase Protein of Vesicular Stomatitis Virus Completely Abolishes Viral mRNA Cap Methylation. *Journal of Virology*, *79*(12), 7327–7337. https://doi.org/10.1128/JVI.79.12.7327-7337.2005
113. Green, T. J., & Luo, M. (2009). Structure of the vesicular stomatitis virus nucleocapsid in complex with the nucleocapsid-binding domain of the small polymerase cofactor, P. *Proceedings of the National Academy of Sciences*, *106*(28), 11713–11718. https://doi.org/10.1073/pnas.0903228106

114. Green, T. J., Zhang, X., Wertz, G. W., & Luo, M. (2006). Structure of the vesicular stomatitis virus nucleoprotein-RNA complex. *Science (New York, N.Y.)*, *313*(5785), 357–360. https://doi.org/10.1126/science.1126953
115. Grütter, M. G., & Luban, J. (2012). TRIM5 structure, HIV-1 capsid recognition, and innate immune signaling. *Current Opinion in Virology*, *2*(2), 142–150. https://doi.org/10.1016/j.coviro.2012.02.003
116. Gu, W., Lewis, S. A., & Cowan, N. J. (1988). Generation of antisera that discriminate among mammalian alpha-tubulins: Introduction of specialized isotypes into cultured cells results in their coassembly without disruption of normal microtubule function. *The Journal of Cell Biology*, *106*(6), 2011–2022. https://doi.org/10.1083/jcb.106.6.2011
117. Guéguen, L., Gaillard, S., Boussau, B., Gouy, M., Groussin, M., Rochette, N. C., Bigot, T., Fournier, D., Pouyet, F., Cahais, V., Bernard, A., Scornavacca, C., Nabholz, B., Haudry, A., Dachary, L., Galtier, N., Belkhir, K., & Dutheil, J. Y. (2013). Bio++: Efficient extensible libraries and tools for computational molecular evolution. *Molecular Biology and Evolution*, *30*(8), 1745–1750. https://doi.org/10.1093/molbev/mst097
118. Guindon, S., Dufayard, J.-F., Lefort, V., Anisimova, M., Hordijk, W., & Gascuel, O. (2010). New algorithms and methods to estimate maximum-likelihood phylogenies: Assessing the performance of PhyML 3.0. *Systematic Biology*, *59*(3), 307–321. https://doi.org/10.1093/sysbio/syq010
119. Gundersen, G. G., Kalnoski, M. H., & Bulinski, J. C. (1984). Distinct populations of microtubules: Tyrosinated and nontyrosinated alpha tubulin are distributed differently in vivo. *Cell*, *38*(3), 779–789. https://doi.org/10.1016/0092-8674(84)90273-3
120. Gurland, G., & Gundersen, G. G. (1995). Stable, detyrosinated microtubules function to localize vimentin intermediate filaments in fibroblasts. *Journal of Cell Biology*, *131*(5), 1275–1290. https://doi.org/10.1083/jcb.131.5.1275
121. Gustin, K. E. (2003). Inhibition of nucleo-cytoplasmic trafficking by RNA viruses: Targeting the nuclear pore complex. *Virus Research*, *95*(1–2), 35–44. https://doi.org/10.1016/S0168-1702(03)00165-5
122. Hagemeijer, M. C., Verheije, M. H., Ulasli, M., Shaltiël, I. A., de Vries, L. A., Reggiori, F., Rottier, P. J. M., & de Haan, C. A. M. (2010). Dynamics of Coronavirus Replication-Transcription Complexes. *Journal of Virology*, *84*(4), 2134–2149. https://doi.org/10.1128/JVI.01716-09
123. Hallak, M. E., Rodriguez, J. A., Barra, H. S., & Caputto, R. (1977). Release of tyrosine from tyrosinated tubulin. Some common factors that affect this process and the assembly of tubulin. *FEBS Letters*, *73*(2), 147–150. https://doi.org/10.1016/0014-5793(77)80968-X
124. Han, R., Wang, R., Zhao, Q., Han, Y., Zong, S., Miao, S., Song, W., & Wang, L. (2016). Trim69 regulates zebrafish brain development by ap-1 pathway. *Scientific Reports*, *6*(1), 24034. https://doi.org/10.1038/srep24034
125. Hanson, R. P. (1952). The natural history of vesicular stomatitis. *Bacteriological Reviews*, *16*(3), 179–204. https://doi.org/10.1128/br.16.3.179-204.1952
126. Hanson, R. P. (1968). DISCUSSION OF THE NATURAL HISTORY OF VESICULAR STOMATITIS. *American Journal of Epidemiology*, *87*(2), 264–266. https://doi.org/10.1093/oxfordjournals.aje.a120815

127. Harashima, A., Guettouche, T., & Barber, G. N. (2010). Phosphorylation of the NFAR proteins by the dsRNA-dependent protein kinase PKR constitutes a novel mechanism of translational regulation and cellular defense. *Genes & Development*, *24*(23), 2640–2653. https://doi.org/10.1101/gad.1965010

128. Hastie, E., Cataldi, M., Moerdyk-Schauwecker, M. J., Felt, S. A., Steuerwald, N., & Grdzelishvili, V. Z. (2016). Novel biomarkers of resistance of pancreatic cancer cells to oncolytic vesicular stomatitis virus. *Oncotarget*, *7*(38), 61601–61618. https://doi.org/10.18632/oncotarget.11202

129. Hatakeyama, S. (2017). TRIM Family Proteins: Roles in Autophagy, Immunity, and Carcinogenesis. *Trends in Biochemical Sciences*, *42*(4), 297–311. https://doi.org/10.1016/j.tibs.2017.01.002

130. Hatziioannou, T., Cowan, S., von Schwedler, U. K., Sundquist, W. I., & Bieniasz, P. D. (2004). Species-Specific Tropism Determinants in the Human Immunodeficiency Virus Type 1 Capsid. *Journal of Virology*, *78*(11), 6005–6012. https://doi.org/10.1128/JVI.78.11.6005-6012.2004

131. Heinrich, B. S., Cureton, D. K., Rahmeh, A. A., & Whelan, S. P. J. (2010). Protein Expression Redirects Vesicular Stomatitis Virus RNA Synthesis to Cytoplasmic Inclusions. *PLoS Pathogens*, *6*(6), e1000958. https://doi.org/10.1371/journal.ppat.1000958

132. Heinrich, B. S., Maliga, Z., Stein, D. A., Hyman, A. A., & Whelan, S. P. J. (2018). Phase Transitions Drive the Formation of Vesicular Stomatitis Virus Replication Compartments. *MBio*, *9*(5), e02290-17. https://doi.org/10.1128/mBio.02290-17

133. Hennig, J., Bresell, A., Sandberg, M., Hennig, K. D. M., Wahren-Herlenius, M., Persson, B., & Sunnerhagen, M. (2008). The Fellowship of the RING: The RING–B-Box Linker Region Interacts with the RING in TRIM21/Ro52, Contains a Native Autoantigenic Epitope in Sjögren Syndrome, and is an Integral and Conserved Region in TRIM Proteins. *Journal of Molecular Biology*, *377*(2), 431–449. https://doi.org/10.1016/j.jmb.2008.01.005

134. Hill, V. M., Harmon, S. A., & Summers, D. F. (1986). Stimulation of vesicular stomatitis virus in vitro RNA synthesis by microtubule-associated proteins. *Proceedings of the National Academy of Sciences*, *83*(15), 5410–5413. https://doi.org/10.1073/pnas.83.15.5410

135. Hill, V. M., & Summers, D. F. (1990). A minor microtubule-associated protein is responsible for the stimulation of vesicular stomatitis virus transcription in vitro. *Journal of General Virology*, *71*(2), 289–298. https://doi.org/10.1099/0022-1317-71-2-289

136. Hirokawa, N., Noda, Y., Tanaka, Y., & Niwa, S. (2009). Kinesin superfamily motor proteins and intracellular transport. *Nature Reviews Molecular Cell Biology*, *10*(10), 682–696. https://doi.org/10.1038/nrm2774

137. Hoffmann, M., Wu, Y.-J., Gerber, M., Berger-Rentsch, M., Heimrich, B., Schwemmle, M., & Zimmer, G. (2010). Fusion-active glycoprotein G mediates the cytotoxicity of vesicular stomatitis virus M mutants lacking host shut-off activity. *Journal of General Virology*, *91*(11), 2782–2793. https://doi.org/10.1099/vir.0.023978-0

138. Holzbaur, E. (2010). Axonal transport: CDKs as traffic signals for motor-ists along the axon? *Current Biology: CB*, *20*(15), R641-642. https://doi.org/10.1016/j.cub.2010.06.016

139. Horio, T., & Hotani, H. (1986). Visualization of the dynamic instability of individual microtubules by dark-field microscopy. *Nature*, *321*(6070), 605–607. https://doi.org/10.1038/321605a0

140. Hornung, V., Ellegast, J., Kim, S., Brzózka, K., Jung, A., Kato, H., Poeck, H., Akira, S., Conzelmann, K.-K., Schlee, M., Endres, S., & Hartmann, G. (2006). 5'-Triphosphate RNA is the ligand for RIG-I. *Science (New York, N.Y.)*, *314*(5801), 994–997. https://doi.org/10.1126/science.1132505

141. Hou, W., Li, Y., Shan, Y., Wang, S., & Liu, F. (n.d.). Dynamic Dissection of Dynein and Kinesin-1 Cooperatively Mediated Intercellular Transport of Porcine Epidemic Diarrhea Coronavirus along Microtubule Using Single Virus Tracking. *Virulence*, *12*(1), 615–629. https://doi.org/10.1080/21505594.2021.1878748

142. Howatson, A. F. (1970). Vesicular Stomatitis And Related Viruses. In *Advances in Virus Research* (Vol. 16, pp. 195–256). Elsevier. https://doi.org/10.1016/S0065-3527(08)60024-X

143. Husain, M., & Harrod, K. S. (2011). Enhanced acetylation of alpha-tubulin in influenza A virus infected epithelial cells. *FEBS Letters*, *585*(1), 128–132. https://doi.org/10.1016/j.febslet.2010.11.023

144. Iomini, C., Bré, M. H., Levilliers, N., & Justine, J. L. (1998). Tubulin polyglycylation in Platyhelminthes: Diversity among stable microtubule networks and very late occurrence during spermiogenesis. *Cell Motility and the Cytoskeleton*, *39*(4), 318–330. https://doi.org/10.1002/(SICI)1097-0169(1998)39:4<318::AID-CM6>3.0.CO;2-Z

145. Ivanov, A. V., Peng, H., Yurchenko, V., Yap, K. L., Negorev, D. G., Schultz, D. C., Psulkowski, E., Fredericks, W. J., White, D. E., Maul, G. G., Sadofsky, M. J., Zhou, M.-M., & Rauscher, F. J. (2007). PHD Domain-Mediated E3 Ligase Activity Directs Intramolecular Sumoylation of an Adjacent Bromodomain Required for Gene Silencing. *Molecular Cell*, *28*(5), 823–837. https://doi.org/10.1016/j.molcel.2007.11.012

146. Iverson, L. E., & Rose, J. K. (1981). Localized attenuation and discontinuous synthesis during vesicular stomatitis virus transcription. *Cell*, *23*(2), 477–484. https://doi.org/10.1016/0092-8674(81)90143-4

147. Jackson, C. B., Farzan, M., Chen, B., & Choe, H. (2022). Mechanisms of SARS-CoV-2 entry into cells. *Nature Reviews Molecular Cell Biology*, *23*(1), 3–20. https://doi.org/10.1038/s41580-021-00418-x

148. Jacob, Y., Badrane, H., Ceccaldi, P. E., & Tordo, N. (2000). Cytoplasmic dynein LC8 interacts with lyssavirus phosphoprotein. *Journal of Virology*, *74*(21), 10217–10222. https://doi.org/10.1128/jvi.74.21.10217-10222.2000

149. James, L. C., Keeble, A. H., Khan, Z., Rhodes, D. A., & Trowsdale, J. (2007). Structural basis for PRYSPRY-mediated tripartite motif (TRIM) protein function. *Proceedings of the National Academy of Sciences of the United States of America*, *104*(15), 6200–6205. https://doi.org/10.1073/pnas.0609174104

150. Jamin, M., & Yabukarski, F. (2017). Nonsegmented Negative-Sense RNA Viruses-Structural Data Bring New Insights Into Nucleocapsid Assembly. *Advances in Virus Research*, *97*, 143–185. https://doi.org/10.1016/bs.aivir.2016.09.001

151. Janelle, V., Brassard, F., Lapierre, P., Lamarre, A., & Poliquin, L. (2011). Mutations in the Glycoprotein of Vesicular Stomatitis Virus Affect Cytopathogenicity: Potential for

Oncolytic Virotherapy. *Journal of Virology*, *85*(13), 6513–6520. https://doi.org/10.1128/JVI.02484-10

152. Janke, C., & Chloë Bulinski, J. (2011). Post-translational regulation of the microtubule cytoskeleton: Mechanisms and functions. *Nature Reviews Molecular Cell Biology*, *12*(12), 773–786. https://doi.org/10.1038/nrm3227
153. Janke, C., & Magiera, M. M. (2020). The tubulin code and its role in controlling microtubule properties and functions. *Nature Reviews Molecular Cell Biology*, *21*(6), 307–326. https://doi.org/10.1038/s41580-020-0214-3
154. Janke, C., Rogowski, K., Wloga, D., Regnard, C., Kajava, A. V., Strub, J.-M., Temurak, N., van Dijk, J., Boucher, D., van Dorsselaer, A., Suryavanshi, S., Gaertig, J., & Eddé, B. (2005). Tubulin polyglutamylase enzymes are members of the TTL domain protein family. *Science (New York, N.Y.)*, *308*(5729), 1758–1762. https://doi.org/10.1126/science.1113010
155. Jenni, S., Bloyet, L.-M., Diaz-Avalos, R., Liang, B., Whelan, S. P. J., Grigorieff, N., & Harrison, S. C. (2020). Structure of the Vesicular Stomatitis Virus L Protein in Complex with Its Phosphoprotein Cofactor. *Cell Reports*, *30*(1), 53-60.e5. https://doi.org/10.1016/j.celrep.2019.12.024
156. Joazeiro, C. A. P., & Weissman, A. M. (2000). RING Finger Proteins. *Cell*, *102*(5), 549–552. https://doi.org/10.1016/S0092-8674(00)00077-5
157. Johannsdottir, H. K., Mancini, R., Kartenbeck, J., Amato, L., & Helenius, A. (2009). Host Cell Factors and Functions Involved in Vesicular Stomatitis Virus Entry. *Journal of Virology*, *83*(1), 440–453. https://doi.org/10.1128/JVI.01864-08
158. Jovasevic, V., Naghavi, M. H., & Walsh, D. (2015). Microtubule plus end–associated CLIP-170 initiates HSV-1 retrograde transport in primary human cells. *The Journal of Cell Biology*, *211*(2), 323–337. https://doi.org/10.1083/jcb.201505123
159. Källberg, M., Wang, H., Wang, S., Peng, J., Wang, Z., Lu, H., & Xu, J. (2012). Template-based protein structure modeling using the RaptorX web server. *Nature Protocols*, *7*(8), 1511–1522. https://doi.org/10.1038/nprot.2012.085
160. Kannan, H., Fan, S., Patel, D., Bossis, I., & Zhang, Y.-J. (2009). The hepatitis E virus open reading frame 3 product interacts with microtubules and interferes with their dynamics. *Journal of Virology*, *83*(13), 6375–6382. https://doi.org/10.1128/JVI.02571-08
161. Kapitein, L. C., & Hoogenraad, C. C. (2015). Building the Neuronal Microtubule Cytoskeleton. *Neuron*, *87*(3), 492–506. https://doi.org/10.1016/j.neuron.2015.05.046
162. Kato, H., Takeuchi, O., Sato, S., Yoneyama, M., Yamamoto, M., Matsui, K., Uematsu, S., Jung, A., Kawai, T., Ishii, K. J., Yamaguchi, O., Otsu, K., Tsujimura, T., Koh, C.-S., Reis e Sousa, C., Matsuura, Y., Fujita, T., & Akira, S. (2006). Differential roles of MDA5 and RIG-I helicases in the recognition of RNA viruses. *Nature*, *441*(7089), 101–105. https://doi.org/10.1038/nature04734
163. Khwaja, S., Kumar, K., Das, R., & Negi, A. S. (2021). Microtubule associated proteins as targets for anticancer drug development. *Bioorganic Chemistry*, *116*, 105320. https://doi.org/10.1016/j.bioorg.2021.105320
164. Kim, K., Dauphin, A., Komurlu, S., McCauley, S. M., Yurkovetskiy, L., Carbone, C., Diehl, W. E., Strambio-De-Castillia, C., Campbell, E. M., & Luban, J. (2019). Cyclophilin A protects

HIV-1 from restriction by human TRIM5α. *Nature Microbiology*, *4*(12), 2044–2051. https://doi.org/10.1038/s41564-019-0592-5

165. Kirtipal, N., Bharadwaj, S., & Kang, S. G. (2020). From SARS to SARS-CoV-2, insights on structure, pathogenicity and immunity aspects of pandemic human coronaviruses. *Infection, Genetics and Evolution*, *85*, 104502. https://doi.org/10.1016/j.meegid.2020.104502
166. Knudson, D. L. (1973). Rhabdoviruses. *Journal of General Virology*, *20*(Supplement), 105–130. https://doi.org/10.1099/0022-1317-20-Supplement-105
167. Koepke, L., Gack, M. U., & Sparrer, K. M. (2021a). The antiviral activities of TRIM proteins. *Current Opinion in Microbiology*, *59*, 50–57. https://doi.org/10.1016/j.mib.2020.07.005
168. Koepke, L., Gack, M. U., & Sparrer, K. M. (2021b). The antiviral activities of TRIM proteins. *Current Opinion in Microbiology*, *59*, 50–57. https://doi.org/10.1016/j.mib.2020.07.005
169. Krishnamoorthy, J., Mounir, Z., Raven, J. F., & Koromilas, A. E. (2008). The eIF2alpha kinases inhibit vesicular stomatitis virus replication independently of eIF2alpha phosphorylation. *Cell Cycle (Georgetown, Tex.)*, *7*(15), 2346–2351. https://doi.org/10.4161/cc.6323
170. Kueck, T., Bloyet, L.-M., Cassella, E., Zang, T., Schmidt, F., Brusic, V., Tekes, G., Pornillos, O., Whelan, S. P. J., & Bieniasz, P. D. (2019). Vesicular Stomatitis Virus Transcription Is Inhibited by TRIM69 in the Interferon-Induced Antiviral State. *Journal of Virology*, *93*(24), e01372-19. https://doi.org/10.1128/JVI.01372-19
171. Kumar, N., & Flavin, M. (1981). Preferential action of a brain detyrosinolating carboxypeptidase on polymerized tubulin. *The Journal of Biological Chemistry*, *256*(14), 7678–7686.
172. Kyrylenko, S., Kyrylenko, O., Suuronen, T., & Salminen, A. (2003). Differential regulation of the Sir2 histone deacetylase gene family by inhibitors of class I and II histone deacetylases. *Cellular and Molecular Life Sciences: CMLS*, *60*(9), 1990–1997. https://doi.org/10.1007/s00018-003-3090-z
173. Laguette, N., Sobhian, B., Casartelli, N., Ringeard, M., Chable-Bessia, C., Ségéral, E., Yatim, A., Emiliani, S., Schwartz, O., & Benkirane, M. (2011). SAMHD1 is the dendritic- and myeloid-cell-specific HIV-1 restriction factor counteracted by Vpx. *Nature*, *474*(7353), 654–657. https://doi.org/10.1038/nature10117
174. Le Blanc, I., Luyet, P.-P., Pons, V., Ferguson, C., Emans, N., Petiot, A., Mayran, N., Demaurex, N., Fauré, J., Sadoul, R., Parton, R. G., & Gruenberg, J. (2005). Endosome-to-cytosol transport of viral nucleocapsids. *Nature Cell Biology*, *7*(7), 653–664. https://doi.org/10.1038/ncb1269
175. LeDizet, M., & Piperno, G. (1987). Identification of an acetylation site of Chlamydomonas alpha-tubulin. *Proceedings of the National Academy of Sciences of the United States of America*, *84*(16), 5720–5724. https://doi.org/10.1073/pnas.84.16.5720
176. Letchworth, G. J., Rodriguez, L. L., & Del cbarrera, J. (1999). Vesicular stomatitis. *Veterinary Journal (London, England: 1997)*, *157*(3), 239–260. https://doi.org/10.1053/tvjl.1998.0303

177. Levy, J. A., Shimabukuro, J., Hollander, H., Mills, J., & Kaminsky, L. (1985). Isolation of AIDS-associated retroviruses from cerebrospinal fluid and brain of patients with neurological symptoms. *Lancet (London, England)*, *2*(8455), 586–588.

178. L'Hernault, S. W., & Rosenbaum, J. L. (1985). Reversal of the posttranslational modification on Chlamydomonas flagellar alpha-tubulin occurs during flagellar resorption. *The Journal of Cell Biology*, *100*(2), 457–462. https://doi.org/10.1083/jcb.100.2.457

179. Li, R., & Gundersen, G. G. (2008). Beyond polymer polarity: How the cytoskeleton builds a polarized cell. *Nature Reviews. Molecular Cell Biology*, *9*(11), 860–873. https://doi.org/10.1038/nrm2522

180. Li, Y.-L., Chandrasekaran, V., Carter, S. D., Woodward, C. L., Christensen, D. E., Dryden, K. A., Pornillos, O., Yeager, M., Ganser-Pornillos, B. K., Jensen, G. J., & Sundquist, W. I. (2016). Primate TRIM5 proteins form hexagonal nets on HIV-1 capsids. *ELife*, *5*, e16269. https://doi.org/10.7554/eLife.16269

181. Liang, B., Li, Z., Jenni, S., Rahmeh, A. A., Morin, B. M., Grant, T., Grigorieff, N., Harrison, S. C., & Whelan, S. P. J. (2015). Structure of the L Protein of Vesicular Stomatitis Virus from Electron Cryomicroscopy. *Cell*, *162*(2), 314–327. https://doi.org/10.1016/j.cell.2015.06.018

182. Liang, G., Zhang, X. D., Wang, L. J., Sha, Y. S., Zhang, J. C., Miao, S. Y., Zong, S. D., Wang, L. F., & Koide, S. (2004). Identification of differentially expressed genes of primary spermatocyte against round spermatid isolated from human testis using the laser capture microdissection technique. *Cell Research*, *14*(6), 507–512. https://doi.org/10.1038/sj.cr.7290254

183. Liao, D. J., Wang, Y., Wu, J., Adsay, N. V., Grignon, D., Khanani, F., & Sarkar, F. H. (2006). Characterization of pancreatic lesions from MT-tgf alpha, Ela-myc and MT-tgf alpha/Ela-myc single and double transgenic mice. *Journal of Carcinogenesis*, *5*, 19. https://doi.org/10.1186/1477-3163-5-19

184. Liberatore, R. A., Mastrocola, E. J., Powell, C., & Bieniasz, P. D. (2017). Tetherin Inhibits Cell-Free Virus Dissemination and Retards Murine Leukemia Virus Pathogenesis. *Journal of Virology*, *91*(12), e02286-16. https://doi.org/10.1128/JVI.02286-16

185. Lichty, B. D., Power, A. T., Stojdl, D. F., & Bell, J. C. (2004). Vesicular stomatitis virus: Re-inventing the bullet. *Trends in Molecular Medicine*, *10*(5), 210–216. https://doi.org/10.1016/j.molmed.2004.03.003

186. Liu, G., Cao, W., Salawudeen, A., Zhu, W., Emeterio, K., Safronetz, D., & Banadyga, L. (2021). Vesicular Stomatitis Virus: From Agricultural Pathogen to Vaccine Vector. *Pathogens*, *10*(9), 1092. https://doi.org/10.3390/pathogens10091092

187. Liu, S., Hard, R., Rankin, S., Hennessey, T., & Pennock, D. G. (2004). Disruption of genes encoding predicted inner arm dynein heavy chains causes motility phenotypes in Tetrahymena. *Cell Motility and the Cytoskeleton*, *59*(3), 201–214. https://doi.org/10.1002/cm.20034

188. Liu, S.-Y., Aliyari, R., Chikere, K., Li, G., Marsden, M. D., Smith, J. K., Pernet, O., Guo, H., Nusbaum, R., Zack, J. A., Freiberg, A. N., Su, L., Lee, B., & Cheng, G. (2013). Interferon-Inducible Cholesterol-25-Hydroxylase Broadly Inhibits Viral Entry by Production of 25-Hydroxycholesterol. *Immunity*, *38*(1), 92–105. https://doi.org/10.1016/j.immuni.2012.11.005

189. Liu, X., Wang, H., Zhu, J., Xie, Y., Liang, X., Chen, Z., Feng, Y., & Zhang, Y. (2019). Structural insights into tubulin detyrosination by vasohibins-SVBP complex. *Cell Discovery*, *5*(1), 1–5. https://doi.org/10.1038/s41421-019-0133-7

190. Lloyd, C., & Hussey, P. (2001). Microtubule-associated proteins in plants—Why we need a MAP. *Nature Reviews. Molecular Cell Biology*, *2*(1), 40–47. https://doi.org/10.1038/35048005

191. Loh, E., Peter, F., Subramaniam, V. N., & Hong, W. (2005). Mammalian Bet3 functions as a cytosolic factor participating in transport from the ER to the Golgi apparatus. *Journal of Cell Science*, *118*(6), 1209–1222. https://doi.org/10.1242/jcs.01723

192. Lopes, D., & Maiato, H. (2020). The Tubulin Code in Mitosis and Cancer. *Cells*, *9*(11), 2356. https://doi.org/10.3390/cells9112356

193. Lu, W., Zhang, S., Chen, B., Chen, J., Xian, J., Lin, Y., Shan, H., & Su, Z. Z. (2020). A Clinical Study of Noninvasive Assessment of Lung Lesions in Patients with Coronavirus Disease-19 (COVID-19) by Bedside Ultrasound. *Ultraschall in der Medizin - European Journal of Ultrasound*, *41*(03), 300–307. https://doi.org/10.1055/a-1154-8795

194. Lu, X., Pan, J., Tao, J., & Guo, D. (2011). SARS-CoV nucleocapsid protein antagonizes IFN-β response by targeting initial step of IFN-β induction pathway, and its C-terminal region is critical for the antagonism. *Virus Genes*, *42*(1), 37–45. https://doi.org/10.1007/s11262-010-0544-x

195. Luban, J., Bossolt, K. L., Franke, E. K., Kalpana, G. V., & Goff, S. P. (1993). Human immunodeficiency virus type 1 Gag protein binds to cyclophilins A and B. *Cell*, *73*(6), 1067–1078. https://doi.org/10.1016/0092-8674(93)90637-6

196. Luo, M. (2012). The nucleocapsid of vesicular stomatitis virus. *Science China Life Sciences*, *55*(4), 291–300. https://doi.org/10.1007/s11427-012-4307-x

197. Luo, M., Green, T. J., Zhang, X., Tsao, J., & Qiu, S. (2007). Conserved characteristics of the rhabdovirus nucleoprotein. *Virus Research*, *129*(2), 246–251. https://doi.org/10.1016/j.virusres.2007.07.011

198. Lusic, M., & Siliciano, R. F. (2017). Nuclear landscape of HIV-1 infection and integration. *Nature Reviews Microbiology*, *15*(2), 69–82. https://doi.org/10.1038/nrmicro.2016.162

199. Lyles, D. S. (2013). Assembly and Budding of Negative-Strand RNA Viruses. In *Advances in Virus Research* (Vol. 85, pp. 57–90). Elsevier. https://doi.org/10.1016/B978-0-12-408116-1.00003-3

200. Magiera, M. M., Singh, P., Gadadhar, S., & Janke, C. (2018). Tubulin Posttranslational Modifications and Emerging Links to Human Disease. *Cell*, *173*(6), 1323–1327. https://doi.org/10.1016/j.cell.2018.05.018

201. Malfavon-Borja, R., Sawyer, S. L., Wu, L. I., Emerman, M., & Malik, H. S. (2013). An Evolutionary Screen Highlights Canonical and Noncanonical Candidate Antiviral Genes within the Primate TRIM Gene Family. *Genome Biology and Evolution*, *5*(11), 2141–2154. https://doi.org/10.1093/gbe/evt163

202. Malikov, V., da Silva, E. S., Jovasevic, V., Bennett, G., de Souza Aranha Vieira, D. A., Schulte, B., Diaz-Griffero, F., Walsh, D., & Naghavi, M. H. (2015). HIV-1 capsids bind and exploit the kinesin-1 adaptor FEZ1 for inward movement to the nucleus. *Nature Communications*, *6*(1), 6660. https://doi.org/10.1038/ncomms7660

203. Malim, M. H., & Bieniasz, P. D. (2012). HIV Restriction Factors and Mechanisms of Evasion. *Cold Spring Harbor Perspectives in Medicine*, *2*(5), a006940–a006940. https://doi.org/10.1101/cshperspect.a006940

204. Mallery, D. L., McEwan, W. A., Bidgood, S. R., Towers, G. J., Johnson, C. M., & James, L. C. (2010). Antibodies mediate intracellular immunity through tripartite motif-containing 21 (TRIM21). *Proceedings of the National Academy of Sciences*, *107*(46), 19985–19990. https://doi.org/10.1073/pnas.1014074107

205. Manka, S. W., & Moores, C. A. (2018). The role of tubulin–tubulin lattice contacts in the mechanism of microtubule dynamic instability. *Nature Structural & Molecular Biology*, *25*(7), 607–615. https://doi.org/10.1038/s41594-018-0087-8

206. Marcaurelle, L. A., Comer, E., Dandapani, S., Duvall, J. R., Gerard, B., Kesavan, S., Lee, M. D., Liu, H., Lowe, J. T., Marie, J.-C., Mulrooney, C. A., Pandya, B. A., Rowley, A., Ryba, T. D., Suh, B.-C., Wei, J., Young, D. W., Akella, L. B., Ross, N. T., … Foley, M. A. (2010). An aldol-based build/couple/pair strategy for the synthesis of medium- and large-sized rings: Discovery of macrocyclic histone deacetylase inhibitors. *Journal of the American Chemical Society*, *132*(47), 16962–16976. https://doi.org/10.1021/ja105119r

207. Marín, I. (2012). Origin and Diversification of TRIM Ubiquitin Ligases. *PLoS ONE*, *7*(11), e50030. https://doi.org/10.1371/journal.pone.0050030

208. Marquis, K. A., Becker, R. L., Weiss, A. N., Morris, M. C., & Ferran, M. C. (2020). The VSV Matrix protein inhibits NF-κB and the interferon response independently in mouse L929 cells. *Virology*, *548*, 117–123. https://doi.org/10.1016/j.virol.2020.06.013

209. Martin, M., & Akhmanova, A. (2018). Coming into Focus: Mechanisms of Microtubule Minus-End Organization. *Trends in Cell Biology*, *28*(7), 574–588. https://doi.org/10.1016/j.tcb.2018.02.011

210. Masters, P. S., & Banerjee, A. K. (1988). Complex formation with vesicular stomatitis virus phosphoprotein NS prevents binding of nucleocapsid protein N to nonspecific RNA. *Journal of Virology*, *62*(8), 2658–2664. https://doi.org/10.1128/JVI.62.8.2658-2664.1988

211. Matsuyama, A., Shimazu, T., Sumida, Y., Saito, A., Yoshimatsu, Y., Seigneurin-Berny, D., Osada, H., Komatsu, Y., Nishino, N., Khochbin, S., Horinouchi, S., & Yoshida, M. (2002). In vivo destabilization of dynamic microtubules by HDAC6-mediated deacetylation. *The EMBO Journal*, *21*(24), 6820–6831. https://doi.org/10.1093/emboj/cdf682

212. McCreedy, B. J., & Lyles, D. S. (1989). Distribution of M protein and nucleocapsid protein of vesicular stomatitis virus in infected cell plasma membranes. *Virus Research*, *14*(3), 189–205. https://doi.org/10.1016/0168-1702(89)90001-4

213. McDonald, D., Vodicka, M. A., Lucero, G., Svitkina, T. M., Borisy, G. G., Emerman, M., & Hope, T. J. (2002). Visualization of the intracellular behavior of HIV in living cells. *The Journal of Cell Biology*, *159*(3), 441–452. https://doi.org/10.1083/jcb.200203150

214. McEwan, W. A., Mallery, D. L., Rhodes, D. A., Trowsdale, J., & James, L. C. (2011). Intracellular antibody-mediated immunity and the role of TRIM21: Insights & Perspectives. *BioEssays*, *33*(11), 803–809. https://doi.org/10.1002/bies.201100093

215. McEwan, W. A., Tam, J. C. H., Watkinson, R. E., Bidgood, S. R., Mallery, D. L., & James, L. C. (2013). Intracellular antibody-bound pathogens stimulate immune signaling via the Fc receptor TRIM21. *Nature Immunology*, *14*(4), 327–336. https://doi.org/10.1038/ni.2548

216. McKenney, R. J., Huynh, W., Vale, R. D., & Sirajuddin, M. (2016). Tyrosination of α-tubulin controls the initiation of processive dynein–dynactin motility. *The EMBO Journal*, *35*(11), 1175–1185. https://doi.org/10.15252/embj.201593071
217. McNab, F. W., Rajsbaum, R., Stoye, J. P., & O'Garra, A. (2011). Tripartite-motif proteins and innate immune regulation. *Current Opinion in Immunology*, *23*(1), 46–56. https://doi.org/10.1016/j.coi.2010.10.021
218. McNally, F. J., & Roll-Mecak, A. (2018). Microtubule-severing enzymes: From cellular functions to molecular mechanism. *Journal of Cell Biology*, *217*(12), 4057–4069. https://doi.org/10.1083/jcb.201612104
219. McNally, F. J., & Vale, R. D. (1993). Identification of katanin, an ATPase that severs and disassembles stable microtubules. *Cell*, *75*(3), 419–429. https://doi.org/10.1016/0092-8674(93)90377-3
220. Mebatsion, T. (2001). Extensive attenuation of rabies virus by simultaneously modifying the dynein light chain binding site in the P protein and replacing Arg333 in the G protein. *Journal of Virology*, *75*(23), 11496–11502. https://doi.org/10.1128/JVI.75.23.11496-11502.2001
221. Mebatsion, T., Weiland, F., & Conzelmann, K. K. (1999). Matrix protein of rabies virus is responsible for the assembly and budding of bullet-shaped particles and interacts with the transmembrane spike glycoprotein G. *Journal of Virology*, *73*(1), 242–250. https://doi.org/10.1128/JVI.73.1.242-250.1999
222. Mellon, M. G., & Emerson, S. U. (1978). Rebinding of transcriptase components (L and NS proteins) to the nucleocapsid template of vesicular stomatitis virus. *Journal of Virology*, *27*(3), 560–567. https://doi.org/10.1128/JVI.27.3.560-567.1978
223. Mercer, B. A., & D'Armiento, J. M. (2006). Emerging role of MAP kinase pathways as therapeutic targets in COPD. *International Journal of Chronic Obstructive Pulmonary Disease*, *1*(2), 137–150. https://doi.org/10.2147/copd.2006.1.2.137
224. Meroni, G., & Diez-Roux, G. (2005). TRIM/RBCC, a novel class of 'single protein RING finger' E3 ubiquitin ligases. *BioEssays*, *27*(11), 1147–1157. https://doi.org/10.1002/bies.20304
225. Miller, J., McLachlan, A. D., & Klug, A. (1985). Repetitive zinc-binding domains in the protein transcription factor IIIA from Xenopus oocytes. *The EMBO Journal*, *4*(6), 1609–1614. https://doi.org/10.1002/j.1460-2075.1985.tb03825.x
226. Mire, C. E., White, J. M., & Whitt, M. A. (2010). A Spatio-Temporal Analysis of Matrix Protein and Nucleocapsid Trafficking during Vesicular Stomatitis Virus Uncoating. *PLoS Pathogens*, *6*(7), e1000994. https://doi.org/10.1371/journal.ppat.1000994
227. Mitchison, T., & Kirschner, M. (1984). Dynamic instability of microtubule growth. *Nature*, *312*(5991), 237–242. https://doi.org/10.1038/312237a0
228. Mitra, S., Shanmugapriya, S., Santos da Silva, E., & Naghavi, M. H. (2020). HIV-1 Exploits CLASP2 To Induce Microtubule Stabilization and Facilitate Virus Trafficking to the Nucleus. *Journal of Virology*, *94*(14), e00404-20. https://doi.org/10.1128/JVI.00404-20
229. Mogensen, T. H. (2019). IRF and STAT Transcription Factors—From Basic Biology to Roles in Infection, Protective Immunity, and Primary Immunodeficiencies. *Frontiers in Immunology*, *9*, 3047. https://doi.org/10.3389/fimmu.2018.03047

230. Morin, B., Rahmeh, A. A., & Whelan, S. P. J. (2012). Mechanism of RNA synthesis initiation by the vesicular stomatitis virus polymerase. *The EMBO Journal*, *31*(5), 1320–1329. https://doi.org/10.1038/emboj.2011.483

231. Moyer, S. A., Baker, S. C., & Lessard, J. L. (1986). Tubulin: A factor necessary for the synthesis of both Sendai virus and vesicular stomatitis virus RNAs. *Proceedings of the National Academy of Sciences*, *83*(15), 5405–5409. https://doi.org/10.1073/pnas.83.15.5405

232. Mukai, M., Ikegami, K., Sugiura, Y., Takeshita, K., Nakagawa, A., & Setou, M. (2009). Recombinant mammalian tubulin polyglutamylase TTLL7 performs both initiation and elongation of polyglutamylation on beta-tubulin through a random sequential pathway. *Biochemistry*, *48*(5), 1084–1093. https://doi.org/10.1021/bi802047y

233. Mukherjee, S., Valencia, J. D. D., Stewman, S., Metz, J., Monnier, S., Rath, U., Asenjo, A. B., Charafeddine, R. A., Sosa, H. J., Ross, J. L., Ma, A., & Sharp, D. J. (2012). Human Fidgetin is a microtubule severing the enzyme and minus-end depolymerase that regulates mitosis. *Cell Cycle*, *11*(12), 2359–2366. https://doi.org/10.4161/cc.20849

234. Naghavi, M. H. (2014). Stable microtubule subsets facilitate early HIV-1 infection. *AIDS Research and Human Retroviruses*, *30*(3), 211–212. https://doi.org/10.1089/aid.2014.0026

235. Naghavi, M. H. (2021). HIV-1 capsid exploitation of the host microtubule cytoskeleton during early infection. *Retrovirology*, *18*(1), 19. https://doi.org/10.1186/s12977-021-00563-3

236. Naghavi, M. H., Gundersen, G. G., & Walsh, D. (2013). Plus-end tracking proteins, CLASPs, and a viral Akt mimic regulate herpesvirus-induced stable microtubule formation and virus spread. *Proceedings of the National Academy of Sciences of the United States of America*, *110*(45), 18268–18273. https://doi.org/10.1073/pnas.1310760110

237. Napolitano, L. M., & Meroni, G. (2012). TRIM family: Pleiotropy and diversification through homomultimer and heteromultimer formation. *IUBMB Life*, *64*(1), 64–71. https://doi.org/10.1002/iub.580

238. Naranatt, P. P., Krishnan, H. H., Smith, M. S., & Chandran, B. (2005). Kaposi's sarcoma-associated herpesvirus modulates microtubule dynamics via RhoA-GTP-diaphanous 2 signaling and utilizes the dynein motors to deliver its DNA to the nucleus. *Journal of Virology*, *79*(2), 1191–1206. https://doi.org/10.1128/JVI.79.2.1191-1206.2005

239. Nehlig, A., Molina, A., Rodrigues-Ferreira, S., Honoré, S., & Nahmias, C. (2017). Regulation of end-binding protein EB1 in the control of microtubule dynamics. *Cellular and Molecular Life Sciences*, *74*(13), 2381–2393. https://doi.org/10.1007/s00018-017-2476-2

240. Neuman, B. W., Kiss, G., Kunding, A. H., Bhella, D., Baksh, M. F., Connelly, S., Droese, B., Klaus, J. P., Makino, S., Sawicki, S. G., Siddell, S. G., Stamou, D. G., Wilson, I. A., Kuhn, P., & Buchmeier, M. J. (2011). A structural analysis of M protein in coronavirus assembly and morphology. *Journal of Structural Biology*, *174*(1), 11–22. https://doi.org/10.1016/j.jsb.2010.11.021

241. Nieuwenhuis, J., Adamopoulos, A., Bleijerveld, O. B., Mazouzi, A., Stickel, E., Celie, P., Altelaar, M., Knipscheer, P., Perrakis, A., Blomen, V. A., & Brummelkamp, T. R. (2017).

Vasohibins encode tubulin detyrosinating activity. *Science*, *358*(6369), 1453–1456. https://doi.org/10.1126/science.aao5676

242. Nikolic, J., Belot, L., Raux, H., Legrand, P., Gaudin, Y., & A. Albertini, A. (2018). Structural basis for the recognition of LDL-receptor family members by VSV glycoprotein. *Nature Communications*, *9*(1), 1029. https://doi.org/10.1038/s41467-018-03432-4
243. Nikolic, J., Le Bars, R., Lama, Z., Scrima, N., Lagaudrière-Gesbert, C., Gaudin, Y., & Blondel, D. (2017). Negri bodies are viral factories with properties of liquid organelles. *Nature Communications*, *8*(1), 58. https://doi.org/10.1038/s41467-017-00102-9
244. Nishida, Y., Hirano, K., Tsukamoto, K., Nagano, M., Ikegami, C., Roomp, K., Ishihara, M., Sakane, N., Zhang, Z., Tsujii Ki, K., Matsuyama, A., Ohama, T., Matsuura, F., Ishigami, M., Sakai, N., Hiraoka, H., Hattori, H., Wellington, C., Yoshida, Y., … Matsuzawa, Y. (2002). Expression and functional analyses of novel mutations of ATP-binding cassette transporter-1 in Japanese patients with high-density lipoprotein deficiency. *Biochemical and Biophysical Research Communications*, *290*(2), 713–721. https://doi.org/10.1006/bbrc.2001.6219
245. Nisole, S., Stoye, J. P., & Saïb, A. (2005a). TRIM family proteins: Retroviral restriction and antiviral defence. *Nature Reviews Microbiology*, *3*(10), 799–808. https://doi.org/10.1038/nrmicro1248
246. Nisole, S., Stoye, J. P., & Saïb, A. (2005b). TRIM family proteins: Retroviral restriction and antiviral defence. *Nature Reviews Microbiology*, *3*(10), 799–808. https://doi.org/10.1038/nrmicro1248
247. Nogales, E., & Wang, H.-W. (2006). Structural intermediates in microtubule assembly and disassembly: How and why? *Current Opinion in Cell Biology*, *18*(2), 179–184. https://doi.org/10.1016/j.ceb.2006.02.009
248. Nogales, E., Wolf, S. G., & Downing, K. H. (1998). Structure of the αβ tubulin dimer by electron crystallography. *Nature*, *391*(6663), 199–203. https://doi.org/10.1038/34465
249. Norris, V., & Ovádi, J. (2021). Role of Multifunctional Cytoskeletal Filaments in Coronaviridae Infections: Therapeutic Opportunities for COVID-19 in a Nutshell. *Cells*, *10*(7), 1818. https://doi.org/10.3390/cells10071818
250. Ogawa, S., Goto, W., Orimo, A., Hosoi, T., Ouchi, Y., Muramatsu, M., & Inoue, S. (1998). Molecular Cloning of a Novel RING Finger-B Box-Coiled Coil (RBCC) Protein, terf, Expressed in the Testis. *Biochemical and Biophysical Research Communications*, *251*(2), 515–519. https://doi.org/10.1006/bbrc.1998.9502
251. Ogino, T., & Green, T. J. (2019). Transcriptional Control and mRNA Capping by the GDP Polyribonucleotidyltransferase Domain of the Rabies Virus Large Protein. *Viruses*, *11*(6), 504. https://doi.org/10.3390/v11060504
252. Ostertag, D., Hoblitzell-Ostertag, T. M., & Perrault, J. (2007). Overproduction of Double-Stranded RNA in Vesicular Stomatitis Virus-Infected Cells Activates a Constitutive Cell-Type-Specific Antiviral Response. *Journal of Virology*, *81*(2), 503–513. https://doi.org/10.1128/JVI.01218-06
253. Ozato, K., Shin, D.-M., Chang, T.-H., & Morse, H. C. (2008). TRIM family proteins and their emerging roles in innate immunity. *Nature Reviews. Immunology*, *8*(11), 849–860. https://doi.org/10.1038/nri2413

254. Park, I. Y., Chowdhury, P., Tripathi, D. N., Powell, R. T., Dere, R., Terzo, E. A., Rathmell, W. K., & Walker, C. L. (2016). Methylated α-tubulin antibodies recognize a new microtubule modification on mitotic microtubules. *MAbs*, *8*(8), 1590–1597. https://doi.org/10.1080/19420862.2016.1228505

255. Parthasarathy, K., Ng, L., Lin, X., Liu, D. X., Pervushin, K., Gong, X., & Torres, J. (2008). Structural Flexibility of the Pentameric SARS Coronavirus Envelope Protein Ion Channel. *Biophysical Journal*, *95*(6), L39–L41. https://doi.org/10.1529/biophysj.108.133041

256. Pasick, J. M., Kalicharran, K., & Dales, S. (1994). Distribution and trafficking of JHM coronavirus structural proteins and virions in primary neurons and the OBL-21 neuronal cell line. *Journal of Virology*, *68*(5), 2915–2928.

257. Paturle-Lafanechère, L., Eddé, B., Denoulet, P., Van Dorsselaer, A., Mazarguil, H., Le Caer, J. P., Wehland, J., & Job, D. (1991). Characterization of a major brain tubulin variant which cannot be tyrosinated. *Biochemistry*, *30*(43), 10523–10528. https://doi.org/10.1021/bi00107a022

258. Pawlica, P., & Berthoux, L. (2014). Cytoplasmic dynein promotes HIV-1 uncoating. *Viruses*, *6*(11), 4195–4211. https://doi.org/10.3390/v6114195

259. Peluso, R. W. (1988). Kinetic, quantitative, and functional analysis of multiple forms of the vesicular stomatitis virus nucleocapsid protein in infected cells. *Journal of Virology*, *62*(8), 2799–2807. https://doi.org/10.1128/JVI.62.8.2799-2807.1988

260. Peluso, R. W., Richardson, J. C., Talon, J., & Lock, M. (1996). Identification of a set of proteins (C' and C) encoded by the bicistronic P gene of the Indiana serotype of vesicular stomatitis virus and analysis of their effect on transcription by the viral RNA polymerase. *Virology*, *218*(2), 335–342. https://doi.org/10.1006/viro.1996.0202

261. Permanyer, M., Ballana, E., & Esté, J. A. (2010). Endocytosis of HIV: Anything goes. *Trends in Microbiology*, *18*(12), 543–551. https://doi.org/10.1016/j.tim.2010.09.003

262. Petersen, J. M., Her, L. S., Varvel, V., Lund, E., & Dahlberg, J. E. (2000). The matrix protein of vesicular stomatitis virus inhibits nucleocytoplasmic transport when it is in the nucleus and associated with nuclear pore complexes. *Molecular and Cellular Biology*, *20*(22), 8590–8601. https://doi.org/10.1128/MCB.20.22.8590-8601.2000

263. Picard, L., Ganivet, Q., Allatif, O., Cimarelli, A., Guéguen, L., & Etienne, L. (2020). DGINN, an automated and highly-flexible pipeline for the detection of genetic innovations on protein-coding genes. *Nucleic Acids Research*, *48*(18), e103–e103. https://doi.org/10.1093/nar/gkaa680

264. Poch, O., Blumberg, B. M., Bougueleret, L., & Tordo, N. (1990). Sequence comparison of five polymerases (L proteins) of unsegmented negative-strand RNA viruses: Theoretical assignment of functional domains. *The Journal of General Virology*, *71 (Pt 5)*, 1153–1162. https://doi.org/10.1099/0022-1317-71-5-1153

265. Pond, S. L. K., Frost, S. D. W., & Muse, S. V. (2005). HyPhy: Hypothesis testing using phylogenies. *Bioinformatics (Oxford, England)*, *21*(5), 676–679. https://doi.org/10.1093/bioinformatics/bti079

266. Rahmeh, A. A., Schenk, A. D., Danek, E. I., Kranzusch, P. J., Liang, B., Walz, T., & Whelan, S. P. J. (2010). Molecular architecture of the vesicular stomatitis virus RNA polymerase. *Proceedings of the National Academy of Sciences of the United States of America*, *107*(46), 20075–20080. https://doi.org/10.1073/pnas.1013559107

267. Rajsbaum, R., García-Sastre, A., & Versteeg, G. A. (2014). TRIMmunity: The roles of the TRIM E3-ubiquitin ligase family in innate antiviral immunity. *Journal of Molecular Biology*, *426*(6), 1265–1284. https://doi.org/10.1016/j.jmb.2013.12.005

268. Ramos, H. J., & Gale, M. (2011). RIG-I like receptors and their signaling crosstalk in the regulation of antiviral immunity. *Current Opinion in Virology*, *1*(3), 167–176. https://doi.org/10.1016/j.coviro.2011.04.004

269. Raux, H., Obiang, L., Richard, N., Harper, F., Blondel, D., & Gaudin, Y. (2010). The Matrix Protein of Vesicular Stomatitis Virus Binds Dynamin for Efficient Viral Assembly. *Journal of Virology*, *84*(24), 12609–12618. https://doi.org/10.1128/JVI.01400-10

270. Redeker, V., Le Caer, J. P., Rossier, J., & Promé, J. C. (1991). Structure of the polyglutamyl side chain posttranslationally added to alpha-tubulin. *The Journal of Biological Chemistry*, *266*(34), 23461–23466.

271. Reymond, A., Meroni, G., Fantozzi, A., Merla, G., Cairo, S., Luzi, L., Riganelli, D., Zanaria, E., Messali, S., Cainarca, S., Guffanti, A., Minucci, S., Pelicci, P. G., & Ballabio, A. (2001). The tripartite motif family identifies cell compartments. *The EMBO Journal*, *20*(9), 2140–2151. https://doi.org/10.1093/emboj/20.9.2140

272. Riedel, C., Hennrich, A. A., & Conzelmann, K.-K. (2020). Components and Architecture of the Rhabdovirus Ribonucleoprotein Complex. *Viruses*, *12*(9), 959. https://doi.org/10.3390/v12090959

273. Rihn, S. J., Aziz, M. A., Stewart, D. G., Hughes, J., Turnbull, M. L., Varela, M., Sugrue, E., Herd, C. S., Stanifer, M., Sinkins, S. P., Palmarini, M., & Wilson, S. J. (2019). TRIM69 Inhibits Vesicular Stomatitis Indiana Virus. *Journal of Virology*, *93*(20). https://doi.org/10.1128/JVI.00951-19

274. Rizzo, M. A., Davidson, M. W., & Piston, D. W. (2009). Fluorescent Protein Tracking and Detection: Fluorescent Protein Structure and Color Variants. *Cold Spring Harbor Protocols*, *2009*(12), pdb.top63. https://doi.org/10.1101/pdb.top63

275. Robert, X., & Gouet, P. (2014). Deciphering key features in protein structures with the new ENDscript server. *Nucleic Acids Research*, *42*(Web Server issue), W320-324. https://doi.org/10.1093/nar/gku316

276. Roche, S., Bressanelli, S., Rey, F. A., & Gaudin, Y. (2006). Crystal structure of the low-pH form of the vesicular stomatitis virus glycoprotein G. *Science (New York, N.Y.)*, *313*(5784), 187–191. https://doi.org/10.1126/science.1127683

277. Roche, S., Rey, F. A., Gaudin, Y., & Bressanelli, S. (2007). Structure of the Prefusion Form of the Vesicular Stomatitis Virus Glycoprotein G. *Science*, *315*(5813), 843–848. https://doi.org/10.1126/science.1135710

278. Rodrigues, J. C. V., Rodriguez, C. M., Moreira, L., Villalobos, W., Rivera, C., & Childers, C. C. (2002). Occurrence of Coffee ringspot virus, a Brevipalpus Miteborne Virus in Coffee in Costa Rica. *Plant Disease*, *86*(5), 564. https://doi.org/10.1094/PDIS.2002.86.5.564B

279. Rodríguez, L. L. (2002). Emergence and re-emergence of vesicular stomatitis in the United States. *Virus Research*, *85*(2), 211–219. https://doi.org/10.1016/S0168-1702(02)00026-6

280. Rogowski, K., Dijk, J. van, Magiera, M. M., Bosc, C., Deloulme, J.-C., Bosson, A., Peris, L., Gold, N. D., Lacroix, B., Grau, M. B., Bec, N., Larroque, C., Desagher, S., Holzer, M., Andrieux, A., Moutin, M.-J., & Janke, C. (2010). A Family of Protein-Deglutamylating

Enzymes Associated with Neurodegeneration. *Cell*, *143*(4), 564–578. https://doi.org/10.1016/j.cell.2010.10.014

281. Roll-Mecak, A., & Vale, R. D. (2005). The Drosophila Homologue of the Hereditary Spastic Paraplegia Protein, Spastin, Severs and Disassembles Microtubules. *Current Biology*, *15*(7), 650–655. https://doi.org/10.1016/j.cub.2005.02.029
282. Roostalu, J., & Surrey, T. (2017). Microtubule nucleation: Beyond the template. *Nature Reviews Molecular Cell Biology*, *18*(11), 702–710. https://doi.org/10.1038/nrm.2017.75
283. Sabo, Y., Walsh, D., Barry, D. S., Tinaztepe, S., de los Santos, K., Goff, S. P., Gundersen, G. G., & Naghavi, M. H. (2013). HIV-1 Induces the Formation of Stable Microtubules to Enhance Early Infection. *Cell Host & Microbe*, *14*(5), 535–546. https://doi.org/10.1016/j.chom.2013.10.012
284. Santos da Silva, E., Shanmugapriya, S., Malikov, V., Gu, F., Delaney, M. K., & Naghavi, M. H. (2020). HIV-1 capsids mimic a microtubule regulator to coordinate early stages of infection. *The EMBO Journal*, *39*(20), e104870. https://doi.org/10.15252/embj.2020104870
285. Sardiello, M., Cairo, S., Fontanella, B., Ballabio, A., & Meroni, G. (2008). Genomic analysis of the TRIM family reveals two groups of genes with distinct evolutionary properties. *BMC Evolutionary Biology*, *8*(1), 225. https://doi.org/10.1186/1471-2148-8-225
286. Saurin, A. J., Borden, K. L. B., Boddy, M. N., & Freemont, P. S. (1996). Does this have a familiar RING? *Trends in Biochemical Sciences*, *21*(6), 208–214. https://doi.org/10.1016/S0968-0004(96)80017-X
287. Sawyer, S. L., Wu, L. I., Emerman, M., & Malik, H. S. (2005). Positive selection of primate *TRIM5* α identifies a critical species-specific retroviral restriction domain. *Proceedings of the National Academy of Sciences*, *102*(8), 2832–2837. https://doi.org/10.1073/pnas.0409853102
288. Scales, S. J., Pepperkok, R., & Kreis, T. E. (1997). Visualization of ER-to-Golgi Transport in Living Cells Reveals a Sequential Mode of Action for COPII and COPI. *Cell*, *90*(6), 1137–1148. https://doi.org/10.1016/S0092-8674(00)80379-7
289. Schlegel, R., Tralka, T. S., Willingham, M. C., & Pastan, I. (1983). Inhibition of VSV binding and infectivity by phosphatidylserine: Is phosphatidylserine a VSV-binding site? *Cell*, *32*(2), 639–646. https://doi.org/10.1016/0092-8674(83)90483-x
290. Schmeisser, H., Mejido, J., Balinsky, C. A., Morrow, A. N., Clark, C. R., Zhao, T., & Zoon, K. C. (2010). Identification of Alpha Interferon-Induced Genes Associated with Antiviral Activity in Daudi Cells and Characterization of IFIT3 as a Novel Antiviral Gene. *Journal of Virology*, *84*(20), 10671–10680. https://doi.org/10.1128/JVI.00818-10
291. Schröder, H. C., Wehland, J., & Weber, K. (1985). Purification of brain tubulin-tyrosine ligase by biochemical and immunological methods. *The Journal of Cell Biology*, *100*(1), 276–281. https://doi.org/10.1083/jcb.100.1.276
292. Schweiger, S., Foerster, J., Lehmann, T., Suckow, V., Muller, Y. A., Walter, G., Davies, T., Porter, H., van Bokhoven, H., Lunt, P. W., Traub, P., & Ropers, H. H. (1999). The Opitz syndrome gene product, MID1, associates with microtubules. *Proceedings of the National*

Academy of Sciences of the United States of America, *96*(6), 2794–2799. https://doi.org/10.1073/pnas.96.6.2794

293. Sedbrook, J. C. (2004). MAPs in plant cells: Delineating microtubule growth dynamics and organization. *Current Opinion in Plant Biology*, *7*(6), 632–640. https://doi.org/10.1016/j.pbi.2004.09.017
294. Sehgal, P. B., Yuan, H., Scott, M. F., Deng, Y., Liang, F.-X., & Mackiewicz, A. (2020). Murine GFP-Mx1 forms nuclear condensates and associates with cytoplasmic intermediate filaments: Novel antiviral activity against VSV. *The Journal of Biological Chemistry*, *295*(52), 18023–18035. https://doi.org/10.1074/jbc.RA120.015661
295. Shang, J., Ye, G., Shi, K., Wan, Y., Luo, C., Aihara, H., Geng, Q., Auerbach, A., & Li, F. (2020). Structural basis of receptor recognition by SARS-CoV-2. *Nature*, *581*(7807), 221–224. https://doi.org/10.1038/s41586-020-2179-y
296. Short, K. M., & Cox, T. C. (2006a). Subclassification of the RBCC/TRIM Superfamily Reveals a Novel Motif Necessary for Microtubule Binding. *Journal of Biological Chemistry*, *281*(13), 8970–8980. https://doi.org/10.1074/jbc.M512755200
297. Short, K. M., & Cox, T. C. (2006b). Subclassification of the RBCC/TRIM Superfamily Reveals a Novel Motif Necessary for Microtubule Binding. *Journal of Biological Chemistry*, *281*(13), 8970–8980. https://doi.org/10.1074/jbc.M512755200
298. Shyu, H.-W., Hsu, S.-H., Hsieh-Li, H.-M., & Li, H. (2001). A novel member of the RBCC family, Trif, expressed specifically in the spermatids of mouse testis. *Mechanisms of Development*, *108*(1–2), 213–216. https://doi.org/10.1016/S0925-4773(01)00485-3
299. Sironi, M., Cagliani, R., Forni, D., & Clerici, M. (2015). Evolutionary insights into host-pathogen interactions from mammalian sequence data. *Nature Reviews. Genetics*, *16*(4), 224–236. https://doi.org/10.1038/nrg3905
300. Slack, F. J., & Ruvkun, G. (1998). A novel repeat domain that is often associated with RING finger and B-box motifs. *Trends in Biochemical Sciences*, *23*(12), 474–475. https://doi.org/10.1016/S0968-0004(98)01299-7
301. Sleat, D. E., & Banerjee, A. K. (1993). Transcriptional activity and mutational analysis of recombinant vesicular stomatitis virus RNA polymerase. *Journal of Virology*, *67*(3), 1334–1339. https://doi.org/10.1128/JVI.67.3.1334-1339.1993
302. Sloboda, R. D., Rudolph, S. A., Rosenbaum, J. L., & Greengard, P. (1975). Cyclic AMP-dependent endogenous phosphorylation of a microtubule-associated protein. *Proceedings of the National Academy of Sciences of the United States of America*, *72*(1), 177–181. https://doi.org/10.1073/pnas.72.1.177
303. Sokolskaja, E., Berthoux, L., & Luban, J. (2006). Cyclophilin A and TRIM5α Independently Regulate Human Immunodeficiency Virus Type 1 Infectivity in Human Cells. *Journal of Virology*, *80*(6), 2855–2862. https://doi.org/10.1128/JVI.80.6.2855-2862.2006
304. Sokolskaja, E., & Luban, J. (2006). Cyclophilin, TRIM5, and innate immunity to HIV-1. *Current Opinion in Microbiology*, *9*(4), 404–408. https://doi.org/10.1016/j.mib.2006.06.011
305. Solinger, J. A., Paolinelli, R., Klöss, H., Scorza, F. B., Marchesi, S., Sauder, U., Mitsushima, D., Capuani, F., Stürzenbaum, S. R., & Cassata, G. (2010). The Caenorhabditis elegans Elongator complex regulates neuronal alpha-tubulin acetylation. *PLoS Genetics*, *6*(1), e1000820. https://doi.org/10.1371/journal.pgen.1000820

306. Song, J., Li, M., Li, C., Liu, K., Zhu, Y., & Zhang, H. (2022). Friend or foe: RIG- I like receptors and diseases. *Autoimmunity Reviews*, *21*(10), 103161. https://doi.org/10.1016/j.autrev.2022.103161
307. Spiropoulou, C. F., & Nichol, S. T. (1993). A small highly basic protein is encoded in overlapping frame within the P gene of vesicular stomatitis virus. *Journal of Virology*, *67*(6), 3103–3110. https://doi.org/10.1128/jvi.67.6.3103-3110.1993
308. Stojdl, D. F., Abraham, N., Knowles, S., Marius, R., Brasey, A., Lichty, B. D., Brown, E. G., Sonenberg, N., & Bell, J. C. (2000). The Murine Double-Stranded RNA-Dependent Protein Kinase PKR Is Required for Resistance to Vesicular Stomatitis Virus. *Journal of Virology*, *74*(20), 9580–9585. https://doi.org/10.1128/JVI.74.20.9580-9585.2000
309. Stremlau, M., Owens, C. M., Perron, M. J., Kiessling, M., Autissier, P., & Sodroski, J. (2004). The cytoplasmic body component TRIM5α restricts HIV-1 infection in Old World monkeys. *Nature*, *427*(6977), 848–853. https://doi.org/10.1038/nature02343
310. Stremlau, M., Perron, M., Welikala, S., & Sodroski, J. (2005). Species-Specific Variation in the B30.2(SPRY) Domain of TRIM5α Determines the Potency of Human Immunodeficiency Virus Restriction. *Journal of Virology*, *79*(5), 3139–3145. https://doi.org/10.1128/JVI.79.5.3139-3145.2005
311. Sun, X., Yau, V. K., Briggs, B. J., & Whittaker, G. R. (2005). Role of clathrin-mediated endocytosis during vesicular stomatitis virus entry into host cells. *Virology*, *338*(1), 53–60. https://doi.org/10.1016/j.virol.2005.05.006
312. Sweeney, A., Hammer, R., Evenski, A., & Crim, J. (2016). Fulminant musculoskeletal and neurologic sarcoidosis: Case report and literature update. *Skeletal Radiology*, *45*(11), 1571–1576. https://doi.org/10.1007/s00256-016-2463-y
313. Swinteck, B. D., & Lyles, D. S. (2008). Plasma membrane microdomains containing vesicular stomatitis virus M protein are separate from microdomains containing G protein and nucleocapsids. *Journal of Virology*, *82*(11), 5536–5547. https://doi.org/10.1128/JVI.02407-07
314. Synowiec, A., Szczepański, A., Barreto-Duran, E., Lie, L. K., & Pyrc, K. (2021). Severe Acute Respiratory Syndrome Coronavirus 2 (SARS-CoV-2): A Systemic Infection. *Clinical Microbiology Reviews*, *34*(2), e00133-20. https://doi.org/10.1128/CMR.00133-20
315. Tan, G. S., Preuss, M. A. R., Williams, J. C., & Schnell, M. J. (2007). The dynein light chain 8 binding motif of rabies virus phosphoprotein promotes efficient viral transcription. *Proceedings of the National Academy of Sciences of the United States of America*, *104*(17), 7229–7234. https://doi.org/10.1073/pnas.0701397104
316. Taran, A. S., Shuvalova, L. D., Lagarkova, M. A., & Alieva, I. B. (2020). Huntington's Disease—An Outlook on the Interplay of the HTT Protein, Microtubules and Actin Cytoskeletal Components. *Cells*, *9*(6), 1514. https://doi.org/10.3390/cells9061514
317. Tesh, R., Saidi, S., Javadian, E., Loh, P., & Nadim, A. (1977). Isfahan virus, a new vesiculovirus infecting humans, gerbils, and sandflies in Iran. *The American Journal of Tropical Medicine and Hygiene*, *26*(2), 299–306. https://doi.org/10.4269/ajtmh.1977.26.299
318. Tort, O., Tanco, S., Rocha, C., Bièche, I., Seixas, C., Bosc, C., Andrieux, A., Moutin, M.-J., Avilés, F. X., Lorenzo, J., & Janke, C. (2014). The cytosolic carboxypeptidases CCP2 and

CCP3 catalyze posttranslational removal of acidic amino acids. *Molecular Biology of the Cell*, *25*(19), 3017–3027. https://doi.org/10.1091/mbc.E14-06-1072

319. Towers, G. J., Hatziioannou, T., Cowan, S., Goff, S. P., Luban, J., & Bieniasz, P. D. (2003). Cyclophilin A modulates the sensitivity of HIV-1 to host restriction factors. *Nature Medicine*, *9*(9), 1138–1143. https://doi.org/10.1038/nm910
320. Vallee, R. B. (1986). Purification of brain microtubules and microtubule-associated protein 1 using taxol. *Methods in Enzymology*, *134*, 104–115. https://doi.org/10.1016/0076-6879(86)34079-5
321. Vallee, R. B., Williams, J. C., Varma, D., & Barnhart, L. E. (2004). Dynein: An ancient motor protein involved in multiple modes of transport. *Journal of Neurobiology*, *58*(2), 189–200. https://doi.org/10.1002/neu.10314
322. van Gent, M., Sparrer, K. M. J., & Gack, M. U. (2018). TRIM Proteins and Their Roles in Antiviral Host Defenses. *Annual Review of Virology*, *5*(1), 385–405. https://doi.org/10.1146/annurev-virology-092917-043323
323. van Lohuizen, M., Verbeek, S., Scheljen, B., Wientjens, E., van der Guidon, H., & Berns, A. (1991). Identification of cooperating oncogenes in Eμ-myc transgenic mice by provirus tagging. *Cell*, *65*(5), 737–752. https://doi.org/10.1016/0092-8674(91)90382-9
324. Venuto, S., & Merla, G. (2019). E3 Ubiquitin Ligase TRIM Proteins, Cell Cycle and Mitosis. *Cells*, *8*(5), 510. https://doi.org/10.3390/cells8050510
325. Verdiá-Báguena, C., Nieto-Torres, J. L., Alcaraz, A., DeDiego, M. L., Torres, J., Aguilella, V. M., & Enjuanes, L. (2012). Coronavirus E protein forms ion channels with functionally and structurally-involved membrane lipids. *Virology*, *432*(2), 485–494. https://doi.org/10.1016/j.virol.2012.07.005
326. Verhey, K. J., & Gaertig, J. (2007). The Tubulin Code. *Cell Cycle*, *6*(17), 2152–2160. https://doi.org/10.4161/cc.6.17.4633
327. V'kovski, P., Kratzel, A., Steiner, S., Stalder, H., & Thiel, V. (2021). Coronavirus biology and replication: Implications for SARS-CoV-2. *Nature Reviews Microbiology*, *19*(3), 155–170. https://doi.org/10.1038/s41579-020-00468-6
328. Walls, A. C., Park, Y.-J., Tortorici, M. A., Wall, A., McGuire, A. T., & Veesler, D. (2020). Structure, Function, and Antigenicity of the SARS-CoV-2 Spike Glycoprotein. *Cell*, *183*(6), 1735. https://doi.org/10.1016/j.cell.2020.11.032
329. Wang, K., Zou, C., Wang, X., Huang, C., Feng, T., Pan, W., Wu, Q., Wang, P., & Dai, J. (2018). Interferon-stimulated TRIM69 interrupts dengue virus replication by ubiquitinating viral nonstructural protein 3. *PLoS Pathogens*, *14*(8), e1007287. https://doi.org/10.1371/journal.ppat.1007287
330. Wang, L., & Ning, S. (2021). TRIMming Type I Interferon-Mediated Innate Immune Response in Antiviral and Antitumor Defense. *Viruses*, *13*(2), 279. https://doi.org/10.3390/v13020279
331. Wang, M.-Y., Zhao, R., Gao, L.-J., Gao, X.-F., Wang, D.-P., & Cao, J.-M. (2020). SARS-CoV-2: Structure, Biology, and Structure-Based Therapeutics Development. *Frontiers in Cellular and Infection Microbiology*, *10*, 587269. https://doi.org/10.3389/fcimb.2020.587269
332. Wang, P., Benhenda, S., Wu, H., Lallemand-Breitenbach, V., Zhen, T., Jollivet, F., Peres, L., Li, Y., Chen, S.-J., Chen, Z., de Thé, H., & Meng, G. (2018). RING tetramerization is

required for nuclear body biogenesis and PML sumoylation. *Nature Communications*, *9*(1), 1277. https://doi.org/10.1038/s41467-018-03498-0

333. Warren, J. C., & Cassimeris, L. (2007). The contributions of microtubule stability and dynamic instability to adenovirus nuclear localization efficiency. *Cell Motility and the Cytoskeleton*, *64*(9), 675–689. https://doi.org/10.1002/cm.20215
334. Weaver, S., Shank, S. D., Spielman, S. J., Li, M., Muse, S. V., & Kosakovsky Pond, S. L. (2018). Datamonkey 2.0: A Modern Web Application for Characterizing Selective and Other Evolutionary Processes. *Molecular Biology and Evolution*, *35*(3), 773–777. https://doi.org/10.1093/molbev/msx335
335. Whelan, S. P., & Wertz, G. W. (1999). Regulation of RNA synthesis by the genomic termini of vesicular stomatitis virus: Identification of distinct sequences essential for transcription but not replication. *Journal of Virology*, *73*(1), 297–306. https://doi.org/10.1128/JVI.73.1.297-306.1999
336. White, E. L., & Rock, M. P. (1981). A comparison of thalamocortical and other synaptic inputs to dendrites of two non-spiny neurons in a single barrel of mouse SmI cortex. *The Journal of Comparative Neurology*, *195*(2), 265–277. https://doi.org/10.1002/cne.901950207
337. Whitlow, Z. W., Connor, J. H., & Lyles, D. S. (2008). New mRNAs Are Preferentially Translated during Vesicular Stomatitis Virus Infection. *Journal of Virology*, *82*(5), 2286–2294. https://doi.org/10.1128/JVI.01761-07
338. Wilbourne, M., & Zhang, P. (2021). Visualizing HIV-1 Capsid and Its Interactions with Antivirals and Host Factors. *Viruses*, *13*(2), 246. https://doi.org/10.3390/v13020246
339. Williams, F. P., Haubrich, K., Perez-Borrajero, C., & Hennig, J. (2019). Emerging RNA-binding roles in the TRIM family of ubiquitin ligases. *Biological Chemistry*, *400*(11), 1443–1464. https://doi.org/10.1515/hsz-2019-0158
340. Wilusz, J., Kurilla, M. G., & Keene, J. D. (1983). A host protein (La) binds to a unique species of minus-sense leader RNA during replication of vesicular stomatitis virus. *Proceedings of the National Academy of Sciences of the United States of America*, *80*(19), 5827–5831. https://doi.org/10.1073/pnas.80.19.5827
341. Wloga, D., Joachimiak, E., & Fabczak, H. (2017). Tubulin Post-Translational Modifications and Microtubule Dynamics. *International Journal of Molecular Sciences*, *18*(10), 2207. https://doi.org/10.3390/ijms18102207
342. Wloga, D., Rogowski, K., Sharma, N., Van Dijk, J., Janke, C., Eddé, B., Bré, M.-H., Levilliers, N., Redeker, V., Duan, J., Gorovsky, M. A., Jerka-Dziadosz, M., & Gaertig, J. (2008). Glutamylation on alpha-tubulin is not essential but affects the assembly and functions of a subset of microtubules in Tetrahymena thermophila. *Eukaryotic Cell*, *7*(8), 1362–1372. https://doi.org/10.1128/EC.00084-08
343. Wordeman, L. (2010). How kinesin motor proteins drive mitotic spindle function: Lessons from molecular assays. *Seminars in Cell & Developmental Biology*, *21*(3), 260–268. https://doi.org/10.1016/j.semcdb.2010.01.018
344. Wu, N., Nguyen, X.-N., Wang, L., Appourchaux, R., Zhang, C., Panthu, B., Gruffat, H., Journo, C., Alais, S., Qin, J., Zhang, N., Tartour, K., Catez, F., Mahieux, R., Ohlmann, T., Liu, M., Du, B., & Cimarelli, A. (2019). The interferon stimulated gene 20 protein (ISG20) is an

innate defense antiviral factor that discriminates self versus non-self translation. *PLOS Pathogens*, *15*(10), e1008093. https://doi.org/10.1371/journal.ppat.1008093

345. Xie, X., Muruato, A., Lokugamage, K. G., Narayanan, K., Zhang, X., Zou, J., Liu, J., Schindewolf, C., Bopp, N. E., Aguilar, P. V., Plante, K. S., Weaver, S. C., Makino, S., LeDuc, J. W., Menachery, V. D., & Shi, P.-Y. (2020). An Infectious cDNA Clone of SARS-CoV-2. *Cell Host & Microbe*, *27*(5), 841-848.e3. https://doi.org/10.1016/j.chom.2020.04.004
346. Yacovone, S. K., Smelser, A. M., Macosko, J. C., Holzwarth, G., Ornelles, D. A., & Lyles, D. S. (2016). Migration of Nucleocapsids in Vesicular Stomatitis Virus-Infected Cells Is Dependent on both Microtubules and Actin Filaments. *Journal of Virology*, *90*(13), 6159–6170. https://doi.org/10.1128/JVI.00488-16
347. Yamashita, M., & Engelman, A. N. (2017). Capsid-Dependent Host Factors in HIV-1 Infection. *Trends in Microbiology*, *25*(9), 741–755. https://doi.org/10.1016/j.tim.2017.04.004
348. Yan, R., Zhang, Y., Li, Y., Xia, L., Guo, Y., & Zhou, Q. (2020). Structural basis for the recognition of SARS-CoV-2 by full-length human ACE2. *Science*, *367*(6485), 1444–1448. https://doi.org/10.1126/science.abb2762
349. Yang, W., Gu, Z., Zhang, H., & Hu, H. (2020). To TRIM the Immunity: From Innate to Adaptive Immunity. *Frontiers in Immunology*, *11*, 02157. https://doi.org/10.3389/fimmu.2020.02157
350. Yang, Z. (2007). PAML 4: Phylogenetic analysis by maximum likelihood. *Molecular Biology and Evolution*, *24*(8), 1586–1591. https://doi.org/10.1093/molbev/msm088
351. Yap, M. W., Nisole, S., Lynch, C., & Stoye, J. P. (2004). Trim5α protein restricts both HIV-1 and murine leukemia virus. *Proceedings of the National Academy of Sciences*, *101*(29), 10786–10791. https://doi.org/10.1073/pnas.0402876101
352. Yap, M. W., Nisole, S., & Stoye, J. P. (2005). A Single Amino Acid Change in the SPRY Domain of Human Trim5α Leads to HIV-1 Restriction. *Current Biology*, *15*(1), 73–78. https://doi.org/10.1016/j.cub.2004.12.042
353. Ye, Z., Sun, W., Suryanarayana, K., Justice, P., Robinson, D., & Wagner, R. R. (1994). Membrane-binding domains and cytopathogenesis of the matrix protein of vesicular stomatitis virus. *Journal of Virology*, *68*(11), 7386–7396. https://doi.org/10.1128/JVI.68.11.7386-7396.1994
354. Yea, C., Dembowy, J., Pacione, L., & Brown, M. (2007). Microtubule-mediated and microtubule-independent transport of adenovirus type 5 in HEK293 cells. *Journal of Virology*, *81*(13), 6899–6908. https://doi.org/10.1128/JVI.02330-05
355. Zhang, N., Huang, H., Tan, B., Wei, Y., Xiong, Q., Yan, Y., Hou, L., Wu, N., Siwko, S., Cimarelli, A., Xu, J., Han, H., Qian, M., Liu, M., & Du, B. (2017). Leucine-rich repeat-containing G protein–coupled receptor 4 facilitates vesicular stomatitis virus infection by binding vesicular stomatitis virus glycoprotein. *Journal of Biological Chemistry*, *292*(40), 16527–16538. https://doi.org/10.1074/jbc.M117.802090
356. Zhang, R., Alushin, G. M., Brown, A., & Nogales, E. (2015). Mechanistic Origin of Microtubule Dynamic Instability and Its Modulation by EB Proteins. *Cell*, *162*(4), 849–859. https://doi.org/10.1016/j.cell.2015.07.012

357. Zhang, T., Wong, S. H., Tang, B. L., Xu, Y., & Hong, W. (1999). Morphological and functional association of Sec22b/ERS-24 with the pre-Golgi intermediate compartment. *Molecular Biology of the Cell*, *10*(2), 435–453. https://doi.org/10.1091/mbc.10.2.435

358. Zhang, X., Liu, H., Zhang, Y., Qiao, Y., Miao, S., Wang, L., Zhang, J., Zong, S., & Koide, S. S. (2003). A novel gene, RSD-3/HSD-3.1, encodes a meiotic-related protein expressed in rat and human testis. *Journal of Molecular Medicine*, *81*(6), 380–387. https://doi.org/10.1007/s00109-003-0434-y

359. Zhou, L., Sokolskaja, E., Jolly, C., James, W., Cowley, S. A., & Fassati, A. (2011). Transportin 3 Promotes a Nuclear Maturation Step Required for Efficient HIV-1 Integration. *PLoS Pathogens*, *7*(8), e1002194. https://doi.org/10.1371/journal.ppat.1002194

360. Zinzula, L., Basquin, J., Bohn, S., Beck, F., Klumpe, S., Pfeifer, G., Nagy, I., Bracher, A., Hartl, F. U., & Baumeister, W. (2021). High-resolution structure and biophysical characterization of the nucleocapsid phosphoprotein dimerization domain from the Covid-19 severe acute respiratory syndrome coronavirus 2. *Biochemical and Biophysical Research Communications*, *538*, 54–62. https://doi.org/10.1016/j.bbrc.2020.09.131